



HAL
open science

Overlay Cognitive Radio for IoT satellite communications

Luciano Barros Cardoso da Silva

► **To cite this version:**

Luciano Barros Cardoso da Silva. Overlay Cognitive Radio for IoT satellite communications. Signal and Image processing. Ecole nationale supérieure Mines-Télécom Atlantique, 2020. English. NNT : 2020IMTA0183 . tel-03124005

HAL Id: tel-03124005

<https://theses.hal.science/tel-03124005>

Submitted on 28 Jan 2021

HAL is a multi-disciplinary open access archive for the deposit and dissemination of scientific research documents, whether they are published or not. The documents may come from teaching and research institutions in France or abroad, or from public or private research centers.

L'archive ouverte pluridisciplinaire **HAL**, est destinée au dépôt et à la diffusion de documents scientifiques de niveau recherche, publiés ou non, émanant des établissements d'enseignement et de recherche français ou étrangers, des laboratoires publics ou privés.

THESE DE DOCTORAT DE

L'ÉCOLE NATIONALE SUPERIEURE MINES-TELECOM ATLANTIQUE
BRETAGNE PAYS DE LA LOIRE - IMT ATLANTIQUE

ECOLE DOCTORALE N° 601
*Mathématiques et Sciences et Technologies
de l'Information et de la Communication*
Spécialité : *Télécommunications*

Par

Luciano BARROS CARDOSO DA SILVA

Overlay Cognitive Radio for IoT Satellite Communications

Thèse présentée et soutenue à l'IMT Atlantique – Campus de Toulouse, le 3 Juillet 2020
Unité de recherche : Lab-STICC, UMR 6285
Thèse N° : 2020IMTA0183

Rapporteurs avant soutenance :

Marie-Laure BOUCHERET Professeur des universités, INP-ENSEEIH Toulouse
Christophe JEGO Professeur des universités, ENSEIRB-MATMECA Bordeaux

Composition du Jury :

Président : Karine AMIS, Professeur, IMT Atlantique

Examineurs : Damien ROQUE, Maître de conférences, ISAE SUPAERO
Mathieu DERVIN, Ingénieur R&D, Thales Alenia Space

Rapporteurs : Marie-Laure BOUCHERET, Professeur des universités, INP-ENSEEIH Toulouse
Christophe JEGO, Professeur des universités, ENSEIRB-MATMECA Bordeaux

Dir. de thèse : Laurent FRANCK, Ingénieur, Airbus Defence & Space
Co-dir. de thèse : Tarik BENADDI, Maître de conférences, IMT Atlantique

«Que pour examiner la vérité il est
besoin, une fois dans sa vie, de
mettre toutes choses en doute
autant qu'il se peut.»

René Descartes - Les Principes de la
philosophie (1644)

Acknowledgments

I am very grateful to the *National Institute for Space Research* (INPE) and the *National Council for Scientific and Technological Development* (CNPq) for providing me the opportunity to develop this work, as well as for funding this thesis. In particular, I would like to dedicate this technical work to the *Telecommunications Group* of the *Aerospace Electronics Division* (DEA) of the INPE, of which I am proud and privileged to be a member. Furthermore, I express all my gratitude to the *IMT-Atlantique*, for the warm welcome and the excellent working conditions, which were determinant for the success of this thesis.

I would like to express a few words about the team I had the honour to work with during these last years. I warmly thank my thesis director, Laurent Franck, for trusting me and accepting to direct me during my PhD, with patience with my limitations and inexperience. Laurent possesses the very rare characteristic of cleverly transforming a problem, whatever it may be, into a minor one by the end of an ordinary meeting. This is vital for a great direction! Also, I would like to greatly thank my supervisor Tarik Benaddi. Tarik has always trusted, encouraged and corrected the technical issues of the work. Without his precious interventions, the results of this work would not be achieved. Thank you for all your patience with my technical difficulties and for the countless discussions (anytime and anywhere). I'm sure I'm a much better engineer after working with you! To complete the amazing team of *IMT-Atlantique* (Toulouse site), I would like to express my gratitude to Geneviève, for all the kindness, help and friendship, to Vicente, Daqing (my great reviewer!), Etienne, Walle, Anouar and so many other friends, who supported me in the innumerable days (and nights) of work.

I would like to thank Karine Amis for the honor of chairing the jury of my thesis. My thanks also go to Marie-Laure Boucheret and Christophe Jego for reporting on my thesis. I would also like to thank Damien Roque and Mathieu Dervin for agreeing to examine my thesis.

Agradeço imensamente meus amigos brasileiros (Rafaela, Prêntice, Vinícius, Jognes e tantos outros), que me fizeram sentir em casa e me apoiaram em todos os aspectos. Sem vocês as coisas ficariam bem mais complicadas e muito menos interessantes.

Enfim, agradeço à minha família (Edson, Alzira, André e Juliana) que são os responsáveis por eu ser quem sou. Obrigado pela referência, exemplo, confiança e por me acompanharem (mesmo quando não fisicamente) em todos os desafios, situações e lugares por onde passo. Cada linha desse trabalho tem muito de vocês e de nossa casa.

Abstract

The favorable projection towards the satellite segment could be sustained especially today, since the demand for the rising new services has increased considerably. This is justified by the unique satellite characteristics such as multicast and broadcasting capabilities, mobility aspects and global reach, besides the ability to cover and connect remote areas and hostile environments. As a typical example, we point out the use of satellite to support the Machine-to-Machine (M2M) communications. In this context, one of the main challenges is to develop techniques which enable a better coordination among legacy and future services. It is within this framework that the Cognitive Radio (CR) techniques have also become attractive for space applications. This doctoral thesis studies the feasibility of a secondary service transmission over the primary user infrastructure by using the CR techniques in the overlay paradigm applied to the satellite context. Without going into further details, given that the Cognitive User (CU) has noncausal knowledge about the Primary User (PU) signal and message, its optimal encoding strategy performs: (i) the superposition coding, in order to relay the PU transmission, and (ii) the Dirty-Paper Coding (DPC), which adapts the cognitive signal to the direction of the PU interference. Having this in mind, the first thesis contribution presents a framework for overlay paradigm towards satellite communications. In this sense, a low complexity solution is proposed related to the Trellis Shaping (TS) based DPC encoder for the CU. The performance of both (primary and cognitive) links are characterized in different interference regimes, pointing out the specific degradation caused by the each precoding loss (*i.e.* power, modulo and shaping losses). Subsequently, improving the CU encoder design, we discuss an approach to control the CU output power by addressing the TS technique. Moreover, by using auxiliary bits as well as the proper mapping selection, further constellation expansion is performed in order to increase the number of shaping regions. The relation among these implemented techniques provides a trade-off between power efficiency, by the reduction of the modulo loss, and complexity, by the reduction of the encoder comparisons and operations. As an alternative solution, in our third contribution, a novel method is implemented to recover the modulo loss at the CU receiver side. In this sense, by exploring the lattice theory, a judicious modification at the receiver decoder metric is employed. We underline that, when considering the satellite application, it is eligible as an efficient solution, since the complexity is transferred from the transmitter to the receiver. Finally, we examine the proposed solutions at the light of a realistic satellite scenario, by using examples of Commercial Off-The-Shelf (COTS) parts and assuming practical link budget parameters.

Résumé

La projection favorable vers le segment des satellites pourrait se maintenir, surtout aujourd’hui, puisque la demande de nouveaux services a considérablement augmenté. Cette projection se justifie d’une part par les caractéristiques uniques du satellite, telles que les capacités de multidiffusion et de radiodiffusion, les aspects de mobilité et la portée mondiale, et d’autre part par la capacité de couvrir et de connecter des zones éloignées et hostiles. À titre d’exemple d’une utilisation typique, nous soulignons l’utilisation du satellite pour soutenir les communications de machine à machine (M2M). Dans ce contexte, l’un des principaux défis consiste à développer des techniques permettant une meilleure coordination entre les services existants et futurs. C’est dans ce cadre que les techniques de radio cognitive (CR) sont également devenues attrayantes pour les applications spatiales. Cette thèse de doctorat étudie la faisabilité d’une transmission d’un service secondaire sur l’infrastructure d’un utilisateur primaire en utilisant les techniques de CR dans le paradigme *overlay* appliqué au contexte satellitaire. Sans entrer dans les détails, puisque l’utilisateur cognitif (CU) dispose d’informations non causales du signal et du message de l’utilisateur primaire (PU), sa stratégie d’encodage optimale est mise en place: (i) le codage par superposition, afin de relayer la transmission du PU, et (ii) le *dirty-paper coding* (DPC), qui adapte le signal cognitif à la direction de l’interférence du PU. La première contribution de thèse présente un cadre pour le paradigme *overlay* pour les communications par satellite. Dans ce sens, une solution peu complexe est proposée qui utilise un codeur DPC basé sur le *Trellis Shaping* (TS) pour le CU. Les performances des deux liaisons (primaire et cognitive) sont caractérisées par différents régimes d’interférence, indiquant la dégradation spécifique causées par chaque perte de précodage (c’est-à-dire les pertes de puissance, modulo et de mise en forme). Ensuite, nous discutons d’une approche pour contrôler la puissance de sortie du CU en abordant la technique TS. De plus, en utilisant des bits auxiliaires ainsi qu’une sélection de mapping appropriée, une expansion de la constellation est réalisée afin d’augmenter le nombre de régions de mise en forme. La relation entre ces différentes techniques a permis de proposer une méthodologie de design qui permet d’atteindre un bon compromis entre l’efficacité de la puissance, par la réduction de la perte modulo, et la complexité, par la réduction des opérations du codeur. Comme solution alternative, dans notre troisième contribution, une nouvelle méthode est mise en œuvre pour récupérer la perte modulo du côté du récepteur du CU. Dans ce sens, en explorant la théorie du treillis, une modification judicieuse de la métrique du décodeur du récepteur est employée. Nous soulignons que, lorsque l’on considère l’application satellite, elle est admissible comme solution efficace, puisque la complexité est transférée de l’émetteur au récepteur. Enfin, nous évaluons les solutions proposées à la lumière d’un scénario satellite réaliste en utilisant des exemples de pièces commerciales (COTS) et en supposant des dimensionnement pratiques pour le bilan de liaison.

Contents

Abstract	iii
Résumé	iv
List of Figures	xi
List of Tables	xv
List of Acronyms	xvii
1 Introduction	1
1.1 Problem Description	3
1.2 Contributions	7
1.3 Outline of this Thesis	8
2 Theoretical Background	13
2.1 Introduction	14
2.2 Overlay Cognitive Radio Channel Model	16
2.2.1 Overlay Model in Standard Form	17
2.3 The Capacity of the Overlay Model	19
Primary User Encoding	19
Cognitive User Encoding	20

Encoding and Decoding Procedure	20
2.4 Superposition Strategy	21
Superposition for Overlay Model in Standard Form	23
2.5 Dirty-Paper Coding	24
2.5.1 DPC Theoretical Concepts	25
2.5.2 Analysis of the DPC Capacity	28
Summary of DPC Strategy	31
2.6 Practical DPC Implementation	32
2.6.1 THP Losses Description	35
Power Loss	36
Shaping Loss	36
Modulo Loss	38
2.6.2 THP Performance	40
2.7 Summary	42
3 Cognitive Radio Overlay Paradigm Towards Satellite Communica-	
tions	43
3.1 Introduction	44
3.2 Trellis Shaped Based DPC Encoder	46
3.3 Simulation Approach	49
3.4 Results and Analysis	53
3.4.1 Discussion about the Reference Scheme	53
Shaping Loss	53
Modulo Loss	54

Power Loss	57
3.4.2 Qualitative Analysis for Interfering Scenarios	57
3.4.3 Quantitative Analysis for Interfering Scenarios	63
3.4.4 Main Conclusions	65
3.5 Summary	66
4 A Design Method of Cognitive Overlay Links for Satellite Commu- nications	67
4.1 Introduction	68
4.2 CU Practical Encoder Design for Dirty-Paper Channel	70
4.2.1 CU Transmitted Power Control	71
4.2.2 Constellation Expansion	72
4.2.3 Mapping Discussion	75
4.2.4 Simulation Approach	78
4.2.5 Results and Analysis	81
(i) Low Interference Scenario - $P_P = 3$ dB	82
(ii) Intermediate Interference Scenario - $P_P = 7$ dB	83
(iii) High Interference Scenario - $P_P = 15$ dB	85
(iv) Extremely High Interference Scenario - $P_P = 20$ dB	85
4.3 On the Modulo Loss Recovering at the Decoder	90
4.3.1 Method Description	90
4.3.2 Results and Analysis of the Proposed Metric	98
4.4 Discussion of the Chapter Results	102
4.5 Summary	102

5	On the Feasibility of a Secondary Service Transmission Over an Ex-	103
	istent Satellite Infrastructure	
5.1	Introduction	104
5.2	Practical System Analysis	106
5.2.1	System Engineering Design	106
5.2.2	Techniques Design	106
5.3	Realistic Use Case	107
5.3.1	Primary Service Transmission Analysis	107
5.3.2	Secondary Service Transmission Analysis	109
	CU Results and Analysis	109
	CU Link Budget	112
5.4	Conclusion	113
6	Conclusion and Future Work	115
6.1	Discussion and Summary of Results	115
6.2	Outlook of Future Work	117
7	Résumé de la Thèse	121
7.1	Contexte de la Thèse	121
7.2	Présentation de la Problématique	123
7.3	Discussion et Synthèse des Résultats	127
A	Alternative Proof of the DPC Capacity	129
B	Design Computations for Analysis of the Feasibility of a Secondary	
	Service Transmission	133

B.1	Primary Service Feasibility	133
	B.1.1 Main Specifications for Primary User	133
	B.1.2 Link Budget for Primary User	135
	B.1.3 Primary User Transmission on the Interfering Scenario	138
	Superposition Strategy Computation	139
B.2	Secondary Service Feasibility	139
	B.2.1 Link Budget for Cognitive User	140
B.3	Transmitted Output Power	142
	Bibliography	143

List of Figures

2-1	Satellite scenarios.	15
2-2	Overlay model.	17
2-3	Overlay model in standard form.	18
2-4	Gaussian channel with additive Gaussian state S available noncausally at the encoder.	25
2-5	$I(X_{cc}; Y_s)$, $I(X_{cc}; S)$ and $R = R_c$, as a function of λ , considering $P_{\hat{X}_c} = P_S = N_s = 1$.	31
2-6	DPC encoder with Partial Interference Presubtraction (PIP) in Tomlinson-Harashima Precoding (THP).	33
2-7	Representation of THP transmission and reception without noise.	35
2-8	Shaped 256-QAM constellation.	38
2-9	Representation of Modulo Loss.	39
2-10	SER of THP schemes.	41
3-1	Proposed DPC encoder.	48
3-2	Proposed DPC receiver.	49
3-3	Proposed CU mapping.	51
3-4	Representation of a trellis decoding for a generic C_c considering the parallel transition defined by the mapping of Fig. 3-3.	52
3-5	Histogram of the transmitted signal X_{cc}^{\wedge} for the reference TS AWGN scheme, considering the assumed shaping code C_s and the the mapping defined by Fig. 3-3.	55

3-6	Representation of a received symbol from AWGN channel considering the proposed CU mapping impacted by modulo loss.	56
3-7	Scatter plots of signals constellations at different PU interfering powers.	58
3-8	Histogram of the X_{cc}^n constellation at different PU interfering powers	61
3-9	Histogram of the \hat{X}_c^n signal at different PU interfering powers	62
3-10	BER of the cognitive user	64
4-1	Shaping regions mapping I	75
4-2	Shaping regions mapping II	77
4-3	Shaping regions mapping II for 64-QAM	80
4-4	Example of parallel transitions for <i>Viterbi</i> decoder of trellis shaping at the transmitter, according to mapping of Fig. 4-3.	81
4-5	Results and analysis for $P_P = 3$ dB	84
4-6	Results and analysis for $P_P = 7$ dB	86
4-7	Results and analysis for $P_P = 15$ dB	87
4-8	Results and analysis for $P_P = 20$ dB	89
4-9	Modulo loss recovering at the receiver side	92
4-10	Decision regions of the investigated metrics.	97
4-11	BER of cognitive user considering different TCM decoder metrics at receiver for $P_P = 3$ dB.	99
4-12	BER of cognitive user considering different TCM decoder metrics at receiver for $P_P = 20$ dB.	100
5-1	Overlay model considering realistic satellite link budget.	108
5-2	Results and analysis for CU, considering $10.\log_{10}(P_p/P_c) = 9.5$ dB and $\alpha = 0.85$, according to different constellation expansion.	110

B-1	Relative position of the satellite and the ground station at the farthest communicative distance.	135
B-2	Summary of the power sharing assignment in this design.	140

List of Tables

2.1	Power loss in respect with the square QAM constellation size.	37
4.1	Summary of the investigated receiver metrics on DPC schemes.	101
5.1	Primary User link budget (QPSK coded FEC $R=1/2$).	108
5.2	Cognitive User link budget.	113
B.1	Bit rate (kbps) supported by each DPC scheme of Fig. 5-2e	141

Acronyms

5G	Fifth Generation.
APSK	Amplitude and Phase-Shift Keying.
AWGN	Additive White Gaussian Noise.
BER	Bit Error Rate.
CNPq/Brazil	National Council for Scientific and Technological Development.
CNR	Carrier-to-Noise Ratio.
CORASAT	COgnitive RAdio for SATellite Communications.
COTS	Commercial Off-The-Shelf.
CPM	Continuous Phase Modulation.
CR	Cognitive Radio.
CU	Cognitive User.
DMC	Discrete Memoryless Channel.
DPC	Dirty-Paper Coding.

DVB-S2X	Digital Video Broadcasting - Satellite - Second Generation Extension.
EESS	Earth Exploration Satellite Service.
EIRP	Effective Isotropic Radiated Power.
FCC	Federal Communication Commission.
FEC	Forward Error Correction.
FSK	Frequency-Shift Keying.
GEO	Geosynchronous Equatorial Orbit.
HPA	High Power Amplifier.
INPE/Brazil	National Institute for Space Research.
INR	Interference-to-Noise Ratio.
IoT	Internet of Things.
ISI	Inter-Symbol Interference.
ITU-RR	International Telecommunication Union Radio Regulation.
LEO	Low Earth Orbit.
M2M	Machine-to-Machine.
MEO	Medium Earth Orbit.
MLAN	Modulo-Lattice Additive Noise.

MMSE	Minimum Mean-Square Error.
MUI	Multi-User Interference.
PAPR	Peak-to-Average Power Ratio.
PIP	Partial Interference Presubtraction.
PSK	Phase-Shift Keying.
PU	Primary User.
QAM	Quadrature Amplitude Modulation.
QPSK	Quadrature Phase-Shift Keying.
SDR	Software Defined Radio.
SER	Symbol Error Rate.
SI	State Information.
SINR	Signal-to-Interference-plus-Noise Ratio.
SNR	Signal-to-Noise Ratio.
TCM	Trellis Coded Modulation.
THP	Tomlinson-Harashima Precoding.
TP	Trellis Precoding.
TS	Trellis Shaping.

Chapter 1

Introduction

It can be emphatically stated that the access to space is easier, cheaper and faster than ever before. This is the widespread view among the main satellite players with respect to the unique opportunistic time currently experienced by the space segment. Even when considered the continuous technological developments in terrestrial networks, the satellite communications systems remain as relevant as ever, playing a crucial role in the modern telecommunications world.

With regards to the applications, the favorable projections to this segment could be sustained especially today, since the demand for the rising new services has increased considerably, justified by the unique satellite characteristics such as multicast and broadcasting capabilities, mobility aspects, global reach, besides the ability to cover and connect green space and hostile environments [1].

In this sense, as an actual and typical example, it could be pointed out the use of satellite to support the Machine-to-Machine (M2M) communications, providing connectivity to the end-users anytime, anywhere, for any media and device [2]. The M2M communications are one of the central use cases in the upcoming new Fifth Generation (5G) mobile network [3] as they play a major role in the Internet of Things (IoT). In fact, it is predicted in [4] the deployment of around 1 million devices per km² like sensors/actuators, vehicles, factory machines, beacons *etc.*

In what concerns the technological advances, this satellite era consolidation could be reinforced (but not only) by the recent maturity reached in the manufacturing process, which ultimately drives down the implementation costs and timescale, as

well as the advances on the conceived payload capabilities, also stimulated by the new tendency towards the novel experiments that falls beyond the risk frontiers.

Nonetheless, as a counterpoint, to meet these increasingly challenging requirements while keeping the competitiveness facing the terrestrial technologies, the satellite communication systems need to push the boundaries in the direction to more and more efficient technical solutions. For this purpose, the search for power and bandwidth efficiency as well as the actual trend to low complexity systems must be a paramount concern for system designers, since that, due to the existing trade-offs, equating these factors often becomes a major challenge.

For a given provided service to the end-users, the design requirements of the communication system, in general, are settled by: (i) the service availability, which ultimately specifies the required Bit Error Rate (BER); (ii) the allocated spectral band, which is assigned by the International Telecommunication Union Radio Regulation (ITU-RR) [5], and (iii) the range of the received Carrier-to-Noise Ratio (CNR), measured in the occupied bandwidth, which is limited by the large path loss as well as the nonlinear behavior of the satellite channel. For instance, it could be typically assigned the dynamic range of CNR between -3 and 20 dB, in accordance to the extension recently presented at the Digital Video Broadcasting - Satellite - Second Generation Extension (DVB-S2X) standard [6].

Basically, concerning these bounds, the system can be designed efficiently in power, by decreasing the received power (or equivalently the CNR) necessary to reach the specified BER, for instance by adding redundancy bits in a digital encoding system, or spectral efficient, by increasing the number of bits per hertz into the occupied bandwidth, which ultimately increases the transmitted data rate. Last but not least, the system complexity should be carefully evaluated in order to reduce as low as possible the number of processing operations without degrading the overall performance, especially when on-board systems are considered. The main goal is to equalize the trade-off as a function of the available mission resources.

Besides the aforementioned challenges, the available radio spectrum is today a scarce resource (cf. [7] for example). Hence, another faced challenge is to develop techniques which enable a better coordination between legacy and future services, especially considering this new machine-type communication environment and its large-

scale implementation. Despite the fact that the spectrum regulation and policy are still being considered as a dry subject since the earliest days of radio communication, the need to reconsider the static long-term exclusivity of the spectrum via licensed regulation procedures, as well as the encouragement of the techniques which enable the coexistence of different networks, become a key element to permit an adequate expansion of these new services [8].

It is within this framework that, with the premise of alleviating the increasingly spectral scarcity, the Cognitive Radio (CR) techniques have also become attractive for space applications [9]. Thanks to the recent developments in the space qualified Software Defined Radio (SDR) [10] and also to the acceptability of concepts such as flexible and hosted payloads [11], [12], CR techniques have been further developed these last years, resulting in a smarter spectrum management. In addition, some valuable and precursor research [13] has been acted in spectral awareness and spectral exploitation techniques, which has driven the cognitive satellite communications towards a promising approach in order to improve a secondary service access.

To summarize this scope description, the main theme of this manuscript relates to the coexistence of a secondary service into the existent primary user infrastructure. We propose a general technical solution by highlighting the results of some specific research contributions. The previously context aspects are taken into account aiming at the timeliness and the realistic accuracy for the following models, approaches and results presented throughout this document.

1.1 Problem Description

In light of the previously exposed theme, this work investigates the CR concepts and its associated techniques. In this sense, we propose a solution for a secondary service coexistence by accessing the primary services network in the satellite communications context, concerning the stringent system constraints. In this section, the problem is depicted in a sequential approach in such way to introduce the novelty as well as the specific research contributions of this thesis. Therefore, few words about the CR nomenclature and paradigms are presented along with the main contributions in the literature on this subject.

First of all, by adopting the usual nomenclature in the great majority of the references, the Primary User (PU) is defined as the licensed user to operate into the interested frequency band. On the other hand, the Cognitive User (CU) is defined as unlicensed user, which opportunistically or even concurrently transmits in this same band allocated to the PU, while guaranteeing the same performance to this latter.

Following this definition, the cognitive operation is realized by the CR, originally introduced by Mitola in [14]. This particular radio is formally defined by the *Federal Communication Commission (FCC)* as *a radio or system that perceives its electromagnetic environment being able, autonomously and dynamically, to set its parameters in order to: optimize the transmission rate, control for mitigation of interference, interoperability and access to secondary markets* [15]. In this way, it can envisage two fundamental radio operations that may be separated as: spectral awareness and spectrum exploitation.

In few words, the first activity (spectral awareness) could be performed by techniques such as: spectral sensing, cooperative database, signal-to-noise ratio estimation, cycle-stationarity, etc [16]. The second activity (spectrum exploitation), refers to the signal parameters adaptation to reach efficient transmission schemes. This is usually performed by techniques such as: adaptive control of resources (power, frequency, space), beamforming techniques, modulation and coding adaptation, etc[17].

From the system point of view, three main paradigms classify the radio operation [18]:

- *interweave*, which is based on the idea of opportunistic communication. In short, the CU looks for the *white* spaces that are not used by the PU transmission, which can be scaled in space, time or frequency, and adjusts its operating parameters. It is inferred that, ideally, there is no coexistence between users and, consequently, no power control of the CU transmission is required;
- *underlay*, denominated as *gray* spectrum space, where the CU, by means of a partial knowledge of the PU signal characteristics and channel, adjusts its parameters in such a way as to respect an established interference threshold, for instance a previously required spectral mask. Unlike the interweave operation, in this paradigm two users can transmit simultaneously. However, as the knowledge of the PU signal is required, more sophisticated spectral sensing

techniques must be employed, such as Signal-to-Noise Ratio (SNR) estimation algorithms. Some examples of techniques found in the literature are: dynamic resource control (power and frequency), beamforming with multiple antennas, and spectral spreading [17];

- *overlay*, where the CU, from the full and noncausal knowledge about the PU waveform, message and channel, uses advanced coding and modulation strategies to transmit simultaneously while mitigating the interference. The CR used spectrum space in this last paradigm is called *black*, as it is occupied by the interfering signals and noise, and is not power limited.

It is worth noting that the choice of the paradigm to be used by the CU highly depends on the available information of the PU signal. Briefly, if the available information is only the presence (or absence) of PU, interweave is used. On the other hand, if in addition to the activity, channel states are also known, the CU may operate under the underlay paradigm. Finally, if the coding strategies and the PU transmitted data are completely known, the CU can operate in overlay, contributing to both links.

Considering the previous definitions and regarding space communications, it could be inferred that one of the first significant stimulus on this subject can be attributed to the COgnitive RAdio for SATellite Communications (CORASAT) group [19] [20]. Composed of several research institutes and universities in the European continent, corroborating the fact that the subject is of great interest in both academic and industrial areas, this group was conceived with the purpose of investigating, developing and demonstrate possible cognitive radio techniques appropriate to space systems. In addition, recommendations that might be used as guides for new projects have been published, culminating in an important step towards standardization and regulation [21].

In 2014, alongside the CORASAT project, the first specific PhD thesis [22] was concluded on the subject of cognitive satellite communications. The contributions of both works, Sharma thesis and CORASAT, explore the coexistence between satellite and terrestrial network as well as the dual satellite systems scenario. It is worth noting that, since the highly stringent requirements for overlay paradigm might be not feasible considering the assumed scenarios, the investigated paradigms were in-

terweave and underlay. Among numerous contributions, we underline the research in spectral sensing, SNR estimation methods, beamforming techniques and dynamic resource allocation.

The present doctoral thesis, supported by the *National Institute for Space Research (INPE/Brazil)* and by the *National Council for Scientific and Technological Development (CNPq/Brazil)*, developed at *IMT-Atlantique (Toulouse site)*, investigates the feasibility of a secondary service transmission over the primary user infrastructure using the overlay paradigm of CR techniques. To the best of the author's knowledge, no previous works have been conducted on the overlay paradigm in the context of satellite communications. Considering the general objective of this thesis, we show that this novel approach is well suitable for low data rate M2M applications.

The main reason to propose the overlay paradigm for satellite communications lies in the feasibility of transmitting both unlicensed and licensed services simultaneously from the same satellite towards their respective terminals. We emphasize, due to the priority among users, that the superposition coding strategy is required [23] to relay the PU transmission, unlike the technical solutions adopted for the broadcast channel [24]. Furthermore, the Dirty-Paper Coding (DPC) [25], is implemented to adapt the cognitive signal to the direction of the PU interference.

DPC is a communication technique that allows to mitigate the interference if it is noncausally known at the transmitter side. This technique was introduced by Costa [25] in 1983. However, the first idea of practical scheme was proposed by Erez, Shamai and Zamir [26]. It pointed out the Tomlinson-Harashima Precoding (THP) for Inter-Symbol Interference (ISI) canceling, which can be seen as a DPC application for frequency selective channel. In this technique, the modulo operation is used to pre-subtract the interference with a minimum power increase. Also in this work, the precoding losses, i.e. shaping loss at high SNR regime and the combined modulo and power losses at intermediate/low SNR regimes, was well characterized. Moreover, Eyuboglu and Forney in their seminal paper [27] generalized the combination of the Trellis Shaping (TS) [28], Trellis Coded Modulation (TCM) and THP for Gaussian ISI channels. The so-called Trellis Precoding (TP) performs interference pre-subtraction and allows recovery of the shaping loss. Likewise, a little bit more closer to our application, an extension of TP for multiuser interference was proposed to recover the shaping loss with sufficient high constellation expansion in [29] and [30], where

the TS technique acts as a vectorial quantization, replacing the modulo operator.

In addition to this discussion, a special attention must be paid in the use of modulo operator at the transmitter, as it incurs into nonlinear distortion. This consideration is of high interest, especially in the context of satellite communications, when the embedded High Power Amplifier (HPA) has to work near of saturation for better power efficiency. The mitigation of this effect was studied in [31] and some countermeasures were disposed for satellite channels over ISI. However, this topic remains an open problem for system with modulo processing.

In view of the above, the specific contributions of this thesis present variations aiming to the design of overlay links, considering realistic interference scenarios. A DPC encoder is proposed involving TS and TCM concepts along with properly constellation expansion combined with THP. The discussions lead to a trade-off between power efficiency (reduction of the modulo loss) and complexity, key levers for both satellite onboard processing and terminals.

1.2 Contributions

The first thesis contribution presents a framework for overlay paradigm towards satellite communications. In this sense, a low complexity solution is proposed related to the Trellis Shaping based DPC encoder for the CU. The performance of both (primary and cognitive) links are characterized in different interference regimes, pointing out the specific degradation caused by each precoding loss (*i.e.* power, modulo and shaping losses). A large part of these results was published in [32].

Subsequently, oriented by the results achieved in [32], some improvements in the CU encoder design were introduced in [33]. We discuss an approach to control the CU output power by addressing the TS technique. Moreover, by using auxiliary bits as well as a proper mapping selection, further constellation expansion is performed in order to increase the number of shaping regions. The relation among these implemented techniques exhibits a trade-off between power efficiency, by the reduction of the modulo loss, and complexity, by the reduction of the encoder comparisons and operations.

As an alternative solution, in our third contribution, a novel method is implemented to recover the modulo loss at the CU receiver side. In this sense, by exploring the lattice theory, a judicious modification at the receiver decoder metric is employed. As a result, for the assumed SNR operation range, almost all precoding losses are recovered without high constellation expansion. We underline that, when considering the satellite application, it is eligible as an efficient solution, since the complexity is transferred from the transmitter to the receiver.

Finally, regarding a general approach, we examine the proposed solutions at the light of a realistic satellite scenario. By using examples of Commercial Off-The-Shelf (COTS) parts and assuming practical link budget parameters, we discuss the feasibility of a secondary service transmission over an existing primary user infrastructure. This work was presented in [34] and have its extended version published in EURASIP Journal on Wireless Communications and Networking (in second round of review process), in the special issue "New application domains for the cognitive-based solutions in the context of 5G and beyond". In addition, an inspired solution applied for watermarking transmission for CubeSat was presented in [35] workshop.

1.3 Outline of this Thesis

This introduction aimed to present the scope of this thesis as well as its contributions, contextualized with the state of art identified in the recent literature. The next chapters will detail each explored concepts, going from the general to specific approach. For familiar readers on the subject of CR paradigms and DPC, the author would encourage to start directly from the Chapter 3, where the thesis contributions are introduced step by step (with reference to specific points in the previous chapters when required).

Following the sequence of the manuscript, Chapter 2 presents the theoretical background of this thesis. In the first part of the chapter, a system model is introduced, grounded by the scope and scenarios previously described. This includes the overlay interference model and the analytic development to reach the Additive White Gaussian Noise (AWGN) channel capacity, which is reached by properly CU encoding strategies. Furthermore, the superposition concept is also discussed, highlighting the

implications and proposing countermeasures.

Subsequent to the channel model characterization, the second part of Chapter 2 is totally dedicated to the CU interference mitigation by means of DPC strategy. Firstly, the theoretical concepts are discussed, supported by the Costa's proof [25]. After that, the practical implementation of DPC encoder is presented by considering the THP scheme, deepening our attention to its inherent losses, that serves as a basis for the solution of DPC encoder implemented in the thesis framework.

From this point, regarding these introductory chapters, the author starts to present the thesis contributions.

In Chapter 3, our proposed framework of the overlay interference model is implemented and the first results, considering typical interference values for satellite applications, are analyzed. The concepts of the encoder and decoder are detailed and the relation with the system degradation is evaluated as function of the BER.

A DPC encoder design is refined in the Chapter 4. First of all, a method to control the output power of the CU is derived by using TS concepts. It is worth noting that, due to this approach, the PU performance is the same as in AWGN channel. Regarding the CU link, we show that a bigger expansion of the CU constellation, tied to a proper mapping design for the shaping regions, improves the system performance. In addition, a new solution is proposed for the modulo loss mitigation in order to reducing also the system complexity at the transmitter, which is of paramount importance for satellite communications. Numerous analyses are exposed and discussed.

In the Chapter 5, the realistic parameters and scenario are assumed for application of the proposed techniques. In this sense, the work in this chapter analyses the feasibility of a secondary service over an existent primary user infrastructure. This general contribution uses the concepts described in all previous chapters and intends to validate the specific proposed solutions in a general context.

Finally, Chapter 6 presents the conclusions of this thesis as well as some directions towards interesting research to be done on this subject.

List of Publications

International Journal Article

1. L. B. C. da Silva, T. Benaddi and L. Franck, "On the Feasibility of a Secondary Service Transmission over an Existent Satellite Infrastructure: Design and Analysis," *EURASIP Journal on Wireless Communications and Networking, in the special issue "New application domains for the cognitive-based solutions in the context of 5G and beyond"* v. 2020, n. 1, pp. 1-18, 2020.;

International Conference Paper

2. L. B. C. da Silva, T. Benaddi, and L. Franck, "On the Feasibility of a Secondary Service Transmission over an Existent Satellite Infrastructure," in *14th International Conference on Cognitive Radio Oriented Wireless Networks (CROWN-COM)*, Poznan, Poland, June 2019, pp. 154-167;
3. L. B. C. da Silva, T. Benaddi and L. Franck, "A Design Method of Cognitive Overlay Links for Satellite Communications," in *9th Advanced Satellite Multimedia Systems Conference and the 15th Signal Processing for Space Communications Workshop (ASMS/SPSC)*, Berlin, Germany, Sept. 2018, pp. 1-6;
4. L. B. C. da Silva, T. Benaddi and L. Franck, "Cognitive Radio Overlay Paradigm Towards Satellite Communications," *IEEE International Black Sea Conference on Communications and Networking (BlackSeaCom)*, Batumi, Georgia, June 2018, pp. 1-5;

National Conference Paper

5. L. B. C. da Silva, T. Benaddi and L. Franck, "*Sur la Faisabilité d'une Transmission de Service Secondaire sur une Infrastructure Satellitaire Existante,*" *Colloque GRETSI sur le traitement du Signal*, Lille, France, August 2019;

International Workshop

6. L. B. C. da Silva, T. Benaddi and L. Franck, "A watermarking like scheme for CubeSat communications," in *10th European CubeSat Symposium*, Toulouse, France, December 2018.

Chapter 2

Theoretical Background

Contents

2.1	Introduction	14
2.2	Overlay Cognitive Radio Channel Model	16
2.2.1	Overlay Model in Standard Form	17
2.3	The Capacity of the Overlay Model	19
2.4	Superposition Strategy	21
2.5	Dirty-Paper Coding	24
2.5.1	DPC Theoretical Concepts	25
2.5.2	Analysis of the DPC Capacity	28
2.6	Practical DPC Implementation	32
2.6.1	THP Losses Description	35
2.6.2	THP Performance	40
2.7	Summary	42

In the opening of this manuscript, the satellite context as well as the positioning of our studied theme into the state of art, addressing the Cognitive Radio (CR) techniques, was underlined.

By recalling this topic, when considering the CR interweave paradigm, the Cognitive User (CU) identifies the available spectrum portions for a specific location and

time and transmits the cognitive messages into this *white* space [18]. In this sense, the *activity* side information about the Primary User (PU) is provided to the CU transmitter, in order to allow an efficient spectrum exploitation. Concerning satellite applications, the references [13, 22, 36] discuss techniques considering (i) the hybrid satellite-terrestrial and (ii) the dual satellite coexistence. Examples of interweave cognitive approaches, applied to these investigated scenarios, are: dynamic spectrum sense techniques, geolocation database methods, interference detection and avoidance etc.

Moreover, by considering the CR underlay paradigm, the CU is allowed to transmit simultaneously with the PU, as long as the interference is below a determined threshold. Therefore, in this *gray* space [18], the *channel* side information about the PU is also required to the CU transmitter, in order to allow the spectrum exploitation transmission. Regarding this paradigm, the same coexistence scenarios (i) and (ii) are investigated in [13, 37, 38, 17], introducing CR technical contributions mainly addressed to: beamforming systems, exclusion zone identification, resource allocation (power/carrier), interference alignment and cancellation, beamhopping etc.

In this thesis, we are interested to explore the techniques concerning the overlay paradigm for satellite communications. In this case, the CU transmits simultaneously with the PU by assign part of its transmit power to relay the primary link (superposition strategy). It is worth noting that the *codebook* side information of the PU is required, in order to implement the optimized CU encoding strategies.

In view of above, this Chapter provides the theoretical background to support the contributions presented through this thesis. A large part of the content demonstrated here follows the developments and discussions introduced in the references [23, 24, 25, 39].

2.1 Introduction

Based on the context presented in the introduction of this thesis, the following scenarios are provided as examples where the overlay CR techniques might be applied to satellite communications.

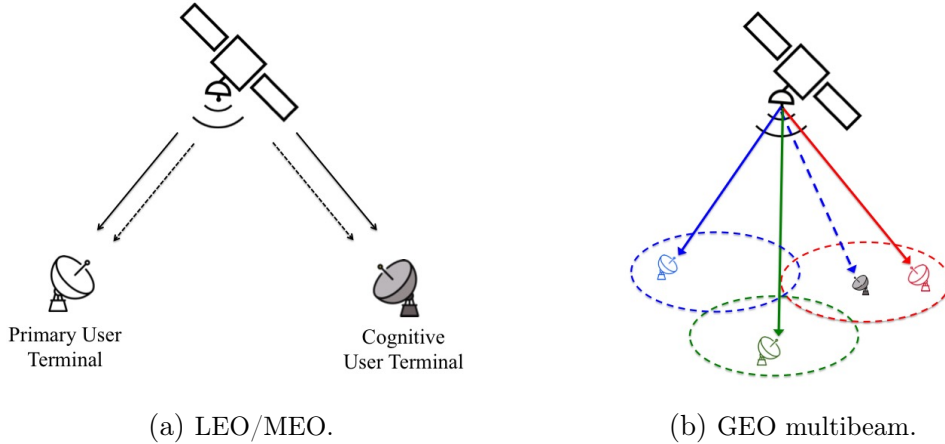


Figure 2-1: Satellite scenarios.

In the first case, presented in the Fig. 2-1a, an ordinary LEO/MEO satellite provides two different services towards different terminals. In this context, a single licensed PU takes priority over the added unlicensed CU. The interference presented at both terminals should be mitigated by properly designed CU encoder, without any changes in the PU communication chain.

In the same way, a GEO multibeam satellite scenario is illustrated in the Fig. 2-1b. In this case, considering the frequency reuse, the CU is able to transmit by using, for instance, the settled blue frequency (or polarization) into the red spot footprint, as far as the interference among adjacent beams is resolved. It is worth noting also that all possible different PU transmissions, represented by several blue spots, should be taken into account in the interference mitigation design. By this way, the total satellite capacity could be increased as well as the spectrum resources better managed.

The main purpose of this Chapter is to present the cognitive radio channel, which could be seen as suitable for the satellite context, and evaluate the highest theoretical rate achieved by the cognitive user. By allowing the coexistence among the cognitive and each primary users, the following obligatory conditions are assumed [23]:

1. The PU performance is not degraded (*i.e.* the primary user rate R_p achieved in the AWGN channel is preserved in the interference channel);
2. The PU infrastructure remains unchanged as in absence of CU transmission or, equivalently, as in the standard AWGN channel. In this sense, the PU receiver implements a *single-user decoder* (for example, the minimum-distance decoder).

Based on the above, the cognitive radio overlay model is characterized in the next section. Subsequently, the CU achievable rate R_c is evaluated, by considering the channel constraints. Finally, a further theoretical description about the CU encoding strategies, superposition and Dirty-Paper Coding (DPC), is presented.

2.2 Overlay Cognitive Radio Channel Model

Equally suitable for both scenarios, the interference model with side information, adapted from [23], is depicted in Figure 2-2. Assuming that the signals are onboard if the processing is performed by the satellite (for transparent satellite, this processing is done by the gateway), the cognitive encoder has full and noncausal knowledge about each i -th PU signal $X_{p,i}^n$ and message, which addresses the main overlay paradigm requirement [13, 40]. In this sense, the encoded cognitive signal X_c^n is a function of both primary and cognitive messages (respectively, $m_{p,i} \in \{1, \dots, M_{p,i}\}$ and $m_c \in \{0, 1, \dots, M_c\}$). We assume that $M_{p,i}$ and M_c are the cardinalities of the corresponding alphabets, and verify $M_{p,i} \leq e^{nR_{p,i}}$ and $M_c \leq e^{nR_c}$, where $R_{p,i}$ and R_c are the achievable i -th primary and cognitive user rates.

Without loss of generality, considering the i -th PU and the added CU, the channel gains $|h_{yx,i}|$ (from the transmitter x to the receiver y) are defined by the losses of the direct paths ($|h_{pp,i}|$ and $|h_{cc}|$), and the interfering paths ($|h_{cp,i}|$ and $|h_{pc,i}|$) (the Fig. 2-2 summarizes these notation). In our context, these factors are computed as function of the each transmission link budget (the Chapter 5 presents an example of these computations by using realistic parameters).

The following equations describe the channel outputs, where n refers to n -uses of the channel:

$$Y_{p,i}^n = |h_{pp,i}| X_{p,i}^n + \overbrace{|h_{pc,i}| X_c^n}^{I_{pc,i}} + Z_{p,i}^n \quad (2.1)$$

$$Y_s^n = |h_{cc}| X_c^n + \underbrace{\sum_{i=1}^N |h_{cp,i}| X_{p,i}^n}_{I_{cp}} + Z_s^n. \quad (2.2)$$

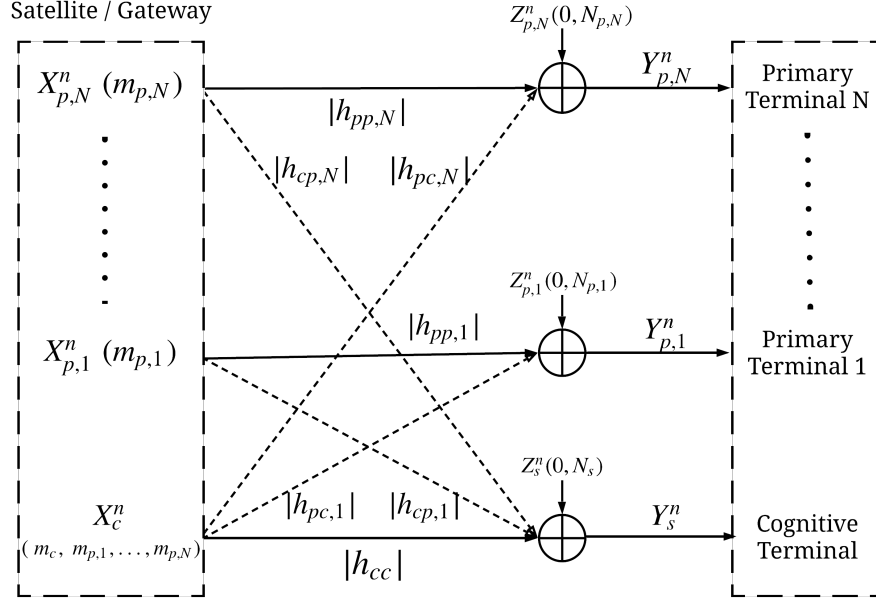


Figure 2-2: Overlay model.

The noise components $Z_{p,i}^n$ and Z_s^n are assumed independent and to follow the normal law $\mathcal{N}(0, N_{p,i})$ (resp. $\mathcal{N}(0, N_s)$). Moreover, the power constraints to be satisfied are $E[\|X_{p,i}^n\|^2] = P_{p,i}$ and $E[\|X_c^n\|^2] \leq P_c$, respectively. We also observe the interfering terms $I_{p,c,i}$ (from the cognitive transmitter to the i -th primary receiver) and I_{cp} (from all N primary transmitters to the cognitive receiver).

Finally, since each PU has the same transmission priority, we highlight that the interference among them could be solved by any precoding technique as proposed, for instance, in DVB-S2X standard [6]. Under this assumption, this thesis provides a design method to permit a secondary service transmission without affecting the PU transmission performance.

2.2.1 Overlay Model in Standard Form

Without loss of generality, given that the terms under the summation sign in Eq. (2.2) are statistically and mutually independent, we assume a model where the interfering term I_{cp} considers only a single Gaussian distributed PU signal (*i.e.* by application of central limit theorem [41]). In addition, in order to ease the analysis and notation, we normalize the terms of the channel output equations Eq. (2.1) and Eq. (2.2) by their

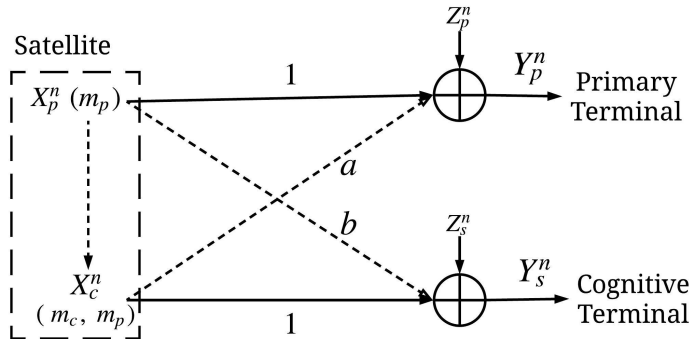


Figure 2-3: Overlay model in standard form.

corresponding direct paths ($|h_{pp}|$ and $|h_{cc}|$). In this sense, the Fig. 2-3 presents an equivalent model, which is described by the pair:

$$Y_p^n = X_p^n + \underbrace{aX_c^n}_{I_{pc}} + Z_p^n \quad (2.3)$$

$$Y_s^n = X_c^n + \underbrace{bX_p^n}_{I_{cp}} + Z_s^n, \quad (2.4)$$

where the normalized interfering path losses a and b are defined as:

$$a = \frac{|h_{pc}|}{|h_{cc}|} \quad b = \frac{|h_{cp}|}{|h_{pp}|} \quad (2.5)$$

We anticipate that this overlay cognitive radio channel model in its standard form, adapted from [23], is implemented to characterize our proposed contributions (especially in Chapter 3 and Chapter 4). In the investigated scenarios, we maintain the powers of PU and CU (respectively, P_p and P_c) fixed, since it could be seen reasonable in most practical applications, and vary the noise power at the CU receiver input Z_s^n . On the other hand, the PU link remains unchanged and operating as in CU absence (*i.e.* as in AWGN channel).

In addition, in some references (for instance, [23, 30]), both Gaussian noise components are assumed as unitary in the interference channel (*i.e.* $Z_{p,i}^n$ and Z_s^n are mapped to $\mathcal{N}(0, 1)$). In this sense, besides the previously considered direct paths normalization, the terms in Eq. (2.3) and Eq. (2.4) are also normalized by the $\sqrt{N_p}$ and $\sqrt{N_c}$ factors. It is worth noting that, for both equations, the second moment of the first term becomes the Signal-to-Noise Ratio (SNR), the second moment of the

middle term becomes the Interference-to-Noise Ratio (INR) and the second moment of the last term is the fixed unitary Gaussian noise, as presented in the following:

$$E[\|Y_p^n\|^2] = \text{SNR}_p + \text{INR}_p + 1 \quad (2.6)$$

$$E[\|Y_s^n\|^2] = \text{SNR}_c + \text{INR}_c + 1. \quad (2.7)$$

In our analysis, this last normalization is not adopted, since the power variation of the Gaussian noise Z_s^n is a key element to characterize the employed encoding technique (as it will be further discussed in the contributions presented in Chapter 3 and Chapter 4).

2.3 The Capacity of the Overlay Model

By considering the previously presented model, this section discusses the optimal encoding strategies for the CU encoder, aiming to mitigate the interference in both links. The referred development is highly inspired in the work presented by [23] and [24].

Let the channel inputs X_p and X_c be real values (\mathbb{R}), such that $\mathcal{X}_p \subset \mathbb{R}$ and $\mathcal{X}_c \subset \mathbb{R}$. In the same way, the channel output alphabets Y_p and Y_s are real values and, respectively, $\mathcal{Y}_p \subset \mathbb{R}$ and $\mathcal{Y}_s \subset \mathbb{R}$.

Primary User Encoding

For the primary receiver, given the practical condition that the PU infrastructure remains unchanged, the transmitted message m_p is decoded from the observation of Y_p^n , by using a *single-user decoder* $D_p^n : \mathcal{Y}_p^n \mapsto \{1, \dots, M_{p,i}\}$. Based on that, the rate R_p is achievable if there exists an encoding strategy $E_p^n : \{1, \dots, M_{p,i}\} \mapsto \mathcal{X}_p^n$ such that the probability of error vanishes as $n \rightarrow \infty$ *i.e.*:

$$P_{e,p} = \frac{1}{M_p} \sum_{k=1}^{M_p} P\left(D_p^n(Y_p^n) \neq k | m_p = k\right) \rightarrow 0, \quad (2.8)$$

under the assumption that m_p is uniformly distributed over $\{1, \dots, M_p\}$.

Cognitive User Encoding

In turn, according to the main overlay paradigm requirement, the cognitive encoder has noncausal knowledge about the primary encoder (codebook) and the message m_p . By expressing the set of all primary encoders as \mathcal{E}_p^n , the sequence of cognitive encoders E_c^n , under the constrained $E[\|X_c^n\|^2] \leq P_c$, is formed as:

$$E_c^n : \mathcal{E}_p^n \times \{1, \dots, M_p\} \times \{1, \dots, M_c\} \mapsto \mathcal{X}_c^n, \quad (2.9)$$

and the cognitive user decoder $D_c^n : \mathcal{Y}_s^n \mapsto \{1, \dots, M_c\}$, which estimates \hat{m}_c from the observation of Y_s^n , is implemented at the cognitive receiver. Thus, the rate R_c is achievable if there exists a sequence of encoders E_c^n such that the following constraints are satisfied:

1. The probability of error for the cognitive user, vanishes as $n \rightarrow \infty$, *i.e.*:

$$P_{e,c} = \frac{1}{e^{n(R_c+R_p)}} \sum_{j=1, k=1}^n P\left(D_c^n(Y_s^n) \neq j | m_p = k, m_c = j\right) \rightarrow 0. \quad (2.10)$$

2. The AWGN channel capacity is always attained by the primary user, *i.e.*:

$$R_p^* = \frac{1}{2} \ln \left(1 + \frac{P_p}{N_p} \right) = C_{AWGN}. \quad (2.11)$$

Encoding and Decoding Procedure

As the existence of a cognitive code that achieves the rate R_c was shown in the last discussion, the following encoding and decoding procedure presents the strategies to attain the AWGN capacity for the CU [23]:

1. Concerning the PU, generate X_p^n in respect to $m_p \in \{1, \dots, e^{nR_p}\}$ by identical and independent distributed (*i.i.d*) coordinates, drawn according the normal law $\mathcal{N}(0, P_p)$;
2. By the noncausal knowledge of the message m_p and the codebook E_p^n , the cognitive user performs the following strategies:

- (a) Superposition, where the CU shares a fraction $\alpha \in [0, 1]$ of its power to construct X_c^n and relay X_p^n (further details in the next Section 2.4);
 - (b) Dirty-Paper Coding (DPC) [25] to transmit the cognitive message m_c through the interference channel (further details in the next Section 2.5).
3. Decode the PU message by the *single-user* primary decoder D_p^n , as implemented in absence of CU transmission;
 4. Decode m_c by the DPC decoder (having knowledge of *binning strategy* imposed by E_c^n).

Thus, by using this procedure, the probability of error for estimating both m_p and m_c vanishes as $n \rightarrow \infty$. In this case, the CU reaches the AWGN capacity, *i.e.*:

$$R_c^* = \frac{1}{2} \ln \left(1 + \frac{(1 - \alpha)P_c}{N_s} \right) = C_{AWGN}. \quad (2.12)$$

Now that we have seen that the optimal CU encoding strategy implements (i) the superposition, to protect the PU link, and (ii) the DPC, to deal with the interference in the CU link, the next sections detail these techniques.

2.4 Superposition Strategy

The purpose of the superposition technique is to ensure that the Signal-to-Noise Ratio (SNR) at each PU receiver is not decreased in the presence of interference. To accomplish this goal, the CU shares part of its power to relay each PU and \hat{X}_c^n is a modified version of the CU message, as it is going to be detailed in the next Section 2.5. Based on that operation and considering the overlay model represented in Fig. 2-2, the CU transmitted signal X_c^n is given by:

$$X_c^n = \hat{X}_c^n + \sum_{i=1}^N \sqrt{\alpha_i \frac{P_c}{P_{p,i}}} X_{p,i}^n, \quad (2.13)$$

where $\alpha_i \in [0, 1]$ is the shared power fraction from P_c to relay each PU message.

By inspection of Eq. (2.13), we notice that the CU transmission (performed by \hat{X}_c^n) is feasible only if the condition $\sum_{i=1}^N \alpha_i < 1$ is satisfied. In this sense, note that the CU data rate R_c should be decreased when aggressive frequency reuse scenarios are considered. Under the assumption that all signals are statistically independent, the new power constraint $P_{\hat{X}_c}$ is defined as:

$$P_{\hat{X}_c} = E[\|\hat{X}_c^n\|^2] \leq (1 - \sum_{i=1}^N \alpha_i) P_c. \quad (2.14)$$

Based on these considerations, by replacing the superposition coded signal X_c (Eq. (2.13)) into the channel outputs given by Eq. (2.1) and Eq. (2.2), we obtain:

$$\begin{aligned} Y_{p,k}^n &= |h_{pp,k}| X_{p,k}^n + |h_{pc,k}| \overbrace{\left(\hat{X}_c^n + \sum_{i=1}^N \sqrt{\alpha_i \frac{P_c}{P_{p,i}}} X_{p,i}^n \right)}^{X_c^n} + Z_{p,k}^n \\ &= |h_{pp,k}| X_{p,k}^n + |h_{pc,k}| \sqrt{\alpha_k \frac{P_c}{P_{p,k}}} X_{p,k}^n + \dots \\ &\dots + \underbrace{|h_{pc,k}| \left(\hat{X}_c^n + \sum_{i=1, i \neq k}^{N-1} \sqrt{\alpha_i \frac{P_c}{P_{p,i}}} X_{p,i}^n \right)}_{I_{cp,k}} + Z_{p,k}^n \end{aligned} \quad (2.15)$$

$$Y_s^n = |h_{cc}| \hat{X}_c^n + \underbrace{\sum_{i=1}^N \left(|h_{cp,i}| + |h_{cc}| \sqrt{\alpha_i \frac{P_c}{P_{p,i}}} \right) X_{p,i}^n}_{S^n} + Z_s^n, \quad (2.16)$$

where S^n in Eq. (2.16) represents the total interference disturbing the cognitive link, which is composed by the PU users signals and the superposition terms.

Apart from that, regarding Eq. (2.15), the first term corresponds to the k -th PU transmission, the second term is the CU power fraction encoded by superposition to relay the PU, the third term represents the interference $I_{cp,k}$ that disturbs the k -th PU link and the last term is the additive Gaussian noise at the k -th PU receiver.

Thus, under the condition of statistical independence among the components in Eq. (2.15), the Signal-to-Interference-plus-Noise Ratio (SINR) at the k -th primary

receiver is given by:

$$\begin{aligned}
\text{SINR}_{p,k} &= \frac{E[\| (|h_{pp,k}| + |h_{pc,k}| \sqrt{\alpha_k \frac{P_c}{P_{p,k}}}) X_{p,k}^n \|^2]}{E[\| |h_{pc,k}| (\hat{X}_c^n + \sum_{i=1, i \neq k}^{N-1} \sqrt{\alpha_i \frac{P_c}{P_{p,i}}} X_{p,i}^n) \|^2] + E[\|Z_{p,k}^n\|^2]} \\
&= \frac{\left(|h_{pp,k}| \sqrt{P_{p,k}} + |h_{pc,k}| \sqrt{\alpha_k P_c} \right)^2}{\|h_{pc,k}\|^2 (1 - \alpha_k) P_c + N_{p,k}} \\
&= \frac{\|h_{pp,k}\|^2 P_{p,k}}{N_{p,k}}. \tag{2.17}
\end{aligned}$$

In this context, the superposition factor $\alpha_k \in [0, 1]$ that guarantees Eq. (2.17), for the interference condition ($|h_{pc,k}| > 0$), which is a generalized form of [23, Eq. 14], is given by:

$$\alpha_k = \left(\frac{|h_{pp,k}| \sqrt{P_{p,k}} \left(\sqrt{N_{p,k}^2 + \|h_{pc,k}\|^2 P_c (N_{p,k} + \|h_{pp,k}\|^2 P_{p,k})} - N_{p,k} \right)}{|h_{pc,k}| \sqrt{P_c} (N_{p,k} + \|h_{pp,k}\|^2 P_{p,k})} \right)^2. \tag{2.18}$$

Superposition for Overlay Model in Standard Form

In the same way, regarding the overlay model in its standard form, defined by the pair Eq. (2.3) and Eq. (2.4), the CU transmitted signal X_c^n is given by:

$$X_c^n = \hat{X}_c^n + \sqrt{\alpha \frac{P_c}{P_p}} X_p^n, \tag{2.19}$$

where $\alpha \in [0, 1]$ and the power constraint is $E[\|\hat{X}_c^n\|^2] \leq (1 - \alpha) P_c$.

Therefore, by considering the power sharing, the channel outputs taking the superposition account may be developed in a straightforward way:

$$Y_p^n = X_p^n + a \sqrt{\alpha \frac{P_c}{P_p}} X_p^n + a \hat{X}_c^n + Z_p^n \tag{2.20}$$

$$Y_s^n = \hat{X}_c^n + \underbrace{\left(b + \sqrt{\alpha \frac{P_c}{P_p}} \right) X_p^n}_{S^n} + Z_s^n, \tag{2.21}$$

where S^n represents the total interference disturbing the cognitive link.

By continuing the analysis, the SINR_p at input of the primary receiver is evaluated as:

$$\text{SINR}_p = \frac{E[\|(1 + a\sqrt{\alpha\frac{P_c}{P_p}})X_p^n\|^2]}{E[\|a\hat{X}_c^n\|^2] + E[\|Z_p^n\|^2]} = \frac{P_p}{N_p}, \quad (2.22)$$

and, under the condition of statistical independence among the components in Eq. (2.22), the superposition factor $\alpha \in [0, 1]$ that maximizes the PU SINR, for interference condition ($a > 0$), is defined by [23]¹:

$$\alpha = \left(\frac{\sqrt{P_p} \left(\sqrt{N_p^2 + a^2(N_p + P_p)P_c} - N_p \right)}{a\sqrt{P_c}(N_p + P_p)} \right)^2. \quad (2.23)$$

It is worth noting from Eq. (2.22) that, in accordance with the interference channel model, despite of the demodulator at the PU terminal receives the specified SINR, the received signal power is increased by the superposition component $(a\sqrt{\alpha^*\frac{P_c}{P_p}})X_p^n$. In this thesis, emphasizing the practical aspects, we assumed that the PU infrastructure is unchanged, including the implemented primary receiver.

The next section presents an overview about the DPC technique, which is implemented to mitigate the interference present on the CU link.

2.5 Dirty-Paper Coding

Once the superposition factors are computed and the CU partially shares its power to relay each PU signal, the next encoding step is to design \hat{X}_c^n efficiently, in order to minimize the PU interference. The optimal strategy uses the theoretical results presented by Costa [25]. On the assumption that the interference is noncausally known at the encoder, a transmitter-based interference presubtraction can be implemented, without any power increase, reaching the AWGN capacity. In this sense, according to the main concept of this technique, the CU adapts its waveform as a function of

¹Without loss of generality, we assume the noise power N_p at PU receiver as unitary in our analyses in Chapter 3 and Chapter 4.

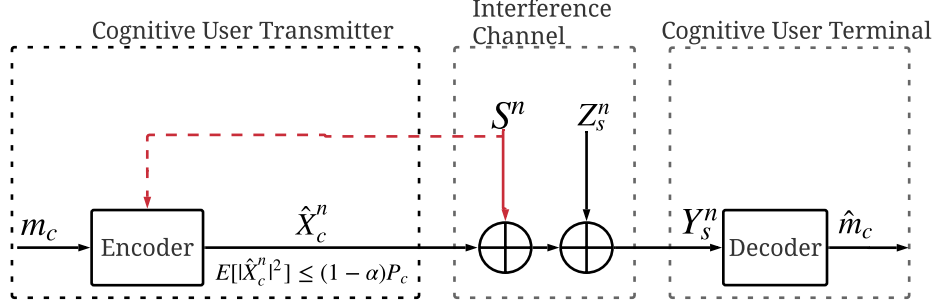


Figure 2-4: Gaussian channel with additive Gaussian state S available noncausally at the encoder.

the channel interference, instead of cancelling it.

Dirty-Paper Coding has several applications in modern communication scenarios, especially regarding broadcast transmission schemes, information hiding [42, 43, 44] and digital watermarking [45, 46, 47, 48]. In the next section we present the theoretical foundations of this technique, based on the original work of Costa [25].

2.5.1 DPC Theoretical Concepts

In the context of the CU link of the overlay cognitive radio model in its standard form (described in Section 2.2.1), consider the Gaussian channel with output $Y_s = \hat{X}_c + S + Z_s$ and input power constraint $E[\|\hat{X}_c^n\|^2] \leq P_{\hat{X}_c}$, as represented in Fig. 2-4. We assume the additive Gaussian state S as a sequence of independent identically distributed (i.i.d) random variables following the normal law $\mathcal{N}(0, P_S)$. In addition, S and the additive Gaussian noise Z_s , which is also distributed according to the normal law $\mathcal{N}(0, N_s)$, are independent. In our context, the state S represents the total interference disturbing the cognitive user channel, which is composed by the PU signal and the amount of CU power shared in the previously discussed superposition strategy. In order to maintain the same reference of the previous model discussion (see Section 2.2), we conserve the same notation in this section.

The encoder aims to send an index $m_c \in \{1, \dots, M_c\}$ towards the receiver in n -uses of the channel. We define that M_c represents the greatest integer in the alphabet set and $M_c \leq e^{nR_c}$, where R_c is the cognitive user rate. The State Information (SI) is available noncausally only at the encoder. Thus, based on m_c and on the knowledge of S , the encoder sends the codeword \hat{X}_c through the channel, which should satisfy the power constraint for $P_{\hat{X}_c}$.

On the other side, the decoder estimates \hat{m}_c based only in the observation of Y_s , without any prior information about the interference S . The error probability $P_{e,c}$ is characterized by:

$$P_{e,c} = \frac{1}{M_c} \sum_{k=1}^{M_c} P(\hat{m}_c \neq k | m_c = k), \quad (2.24)$$

under the assumption that m_c is uniformly distributed over $\{1, \dots, M_c\}$.

The problem of sending information through this channel was abstractly interpreted by Costa [25] such as that of writing a message in a sheet of paper covered with independent dirty spots. In this analogy, the dirty sheet of paper represents our respective channel. The writer (playing the role of the encoder) has a limited amount of ink (or power constraint) and knows the location and normally distributed intensity of the dirt spots over the sheet. On the other side, the reader (representing the decoder) is not able to distinguish between the ink marks, sent from the writer, and the dirt spots. Thus, by means of the "optimum writing strategy", the reader can recover the transmitted message, regardless of the dirt exposed in the paper.

We remind that, if the SI of S is not available at either the encoder and the decoder, the interference is interpreted as another Gaussian source added to the additive noise N_s . Thus, the capacity C is given by [39]:

$$C = \mathfrak{C} \left(\frac{P_{\hat{X}_c}}{P_S + N_s} \right), \quad (2.25)$$

where $\mathfrak{C}(x) = \frac{1}{2} \ln(1 + x)$, $x \geq 0$, is the Gaussian capacity function (in *nats per transmission*) considering the Gaussian channel with SNR x .

On the other hand, we notice that, if the interference S is known at the decoder it can be simply subtracted-off at the receiver, cancelling its effect. In this case, we reach the AWGN channel capacity, given by:

$$C_{SI-D} = \mathfrak{C} \left(\frac{P_{\hat{X}_c}}{N_s} \right). \quad (2.26)$$

Considering now our case, where the SI is available only at the encoder, a simple encoding strategy to transmit the message m_c over the channel of Fig. 2-4 would

be to use a fraction λ of the available power $P_{\hat{X}_c}$ to partially cancel the channel interference S . This transmission scheme is usually rubricated as Partial Interference Presubtraction (PIP) [25, 26, 29]. Thus, for a selected shared fraction $0 \leq \lambda \leq \min(1, P_S/P_{\hat{X}_c})$, the transmitted signal \hat{X}_c is given by:

$$\hat{X}_c = X_{cc} - \sqrt{\lambda \frac{P_{\hat{X}_c}}{P_S}} S, \quad (2.27)$$

where X_{cc} is the coded signal, under the power constraint $E[\|X_{cc}\|^2] \leq (1 - \lambda)P_{\hat{X}_c}$. We observe that the factor λ controls the fractioned interference to be presubtracted.

By considering that, the second moment of Y_s is evaluated as:

$$\begin{aligned} E[\|Y_s\|^2] &= E\left[\| \overbrace{X_{cc} - \sqrt{\lambda \frac{P_{\hat{X}_c}}{P_S}} S}^{\hat{X}_c} + S + Z_s \|^2\right] \\ &= (1 - \lambda)P_{\hat{X}_c} + (\sqrt{\lambda P_{\hat{X}_c}} - \sqrt{P_S})^2 + N_s, \end{aligned} \quad (2.28)$$

where the last step comes from the fact that X_{cc} and S are independent.

Thus, by considering Eq. (2.28), the achievable rate for a scheme where the SI is available only at the encoder, employing PIP and considering an arbitrary λ , is evaluated as [25]:

$$C_{SI-E, \text{ PIP}} = \mathsf{C}\left((1 - \lambda)\frac{P_{\hat{X}_c}}{N_s} + (\sqrt{\lambda P_{\hat{X}_c}} - \sqrt{P_S})^2\right). \quad (2.29)$$

By inspecting Eq. (2.29), we notice that the capacity of AWGN channel (see Eq. (2.26)) is not achieved. In addition, the achievable rate depends on the interference power P_S . To deal with this problem, the approach proposed by Costa seeks for codewords towards the vector S , instead of trying to cancel it. The encoder examines the space surrounding the vector S and chooses codewords that are in accordance with the power constraint $P_{\hat{X}_c}$ and distinguishable at the decoder from the observation of Y_s .

The next section presents Costa's proof, which shows that, by the correct choice of the auxiliary random variable X_{cc} as well as the proper scaling of λ , all rates

$R_c < \mathsf{C}\left(\frac{P_{\hat{X}_c}}{N_s}\right)$ are attainable (*i.e.* the capacity of an interference-free channel is achieved).

2.5.2 Analysis of the DPC Capacity

By considering the extension of *Gelfand-Pinsker* Theorem [49], the capacity of the Discrete Memoryless Channel (DMC), with random state (S) known only at the encoder and with the power constraint $P_{\hat{X}_c}$, is evaluated as²:

$$C_{SI-E} = \max_{p(x_{cc}|s), \hat{x}_c(x_{cc}, s): E[\|\hat{X}_c^n\|^2] \leq P_{\hat{X}_c}} (I(X_{cc}; Y_s) - I(X_{cc}; S)), \quad (2.30)$$

where X_{cc} is a auxiliary random variable of finite alphabet. The encoding and decoding procedures are performed as the following:

- Encoding Procedure:
 1. Generate $e^{n(I(X_{cc}; Y_s) - \epsilon)}$ identical and independent distributed (*i.i.d*) sequences X_{cc} ($\epsilon > 0$, arbitrarily small), uniformly distributed over the typical set X_{cc} ;
 2. Distribute these sequences uniformly over e^{nR_c} bins. These bins are ordered from $\{1, \dots, M_c\}$;
 3. Given the state vector S and the message m_c , look in the bin m_c for a sequence X_{cc} such that (X_{cc}, S) is jointly typical (see Ch. 7.6 of [50], for further clarification about *joint typicality* as well as the theorem proof);
 4. Select \hat{X}_c such that (\hat{X}_c, X_{cc}, S) is jointly typical and transmit it through the channel.
- Decoding Procedure:
 1. Look for the unique sequence X_{cc} such that $(X_{cc}; Y_s)$ is jointly typical;
 2. Declare an error in case of more than one or no sequence exists;

²The proof of the *Gelfand-Pinsker* Theorem can be found in ([39], Ch. 7.6) or in the original work [49]

3. Set the estimate \hat{m}_c equal to the index of the bin containing the obtained sequence X_{cc} ;
4. If $R_c < I(X_{cc}; Y_s) - I(X_{cc}; S) - \epsilon - \delta$ ($\epsilon > 0$ and $\delta > 0$, arbitrarily small), the probability of error averaged over all codes exponentially goes to zero as $n \rightarrow \infty$.

Thus, this procedure shows the existence of a code which achieves the rate R_c . Therefore, it is necessary to properly assign the auxiliary random variable X_{cc} .

As pointed out by [39], since the channel is additive (linear) and Gaussian, it is natural to expect that the optimal distribution of (X_{cc}, \hat{X}_c) given S be Gaussian to reach the AWGN capacity. By considering that, the solution proposed by Costa [25] assigns the auxiliary variable $X_{cc} = \hat{X}_c + \lambda S$, where \hat{X}_c and S are independent random variables and are assumed to follow the normal law $\mathcal{N}(0, P_{\hat{X}_c})$ and $\mathcal{N}(0, P_S)$, respectively. As a consequence, X_{cc} also follows the normal law $\mathcal{N}(0, P_{\hat{X}_c} + \lambda^2 P_S)$. It is worth noting that the adopted solution could be seen as a PIP scheme (see Eq. (2.27)), where the parameter λ should be optimized.

Thus, by evaluating the mutual information terms of Eq. (2.30), with $Y_s = \hat{X}_c + S + Z_s$ and the auxiliary variable $X_{cc} = \hat{X}_c + \lambda S$, we have:

$$\begin{aligned}
I(X_{cc}; Y_s) &= h(\hat{X}_c + S + Z_s) - h(\hat{X}_c + S + Z_s | \hat{X}_c + \lambda S) \\
&= h(\hat{X}_c + S + Z_s) + h(\hat{X}_c + \lambda S) - h(\hat{X}_c + S + Z_s, \hat{X}_c + \lambda S) \\
&= \frac{1}{2} \ln \left(\frac{(P_{\hat{X}_c} + P_S + N_s)(P_{\hat{X}_c} + \lambda^2 P_S)}{P_{\hat{X}_c} P_S (1 - \lambda)^2 + N_s (P_{\hat{X}_c} + \lambda^2 P_S)} \right), \tag{2.31}
\end{aligned}$$

and

$$\begin{aligned}
I(X_{cc}; S) &= h(X_{cc}) - h(X_{cc} | S) \\
&= h(\hat{X}_c + \lambda S) - h(\hat{X}_c + \lambda S | S) \\
&= h(\hat{X}_c + \lambda S) - h(\hat{X}_c | S) \\
&= h(\hat{X}_c + \lambda S) - h(\hat{X}_c) \\
&= \frac{1}{2} \ln \left(\frac{P_{\hat{X}_c} + \lambda^2 P_S}{P_{\hat{X}_c}} \right). \tag{2.32}
\end{aligned}$$

By substituting Eq. (2.31) and Eq. (2.32) in Eq. (2.30), the rate R_c as a function of λ is given by:

$$\begin{aligned} R_c(\lambda) &= I(X_{cc}; Y_s) - I(X_{cc}; S) \\ &= \frac{1}{2} \ln \left(\frac{P_{\hat{X}_c} (P_{\hat{X}_c} + P_S + N_s)}{P_{\hat{X}_c} P_S (1 - \lambda)^2 + N_s (P_{\hat{X}_c} + \lambda^2 P_S)} \right). \end{aligned} \quad (2.33)$$

The value of λ that maximizes Eq. (2.33) is given by:

$$\lambda^* = \frac{P_{\hat{X}_c}}{P_{\hat{X}_c} + N_s} = \frac{\text{SNR}}{\text{SNR} + 1}. \quad (2.34)$$

Then, by application of λ^* in Eq. 2.33, we find that the capacity of the DPC channel is equal to:

$$\max_{\lambda} R_c(\lambda) = R_c(\lambda^*) = \frac{1}{2} \ln \left(1 + \frac{P_{\hat{X}_c}}{N_s} \right) = C_{SI-D}. \quad (2.35)$$

We notice that the capacity of the AWGN channel (no interference), or equivalently, the capacity when the SI of S is available at the decoder, is reached. This development demonstrates the optimality of this scheme, independently of the interference power P_s [25], as expressed in Eq. (2.34) and Eq. (2.35). In addition, the mutual information is evaluated considering the optimum scaling factor λ^* :

$$I(X_{cc}^*; Y_s) = \frac{1}{2} \ln \left(1 + \frac{P_{\hat{X}_c} (P_{\hat{X}_c} + P_S + N_s)}{N_s (P_{\hat{X}_c} + N_s)} \right). \quad (2.36)$$

$$I(X_{cc}^*; S) = \frac{1}{2} \ln \left(1 + \frac{P_{\hat{X}_c} P_S}{(P_{\hat{X}_c} + N_s)^2} \right). \quad (2.37)$$

Fig. 2-5 presents $I(X_{cc}; Y_s)$, $I(X_{cc}; S)$ and R_c as a function of λ . In this case we fixed $P_{\hat{X}_c} = P_S = N_s = 1$. From a geometric point of view, we notice that the rate R_c is given by the difference between the mutual information functions and reaches the maximum according to Eq. (2.35). In addition, by inspecting the mutual information $I(X_{cc}; Y_s)$, we notice that this quantity increases with λ until the point $\lambda = 1$, then start decreasing. The maximum value is actually achieved when the exact amount of

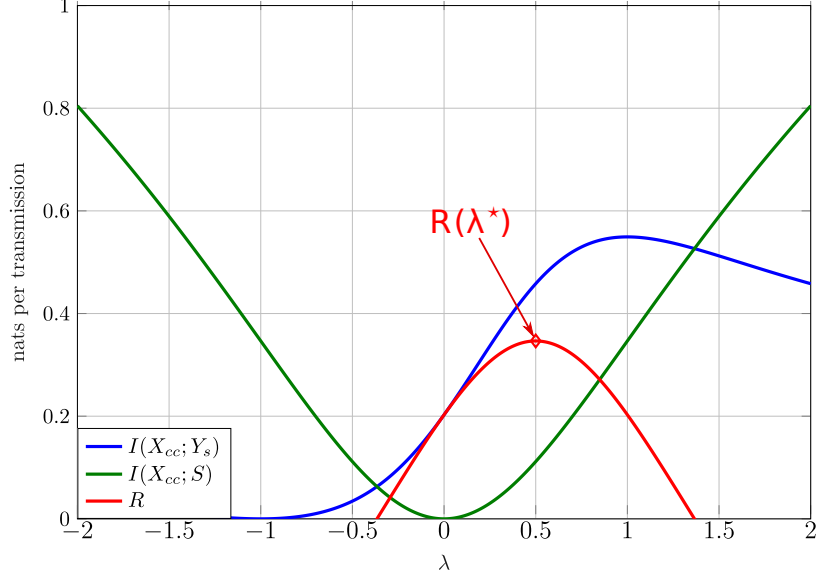


Figure 2-5: $I(X_{cc}; Y_s)$, $I(X_{cc}; S)$ and $R = R_c$, as a function of λ , considering $P_{\hat{X}_c} = P_S = N_s = 1$.

interference (*i.e.* $\lambda = 1$) is presubtracted at the transmitter (see Eq. (2.27)).

Summary of DPC Strategy

Following, we re-examine the encoding and decoding procedure in order to summarize the discussed concepts.

- Encoding Procedure:

1. Generate $e^{n(I(X_{cc}; Y_s) - \epsilon)}$ identical and independent distributed (*i.i.d.*) sequences X_{cc} ($\epsilon > 0$, arbitrarily small), drawn according the normal law $\mathcal{N}(0, P_{\hat{X}_c} + \lambda^2 P_S)$;
2. Allocate these sequences uniformly over $e^{nR} = e^{nC_{DPC} - 2\epsilon}$ bins. Each bin contains the same number of sequences;
3. Given the state vector $S = S_0$ and the message m_c , look in bin m_c for a sequence X_{cc} such that (X_{cc}, S_0) is jointly typical among the X_{cc} in bin m_c . The encoder, equivalently, look for a sequence X_{cc} such that:

$$|(X_{cc}^n - \lambda^* S_0)' S_0| \leq \delta. \quad (2.38)$$

4. Encoder calculates $\hat{X}_{c,0} = X_{cc,0} - \lambda^* S_0$ and transmits it through the channel.
- Decoding Procedure:
 1. Look for the unique sequence X_{cc} such that $(X_{cc}; Y_{s,0})$ is jointly typical;
 2. Declare an error in case of more than one or no sequence exist;
 3. Set the estimate \hat{m}_c equal to the index of the bin containing the obtained sequence $X_{cc,0}$;

2.6 Practical DPC Implementation

Concerning the historical perspective for practical DPC implementations, the use of Tomlinson-Harashima Precoding (THP) [51, 52] for Inter-Symbol Interference (ISI) cancelling was firstly introduced by Erez et al. in [26]. Subsequently, Eyuboglu and Forney [27, 53] developed the Trellis Precoding (TP) technique, also partially recovering the so-called shaping loss by the Trellis Shaping (TS) technique [28]. Finally, the TP technique for Multi-User Interference (MUI), presented in [29] and further developed in [30], formed the basis of the DPC encoder implemented in this thesis.

The Fig. 2-6 presents the diagram of a DPC encoder implemented by the THP scheme [51, 52]. In this configuration, assuming low and intermediate SNR regime, the Partial Interference Presubtraction (PIP) is performed. In this way, the signal \hat{X}_c^n is designed as:

$$\hat{X}_c^n = \left[X_{cc}^n - \lambda S^n \right] \text{MOD}_{\Delta}, \quad (2.39)$$

where X_{cc}^n is the coded signal and the factor λ , as discussed in the Section 2.5.2, regulates the amount of interference to be presubtracted (recall, by inspection of Eq. (2.34), that the factor λ tends to unitary in high SNR regimes). To complete the transmitter chain, the MOD_{Δ} is the complex-valued modulo operation. The modulo amplitude is defined by $\Delta = \sqrt{M}d_{min}$, where M is the number of points of the square Quadrature Amplitude Modulation (QAM) constellation and d_{min} the minimum intersymbol distance.

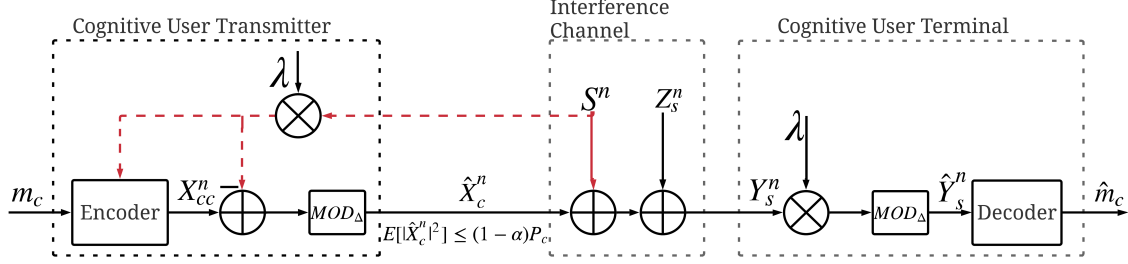


Figure 2-6: DPC encoder with Partial Interference Presubtraction (PIP) in Tomlinson-Harashima Precoding (THP).

It is worth noting the connection between the practical implemented THP scheme and the Costa DPC proof, previously discussed in Section 2.5.2. In fact, we have seen that the PIP is also employed in the choice of the auxiliary random variable X_{cc}^n . Besides, the modulo operation at the transmitter, part of the THP scheme, is implemented in order to guarantee the required power limitation of \hat{X}_c^n (i.e. $E[\|\hat{X}_c^n\|^2] \leq (1 - \alpha)P_c$). However, in order to achieve the DPC capacity Eq. (2.35), we may infer that two main points should be satisfied:

1. The modulo operation should not introduce degradation in the system performance;
2. The coded signal X_{cc}^n should be Gaussian distributed, according to the encoding procedure described in Section 2.5.2.

At the receiver, as also depicted in the Fig. 2-6, the reverse chain is implemented: firstly, Y_s^n is multiplied by the factor λ and, before entering the DPC decoder, the signal is modulo operated again, as the following:

$$\begin{aligned} \hat{Y}_s^n &= \left[(Y_s^n)\lambda \right] \text{MOD}_\Delta \\ &= \left[\lambda\hat{X}_c^n + (\hat{X}_c^n - X_c^n) + \lambda S^n + \lambda Z_s^n \right] \text{MOD}_\Delta \\ &= \left[\lambda\hat{X}_c^n + [X_{cc}^n - \lambda S^n] \text{MOD}_\Delta - \hat{X}_c^n + \lambda S^n + \lambda Z_s^n \right] \text{MOD}_\Delta \quad (2.40) \end{aligned}$$

$$= \left[X_{cc}^n - (1 - \lambda)\hat{X}_c^n + \lambda Z_s^n \right] \text{MOD}_\Delta, \quad (2.41)$$

where in Eq. (2.40), the following property was utilized $[(a)\text{MOD}_\Delta + b]\text{MOD}_\Delta = (a + b)\text{MOD}_\Delta$.

In the light of the lattice theory presented in the Modulo-Lattice Additive Noise (MLAN) channel (see [54], section III for further details and theorem proof), the effective noise N' is defined as:

$$N' = (1 - \lambda)\hat{X}_c^n + \lambda Z_s^n. \quad (2.42)$$

Thus, by considering the Costa's choice[25] for λ in Eq. (2.34), which minimizes the effective noise N' , we obtain:

$$P_{N'} = E \left[\|N'\|^2 \right] = (1 - \lambda)^2 P_{\hat{X}_c} + \lambda^2 N_s = \frac{P_{\hat{X}_c} N_s}{P_{\hat{X}_c} + N_s} = \lambda N_s, \quad (2.43)$$

where we observe that $P_{N'}$ is similar to the second moment of the linear Minimum Mean-Square Error (MMSE) estimation error \mathbf{E} (as pointed out in Eq. (A.2) of the development presented in Appendix A).

In the sequence, Fig. 2-7 presents the transmission of a 16-QAM symbol X_{cc} ($M = 16$ and $d_{min} = 1$) by using THP scheme. The additive Gaussian noise is not considered (which means that λ is unitary) and the channel interference S is known only at the transmitter. The following steps describes the scheme operation:

- ① Consider in this example, at the instant n , the uncoded 16-QAM signal $X_{cc}(n)$ and the channel interference $S(n)$, given by:

$$X_{cc}(n) = 1.5 + j1.5;$$

$$S(n) = 4.25 + j5.25.$$
- ② By the knowledge of the channel interference $S(n)$, the transmitter performs the presubtraction:

$$\hat{X}_c(n) = -2.75 - j3.75.$$
- ③ By performing the modulo operation ($\Delta = 4$), we obtain;

$$\hat{X}_{c,\Delta}(n) = 1.25 + j0.25.$$
- ④ At the cognitive receiver, the received signal $Y_s(n)$ is given by:

$$Y_s(n) = 5.5 + j5.5.$$
- ⑤ Finally, by applying the modulo operation over the signal $Y_s(n)$, we obtain the signal $\hat{Y}_s(n)$ at the decoder input:

$$\hat{Y}_s(n) = 1.5 + j1.5 = X_{cc}(n).$$

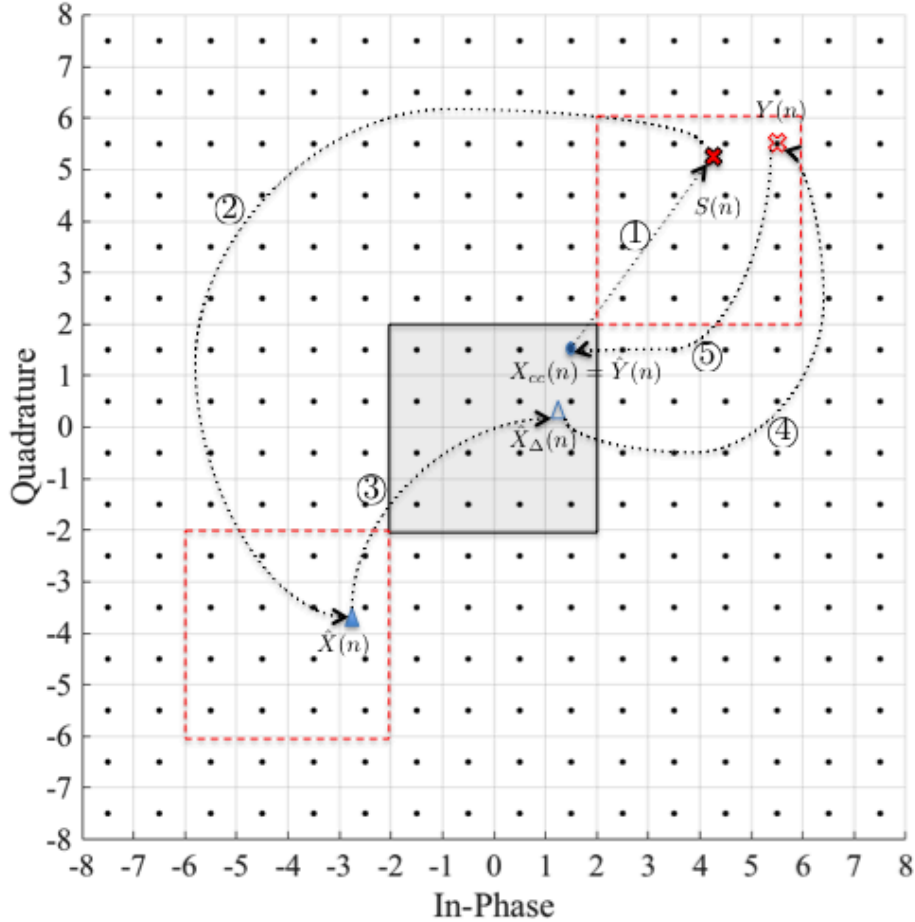


Figure 2-7: Representation of THP transmission and reception without noise.

Thus, without additive noise, we conclude that the transmitted signal X_{cc} can be reconstructed at the decoder, regardless the amount of interference power.

2.6.1 THP Losses Description

When compared with AWGN channel, the performance of THP scheme in the dirty-paper channel is degraded by three separated sources of losses: power loss, modulo loss and shaping loss [29, 26]. In this sense, the goal is to design the coded signal X_{cc}^n in order to mitigate these sources of losses (which is the main subject of the next thesis chapters). The next section presents a brief description about these losses, which serves as a starting point to the further discussion present through this thesis manuscript.

Power Loss

Due to the presubtraction and modulo operation performed at the transmitter (see Eq. (2.39)), when S is large, the signal \hat{X}_c^n is uniformly spread over the modulo region bounded by Δ . As a consequence, the average power of the continuous transmitted signal \hat{X}_c^n in THP scheme is evaluated as [29]:

$$P_{\hat{X}_{c,\text{THP}}} = E \left[\|\hat{X}_c^n\|^2 \right] = \frac{\Delta^2}{6} = \frac{M}{6} d_{min}^2, \quad (2.44)$$

where, as previously defined, $\Delta = \sqrt{M}d_{min}$, such that M is the number of points of the square QAM constellation and d_{min} is the minimum intersymbol distance.

On the other hand, the average power of the discrete squared M-QAM constellation, such that the symbols are uniformly distributed, is computed as [55, 56]:

$$P_{X_{cc,\text{THP}}} = E \left[\|X_{cc}^n\|^2 \right] = \frac{(M-1)}{6} d_{min}^2. \quad (2.45)$$

Thus, the resulting power loss γ_p caused by THP schemes in comparison with the equivalent reference in AWGN channel, is evaluated by:

$$\gamma_p = \frac{P_{\hat{X}_{c,\text{THP}}}}{P_{X_{cc,\text{THP}}}} = \frac{M}{(M-1)} \quad (2.46)$$

We can infer that this loss is always present in the THP scheme, since the transmitted signal \hat{X}_c^n is continuous and has more power than the equivalent discrete version X_{cc}^n . In addition, by inspecting Eq. (2.46), it is noticed that γ_p is significant in low order modulations (*i.e.* low M). The following Table 2.1 summarizes the degradation for square M-QAM constellations:

Shaping Loss

In the previous discussion concerning the DPC theoretical concepts, we have highlighted that, in order to reach the AWGN capacity, the coded signal X_{cc}^n and, consequently, \hat{X}_c^n should be constructed with Gaussian distribution (see Section 2.5.2).

Table 2.1: Power loss in respect with the square QAM constellation size.

QAM (M)	γ_p (dB)
4	1.25
16	0.28
64	0.06
256	0.02
1024	0.00

However, we have also seen that, in THP schemes, the transmitted \hat{X}_c^n is uniformly distributed in the region bounded by Δ . Hence, signaling with uniform distribution (usually rubricated as *n-cube* distribution [57, 58]) causes the so-called shaping loss, which is ultimately evaluated as 1.53 dB (the *n-sphere* distribution, see [58, 28] for further details).

For an arbitrary constellation or shaping scheme the baseline average power (*i.e.* *n-cube* distribution power) is defined as [28]:

$$P_{\oplus} = \frac{2^{R_c}}{6} d_{min}^2, \quad (2.47)$$

where, by conserving our notation, R_c is the data rate and d_{min} is the minimum distance among constellation symbols.

Thus, the shaping gain γ_s is the ratio of the baseline power in Eq. (2.47) to the average power of the transmitted *shaped* signal $P_{\hat{X}_c}$, *i.e.*:

$$\gamma_s = \frac{P_{\oplus}}{P_{\hat{X}_c}}. \quad (2.48)$$

The Trellis Shaping, introduced by Forney (see [28] for further details), is a method of selecting a minimum-weight sequence from an equivalence class of possible transmitted sequences. The selection is performed by a *Viterbi* decoder for a shaping code C_s , placed at the transmitter. In this way, it is possible to minimize the average energy of the transmitted signal.

As an example of the application of this technique, Fig. 2-8 depicts the shaped 256-QAM signal by employing two different shaping codes C_s . Fig. 2-8a implements a 4-state code, rate 1/2, specified by generators $g_{s,1}(D) = 7$ and $g_{s,2}(D) = 5$, which

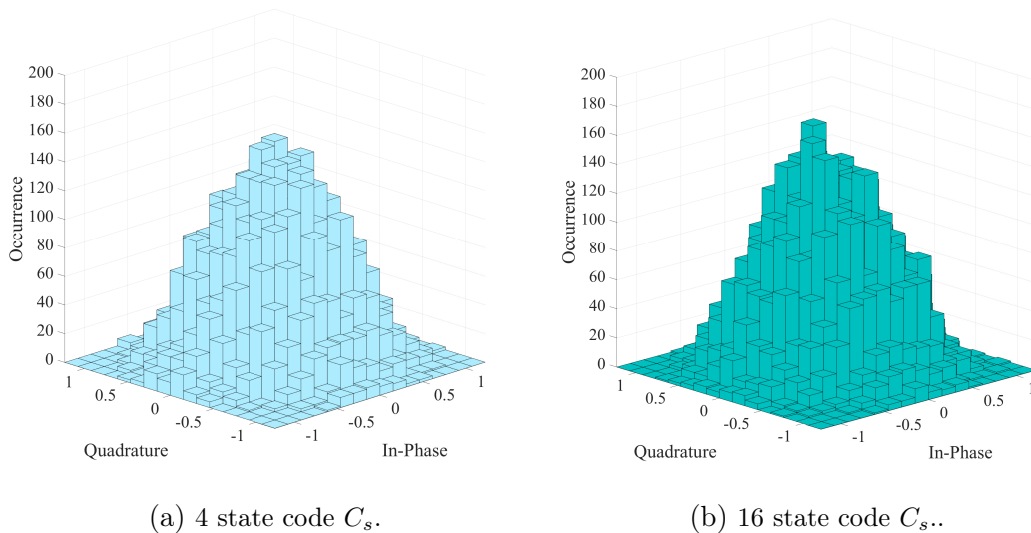


Figure 2-8: Shaped 256-QAM constellation.

provides a shaping gain of $\gamma_s = 0.97$ dB. In turn, by increasing the complexity, in Fig. 2-8b a 16-state, rate $1/2$, shaping code C_s , specified in octal notation by generators $g_1(D) = 31$ and $g_2(D) = 33$, is implemented. In this case, the $\gamma_s = 1.11$ dB is obtained.

As we observed, shaping gains of the order of 1 dB might be obtained with a simple 4-state shaping code. In this thesis, we discuss the TP technique, based on the work presented in [29], which, besides performs the interference presubtraction, also partially recovers the shaping loss. Further discussion, analysis and improvements are presented in the following Chapters.

Modulo Loss

The so-called *modulo loss* is caused by the modulo operation placed at the receiver side (see Fig. 2-6). We have seen, by the previous representation of THP operation steps (Fig. 2-7), that the modulo function collapses all points different of Δ to the same value, so they can be seen as multiple representations of the same point [29].

However, when the symbols are transmitted in the boundary of constellation (corner or edges points) the additive Gaussian noise might causes a mistake by decoding symbols at the opposite side. Fig. 2-9 represents this effect. Notice that, given the transmitted corner symbol $X_{cc}(n)$, the additive channel noise drives the received sym-

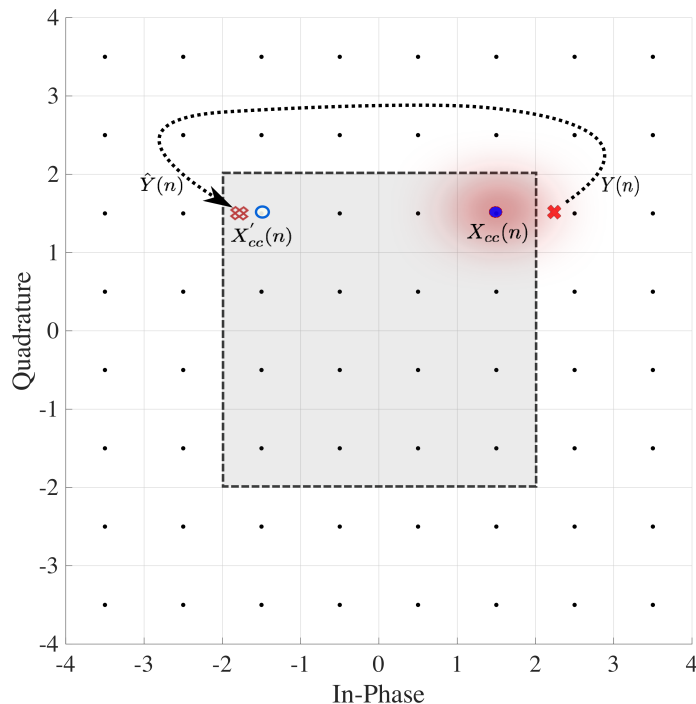


Figure 2-9: Representation of Modulo Loss.

bol $Y_s(n)$ out of shaded area, bounded by Δ . In this sense, due to the receiver modulo operation, the equivalent point $\hat{Y}_s(n)$ is moved to the opposite side. Thus, by considering a minimum distance decoder, the estimated symbol would be $X'_{cc}(n)$, causing a decoding error.

In addition, regarding the uncoded QAM schemes, it is noticed that all constellation points have the same *Voronoi* region \mathcal{V}_{QAM} :

$$\mathcal{V}_{QAM} = |\text{Re}(Z)| \text{ and } |\text{Im}(Z)| < \frac{d_{min}}{2}. \quad (2.49)$$

Thus, we might infer that performance degradation caused by the modulo loss depends on:

- the modulation order M , since in higher order constellations the corners and edges points are proportionally reduced in comparison to the total constellation points;
- the SNR, since that as this quantity increases, the system becomes less suscep-

tible to this loss due to the \mathcal{V}_{QAM} ;

This specific loss is also further stressed in the next chapter. Besides, some countermeasures are proposed to overcome this effect.

2.6.2 THP Performance

To outline this Section 2.6, Fig. 2-10 presents the Symbol Error Rate (SER) of the THP in comparison with the equivalent M-QAM in AWGN channel schemes. The shaping is not considered, which means that a uniform signaling is assigned for both transmission. However, power and modulo losses are present in the THP, causing a performance gap with respect to the reference AWGN scheme.

Before a proper analysis and in order to set out a comparison among the reference, corresponding to the M-QAM schemes in AWGN channel, and the THP curves, we define the SNR_{eff} in terms of:

$$\text{SNR}_{eff} = \frac{E_S}{P_{N'}}, \quad (2.50)$$

where the effective noise N' Eq. (2.42) is considered.

In the 4-QAM scheme (transmitting 2 bits per symbol) we notice a degradation, around 1.8 dB observed at a BER of 10^{-3} and about 1.25 dB at 10^{-6} , when the THP (dashed blue curve) is compared with the reference 4-QAM in AWGN channel. This different gap can be explained by the presence of the modulo loss, which affects the system performance in low and intermediate SNR and is less susceptible in high SNR, where the degradation only corresponds to power loss (see Table 2.1).

In addition, the effect of the modulo loss is represented by the dot-dashed red line. In this plot, we compute the uniform SER of M inner points, by considering the different M-QAM schemes. Hence, as previously highlighted, we notice that this degradation decreases as the SNR increases.

Regarding the 16-QAM, we notice that the degradation is further reduced in comparison with 4-QAM. This is explained due to: (i) the high SNR regime, which highly reduces the modulo loss effect, and (ii) the low power loss, computed as 0.28 dB

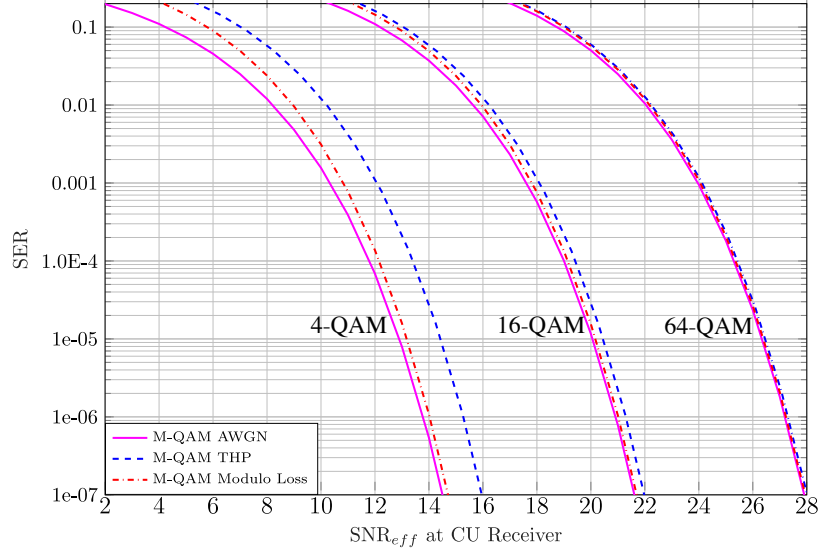


Figure 2-10: SER of THP schemes.

(see Table 2.1). It is worth noting that, considering a BER of 10^{-6} , the degradation is only limited by the power loss.

Finally, for 64-QAM, we notice that the degradation of the THP scheme may be neglected. Since the SNR is high, which is less susceptible to modulo loss, and the power loss is computed as 0.06 dB, the same performance of AWGN channel is achieved.

By considering the above, we conclude that the THP technique is effective in high SNR operation (or, equivalently, in high order modulation) achieving the same performance as AWGN channel, but has a significant performance degradation in low and intermediate SNR. As the context of this thesis considers intermediate SNR (for instance SNR < 14 dB, as usually adopted in satellite communications[6]), some alternatives of DPC encoding are discussed, with the objective to design X_{cc}^n with a good channel code and shaping gain.

The following chapters present the trellis shaping DPC encoder (based on the work [29]) and proposes some improvements in order to deal these losses.

2.7 Summary

This Chapter presented the theoretical background concerning the overlay cognitive radio channel model, suitable for the satellite scenario investigated in this thesis. After the channel description, the achieved capacity of both primary and cognitive users were evaluated, pointing out the optimal encoding strategies of the cognitive user.

In addition, supported by the main references concerning the topic, the superposition and DPC techniques were theoretically discussed, emphasizing the main concepts in order to support the following thesis discussions.

Finally, the well known Tomlinson-Harashima Precoding (THP) for Multi-User Interference (MUI) was briefly introduced, highlighting the sources of losses which degrades the performance when compared to the AWGN channel.

The following chapters further discuss these losses and proposes some encoding design improvements in order to reach the equivalent AWGN performance.

Chapter 3

Cognitive Radio Overlay Paradigm Towards Satellite Communications

Contents

3.1	Introduction	44
3.2	Trellis Shaped Based DPC Encoder	46
3.3	Simulation Approach	49
3.4	Results and Analysis	53
3.4.1	Discussion about the Reference Scheme	53
3.4.2	Qualitative Analysis for Interfering Scenarios	57
3.4.3	Quantitative Analysis for Interfering Scenarios	63
3.4.4	Main Conclusions	65
3.5	Summary	66

The previous chapters have discussed, in some details, the concepts of the Cognitive Radio (CR) overlay paradigm as well as the foundations of its related techniques. Some practical aspects were pointed out, especially regarding to the Tomlinson-Harashima Precoding (THP) system losses in a multiuser interference regime. In the wake of these concepts, this Chapter presents the first contribution of this thesis.

A low complexity scheme is proposed and compared with the classical precoding for multiuser interference presubtraction, introduced in [29] and further explored con-

sidering the overlay context in [30]. The system performance is evaluated in different interfering scenarios, resulting in no degradation for Primary User (PU) and some recovery of the THP losses for the Cognitive User (CU). Beyond the quantitative results, usually measured in terms of the Bit Error Rate (BER), a qualitative analysis is carried out, by inspecting the scatter plot and the histogram of the different components that form the transmitted signal. In this sense, we intend to address separately each precoding loss, evaluating its criticality and providing valuable insights to key parameters.

This chapter can be seen as a point of departure in the sequel of the thesis contributions. By considering the points investigated here, novel solutions are proposed for the cognitive communication system, both in the transmitter and receiver sides (developed in the Chapter 4). A large part of the discussions presented here was published in [32].

3.1 Introduction

The specific focus of this Chapter lies into the exploration of the overlay scheme for satellite communication where both PU and CU transmit concurrently towards two (or even more) different terminals, at the same frequency, time and polarization, without a power constrained threshold. This section presents a short recall of the previous chapters.

In the light of the satellite context exposed in the Chapter 1, the motivation of this work can be seen as achieving the coexistence of a low data rate secondary service with an existing primary user service. To the best of the authors' knowledge, no previous works explored the overlay paradigm in the context of satellite communications.

As previously stated in the same Chapter 1, the CU encoding strategies are implemented based on the assumption that the full and noncausal knowledge of PU signal are available. Both are transmitted from the satellite or, equivalently, from the same satellite gateway. Moreover, we also identified some stringent satellite constraints, especially the trade-off regarding the "design tripod" formed by complexity, power efficiency and bandwidth efficiency.

In the Chapter 2, we discussed the formalized model, which is well suited for our context. In particular, in this Chapter we investigate the same procedure and considerations previously assumed. As a consequence, in order to avoid eventual redundancy or conflict of information (and notation), we leave out here the exposition of the system model, referring to the specific points whenever required.

More specifically, the same adaptation of the overlay cognitive radio model in its standard form is implemented (we recommend the reader to revisit Section 2.2.1 along with its development). In this sense, without loss of generality, we assume that the total interference disturbing the CU link has Gaussian distribution, which satisfies the statistical properties required by the superposition technique (according to Eq. (2.22)) and also makes the analysis valid in a broader sense (as will be further discussed in Section 5.2.2).

Once the channel model is established, Chapter 2 also introduces the DPC theoretical concepts (see Section 2.5) as well as the practical DPC encoder.

Furthermore, in the spirit of the previous discussion concerning the THP losses (see Section 2.6.1), it might be possible to clarify the obtained results allowing a better qualitative interpretation. In this way, we provide a general view of each source of degradation of THP, which is useful for the development of mitigation solutions. We highlight that, unlike the references about the topic (for instance [30, 59]), the approach here studies practical scenarios and intends to explore the relation between different interference power levels and the system performance degradation.

We propose, in this Chapter, a scheme based on the Trellis Shaped DPC encoder with slight constellation expansion combined with THP. Unlike the previous works published in [29, 30], the modulo operation is always part of our transmission system, assuring the required power limitation for the transmitter, given any interference scenario. The system performance degradation caused by this modulo operation is studied and we clearly experience the trade-off between power efficiency and low complexity solutions.

Additionally, we also point out some differences of our scheme with respect to the work carried out by Diaz et al. in [31, 59], which investigates the THP precoding for satellite applications:

- in this thesis, a priority among signals is considered, which implies the use of the superposition technique. In turn, Diaz et al [59] consider a broadcast scenario, where the same power is allocated for all users;
- our implemented encoder is based on [29], which provides three separated gains - coding, shaping and prediction gains - necessary to maintain the received SNR at the satellite terminal into the typical standardized range [6], independently of the interference power level. Conversely, the solution adopted in [59] implements the THP along with Shaping without Scrambling technique, as introduced by Fischer in [57];
- the nonlinear distortion is not considered in this work. Diaz et al., in [31], investigated and compensated the degradation caused by the THP signal incurred in a nonlinear channel, typical in satellite application.

The rest of the Chapter is organized as follows. The Section 3.2 presents the Trellis Shaped Based DPC Encoder, exposing the main operation concepts. The system parameters and details about the implementations are shown in Section 3.3. Simulation results and analysis are presented and discussed in Section 3.4 and the conclusions are exposed in Section 3.5.

3.2 Trellis Shaped Based DPC Encoder

By considering the same adaptation of the overlay cognitive radio model in its standard form, previously discussed in the Section 2.2.1, we have evaluated that the optimum CU encoding strategy is composed by the following techniques: (i) superposition, to protect the PU user link, and (ii) DPC, to mitigate the disturbing interference into the CU link. Moreover, by the described procedure, once the superposition is implemented, the goal is then to design X_{cc}^n (or equivalently \hat{X}_c^n) in such way to presubtract S^n and respect the power constraint $E[|\hat{X}_c^n|^2] \leq (1 - \alpha)P_c$.

This Section presents the foundations of the Trellis Shaped Based DPC Encoder [29], which is implemented in this thesis. The coded signal X_{cc}^n is designed to have a good channel coding gain and near Gaussian distribution to recover the shaping loss. This is reached by combining trellis shaping and THP.

The TS technique was introduced by Forney in [28] and could be seen as a method for sequence optimization to achieve any desired signal property. In our case, the objective is to design X_{cc}^n to be as close as possible to the scaled interference λS^n , without sacrificing the shaping gain as it is the case for THP [29]. The optimal shaping gain is known to be 1.53 dB (see the [28, 53] for further details).

In addition to this preliminaries, as further discussed in the DPC proof, previously presented in the Section 2.5, the main concept to bear in mind is that: the DPC encoder should not intend to cancel but, on the opposite, to adapt itself, by transmitting the best sequence belonged to its subcodebook, with respect to the non-causal observed interference S^n .

In this perspective, both the Trellis Precoding (TP), proposed in [27], and its extension for Multi-User Interference (MUI) [29] could be conceptually seen as a DPC encoder. The sequence of shaping regions plays the role of a subcodeword assigned to the index provided by the trellis coded sequence, which is responsible by the coding gain (robustness against additive Gaussian noise). Following this short remark, we present the encoder description.

The Fig. 3-1 presents the implemented encoder for the cognitive user. Three gains can be achieved by this system: (i) coding gain, represented by the upper part of the diagram; (ii) shaping gain, achieved by the trellis shaping code in the lower part, and (iii) prediction gain (term rubricated by references considering Inter-Symbol Interference (ISI) channels, for instance [57]), achieved by the modulo operation jointly with shaping code.

The two codes work independently. The input bit sequence is split in three parts. The upper part is formed by the coset select code C_c . This later is described by the generator matrix G_c , which encodes the k_c message bits x_c into a n_c coded bits y_c . Additionally, the n_u uncoded bits sequence u selects the constellation points within each coset defined by C_c ¹. In the lower part, the r_s -bits syndrome sequence s passes through an inverse syndrome former H_s^{-T} for the shaping code C_s . This initial sequence t jointly with the channel coded sequence y_c , the uncoded sequence u , and the interference λS^n are fed into the *Viterbi* decoder. This later selects, according to a

¹We anticipate that, in this thesis, as it will be further discussed, the uncoded bits sequence u (represented by the black dashed line) is not implemented. However, the general block diagram is exposed based on [29]

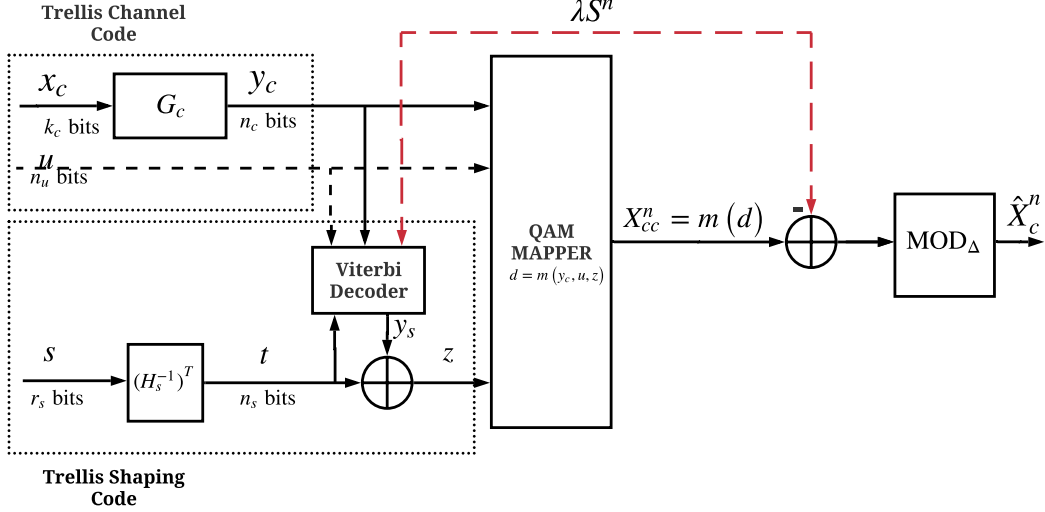


Figure 3-1: Proposed DPC encoder.

well chosen branch metric, the shaping codeword y_s . After that, the shaped sequence z is obtained by the XOR operation between t and y_s . Note that z_s and t are within the same coset, according to the trellis shaping on regions strategy, detailed in [28]. Finally, the output shaped sequence X_{cc}^n is obtained by mapping the d symbols as a function of y_c , u , and the sign mapped bits z .

Similarly to the THP operation (see Eq. (2.39) of the Chapter 2), the coded symbol sequence X_{cc}^n is presubtracted by the scaled interference sequence λS^n and modulo operated in order to limit its power. At the end, the transmitted sequence \hat{X}_c^n is obtained and sent through the interference channel.

The following branch metric Eq. (3.1) is implemented, where the precoder selects the proper region sequence with minimum average power to steer the scaled interference sequence λS^n :

$$\| [X_{cc}^n - \lambda S^n] \text{MOD}_{\Delta} \|^2. \quad (3.1)$$

At the receiver, as depicted in the Fig. 3-2, the reverse chain is implemented: firstly, Y_s^n is multiplied by the factor λ . Before entering the DPC decoder, the signal is modulo operated again. At the decoder, the strategy is the same as implemented for the usual Trellis Coded Modulation (TCM) decoder: the symbols are decoded using the expanded constellation mapping with a *Viterbi* algorithm for C_c . The shaping symbols represent the parallel branches between consecutive state transitions running

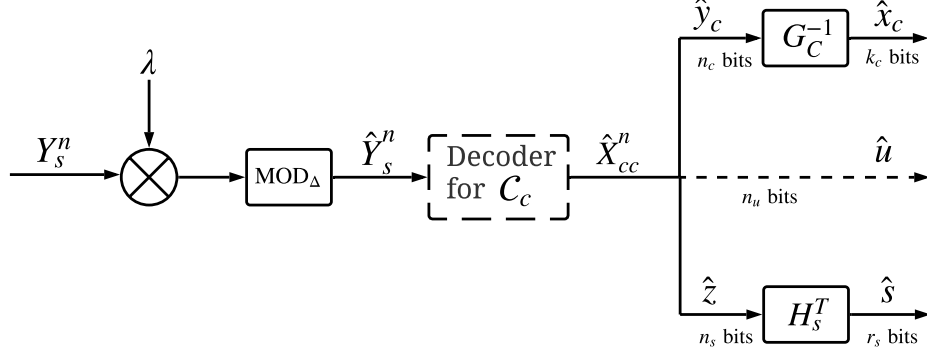


Figure 3-2: Proposed DPC receiver.

into this trellis (the next Section provides an example). At the end of the decoding, the estimated shaping bits \hat{s} are obtained by $\hat{s} = \hat{z}H_s^T$.

Conversely to the contributions presented in [29] and [30], this work proposes the combination of a slight expanded constellation with the THP as DPC encoder. Despite the fact that only part of the losses is recovered, our practice reduces the complexity by having less parallel branches in the shaping *Viterbi* decoder. In addition, the use of the modulo, which guarantees that the transmitted power is limited even in high interference scenarios, is considered in all analysed cases.

The next Section presents the channel parameters as well as the details about the implementation of both user's encoder and decoder. The investigations are performed by considering typical scenarios for satellite communications.

3.3 Simulation Approach

A framework is implemented considering the overlay cognitive radio channel model in its standard form, adapted from [23] (for detailed discussion, see Section 2.2.1). In few words, the channel gains are normalized by their corresponding direct paths, which defines the channel parameters a and b . As a consequence, the powers becomes specified at the receiver input. In our case, without loss of generality, we assume that the parameters a and b are real values and equal to 0.2 (i.e. 4% of the transmitted power disturbs the other link)². We might justify this assigned value from the premise that the receiver station is not properly designed for the other interference

²for instance, at the primary receiver, the incoming interfering signal is given by $I_{pc} = aX_c^n$, whose power is evaluated as $E[|aX_c^n|^2] = a^2P_c$.

service (pointing loss, antenna patterns, geographic localization etc.). In addition, it is noticed that this approach considers two transmission antennas and two different receiver stations, located in different sites and affected by independent noise components.

Regarding the PU transmission, a 4-QAM transmitted signal encoded by a 16-state, rate 1/2, convolutional code C_c , specified in octal notation by generators $g_1(D) = 31$ and $g_2(D) = 33$, is implemented. The transmitted power values P_p of 3, 7 and 15 dB are considered, in accordance with the typical range of received SNRs in satellite communications, for instance, in DVB-S2X standard [6]³.

For the CU, the available remaining received power (after the superposition) is assumed as 10 W. It is worth noting that, on the opposite of a common design approach, where the total available transmitter power is specified and shared in the superposition procedure, in this case, we are interested in observing the behaviour of the coded scheme in different interference regimes. For this reason, we adopted the same received power for CU in our analysis, which maintains the same reference.

In order also to comply to the defined SNR range for satellite communication, it is proposed a typical transmission rate of $R_c = 2$ bits/symbol. The Trellis Shaped based DPC encoder is implemented, with a slight expanded constellation of $n_s = 2$, and modulo operation in its output, previously discussed in Section 3.2 (see Fig. 3-1 for further clarification).

For the coding gain, a systematic 64-state, rate 1/2, convolutional code C_c specified in octal notation by the feedforward polynomial $h_1(D) = 54$ and the feedback polynomial $h_0(D) = 161$ is assumed. Along with this, for the shaping code C_s , the 4-state code, rate 1/2, specified by generators $g_{s,1}(D) = 7$ and $g_{s,2}(D) = 5$ is implemented. In other words, at the DPC transmitter, the 4-QAM coded constellation is replicated four times by the shaping operation (since $n_s = 2$), resulting in an expanded 16-QAM constellation for X_{cc}^n .

In addition, considering the shaping operation, the proposed mapping for X_{cc}^n is based on the sign bit shaping strategy described by Forney in [28]. Following the same notation as in Fig. 3-1, consider now the 16-QAM constellation X_{cc}^n represented

³Without loss of generality, we assume the noise power N_s , at the input of PU receiver, as unitary in our analysis [23].

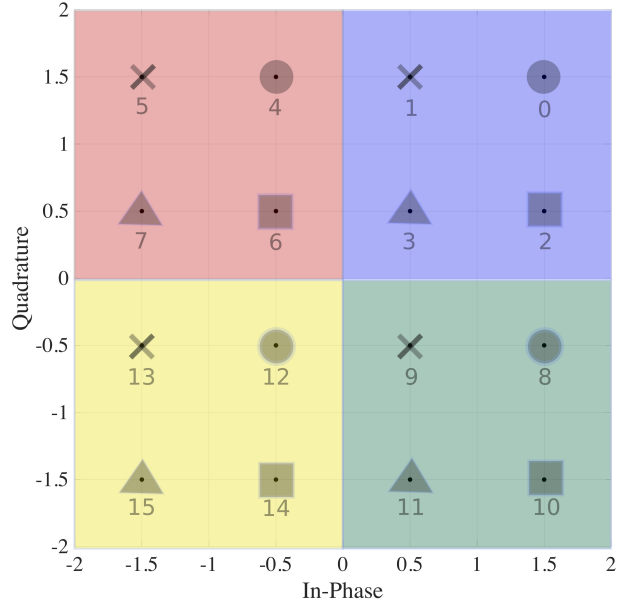


Figure 3-3: Proposed CU mapping.

by the Fig. 3-3. Each symbol is defined by the tuple $(z_1 z_2 y_{c_1} y_{c_2})$, where z_1 and z_2 are the sign bits while y_{c_1} and y_{c_2} are the coset bits. It should also be noted that, to keep the specified rate, which maintains the SNR range, the uncoded bits are not implemented in this scheme (represented by the black dashed line in Fig. 3-1).

Thus, in view of this adopted shaping strategy, the shaping regions are represented by the four different colors that delimit the constellation regions, while the four different markers (\circ , \times , \square or \triangle) represent the convolutional code cosets. The analogy with the *Gelfand - Pinsker* multicoding scheme [49], which is a key concept utilised in the DPC theoretical proof [25] (discussed in Section 2.5.2), is intuitive. Basically, we assign the transmitted "sequence of colors" as the subcodebook, determined by the shaping code C_s , which is indexed by the chosen codeword generated by the convolutional code C_c . In this sense, the described encoder can be conceptually considered as a practical implementation of the DPC encoder.

At the receiver, the decoder employs the same strategy for usual TCM schemes. Fig. 3-4 illustrates an example of trellis for the channel code C_c with the parallel transitions. Since each branch of the trellis corresponds to a signal subset (in this case defined by y_c and labeled by the markers \circ , \times , \square or \triangle), the first step in decoding is to determine the best signal point within each subset (equivalently to determine the

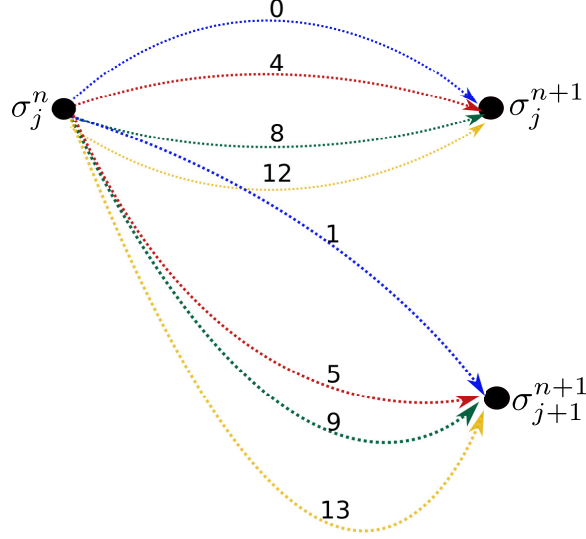


Figure 3-4: Representation of a trellis decoding for a generic C_c considering the parallel transition defined by the mapping of Fig. 3-3.

best shaping region, represented by different colors). This is performed by selecting the point that is closest in Euclidean distance to the received point \hat{Y}_s . After that, the selected signal point and its squared distance metric are applied in the usual *Viterbi* decoder for C_c in order to selected the most likely coded sequence \hat{y}_c [41].

By observing this simple example, the trellis transition from the state σ_j^n to the state σ_j^{n+1} provides $(y_{c_1}y_{c_2})$ mapped to $(0,0)$, which is represented by the marker "○" according with the assigned mapping. Thus, the decoder will perform a hard decision among the four constellation symbols $(0, 4, 8, 12)$, representing the shaping regions, defined by the pair of bits (z_1z_2) . In the same way, the transition from the state σ_j^n to σ_{j+1}^{n+1} provides $(y_{c_1}y_{c_2})$ mapped to $(0,1)$, represented by the marker "X", which decides among the parallel transitions $(1, 5, 9, 13)$.

It is worth noting that an error in the first step of the decoding procedure (*i.e.* error in the parallel transition decision) results in a wrong decoding of the shaping region. This fact significantly increases the degradation caused by the modulo loss in DPC schemes, as will be further discussed in the next Section. We remark that, in order to reduces the system complexity, the state expansion in the *Viterbi* decoder at the receiver [60, 61, 62], which could be an effective strategy for eliminate the parallel transition effect, is not considered in this implementation.

3.4 Results and Analysis

Once the channel parameters are defined and both primary and cognitive communications systems are implemented, the results and analysis are presented here.

Firstly, we provide some details about the reference scheme for CU. In this way, the effects caused by the THP losses are discussed without the channel interference. Continuing the analysis, the interfering scenarios are investigated in both qualitative, by inspection of histograms and scatter plot of the signal constellations involved at encoder processing, and quantitative ways, by evaluation of the BER performance for the PU and CU. At the end of the section, the main conclusions about the interference mitigation techniques for both links, by superposition concerning the PU and by DPC for CU, are presented.

3.4.1 Discussion about the Reference Scheme

Before considering the proposed interfering scenarios (previously assigned in the Section 3.3), it is necessary to define a reference scheme as well as to discuss the effects related to the THP losses without considering the interference disturbance. By this analysis it is possible to discriminate each loss and, consequently, to propose countermeasures for further design improvements (to be presented in the next Chapter 4).

In this thesis, we assumed as a reference the Trellis Shaping scheme in a AWGN channel, with a fixed transmission rate at 2 bits per symbol. In other words, it follows the same scheme depicted in the Fig. 3-1 without the interference presubtraction (i.e. according with our notation, $\hat{X}_c = X_{cc}$). Additionally, regarding the practical aspects, the transmitted signal (16-QAM modulation) is in line with the satellite standards [6].

Shaping Loss

Regarding the THP losses, we begin our analysis by the shaping loss. Supported by the investigation presented in [57, Section 4.4.3], we highlight that the TS technique is not effective for low orders of uncoded QAM constellations. In fact, the power

reduction, specified by the shaping code C_s , is obtained at the transmitter output, but, nevertheless, this gain can not be observed in the BER performance. This could be inferred due to the points that are located close to the axis which, in determined error condition, would lead to wrong shaping region estimation. As observed by Fischer [57], this situation causes the propagation of errors inherent to the syndrome decoder strategy implemented for shaping bits recovering, especially in low SNR regimes. By this reason, the shaping errors should be avoided since that it could cause excessive bit errors even when a single symbol error is occurred at the decoding process. When higher orders constellations are considered, the probability of transmission of these specific constellation points is further decreased, reducing this degradation.

Conversely, by inspection of Fig. 3-3, it is observed that the TS construction increases the minimum Euclidean distance among uncoded bits (i.e. points within each signal subset) due to the inherent TCM implementation. We observe that the *Voronoi*⁴ region of this scheme \mathcal{V}_{TCM} is increased. As a consequence, the error probability related to the wrong shaping region estimation is significantly reduced, even taken into account, as implemented in our system, the hard decision decoding for the parallel transition (as represented in Fig. 3-4).

By considering the shaping code C_s previously assumed in our scheme, the Fig. 3-5 presents the histogram of the transmitted signal X_{cc} (or equivalently \hat{X}_c) for the TS AWGN scheme, with minimum symbol distance $d_{min} = 1$. We can notice that the occurrence is highly concentrated in the four inner points and, on the other hand, the four corners points are practically avoided. However, we still have the transmission of edges constellation points, which implies in degradation when the modulo is applied (as shall discuss below). Quantitatively, according to the previous theory presented in [28], by evaluating Eq. (2.47) and Eq. (2.48) we obtain $\gamma_s = 1.02$ dB⁵.

Modulo Loss

We study now the impact of the modulo loss for the TS AWGN scheme. To introduce this analysis, we revisit the discussions presented in the Fig. 2-10 of the Chapter 2.

⁴We consider *Voronoi* region \mathcal{V} as the decision region around a specific constellation point.

⁵In fact, we attribute $\gamma_s = 0.97$ dB for this shaping code C_s , considering the continuous region delimited by Δ . This small difference of approximately 0.05 dB is related from the imprecision between the continuous approximation and the 16-QAM constellation. When 256-QAM is employed, we obtain $\gamma_s = 0.97$ dB, as presented in the Fig. 2-8a and by Forney in [28].

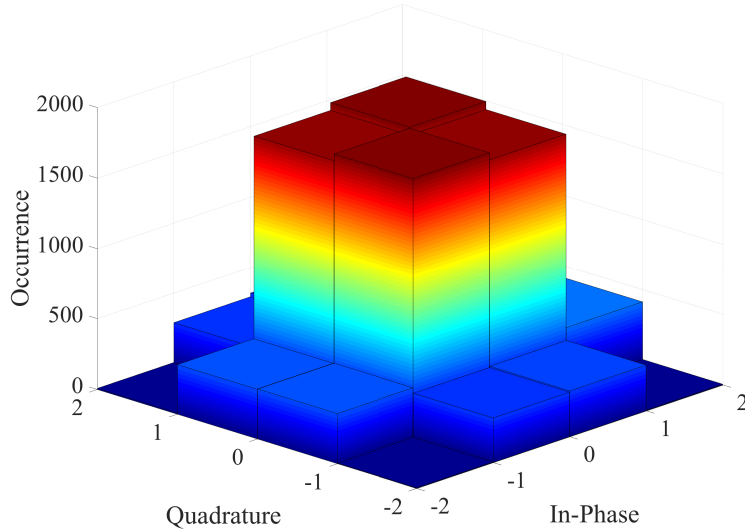


Figure 3-5: Histogram of the transmitted signal X_{cc}^{\wedge} for the reference TS AWGN scheme, considering the assumed shaping code C_s and the the mapping defined by Fig. 3-3.

By recalling the discussions in Section 2.6.1, considering uncoded QAM schemes in AWGN channel bounded by the modulo, an analytical SER approximation was evaluated. In that analysis, we observed that all constellation points have the same *Voronoi* region \mathcal{V}_{QAM} , resulting in a square delimited by $d_{min}/2$. Thus, we can conclude that the modulo loss degradation depends on: (i) the modulation order, since in higher orders constellations the corners and edges points are proportionally reduced in comparison to the total constellation points, and (ii) the SNR level, due to \mathcal{V}_{QAM} .

In order to analyse the modulo loss in the TS AWGN scheme, Fig. 3-6 provides an example which compares the system without modulo (TCM scheme with TS) and with modulo (denominated here as DPC). In this representation, the symbol "0" (corner point) was transmitted and, at the receiver, the signal is corrupted by the additive Gaussian noise, represented by the red dots. As we can observe, firstly for TCM scheme, the received signal should be within the *Voronoi* region \mathcal{V}_{TCM} , in order to avoid a wrong shaping decoding. This region is delimited by the constellation point distance d_{min} in two directions and unlimited in the other two directions.

In turn, when the modulo is applied into the DPC scheme, since this transmitted symbol is located at the constellation corner, the *Voronoi* region \mathcal{V}_{DPC} is highly decreased, which is delimited by the distance $d_{min}/2$ in two directions and d_{min} in the other two directions. It is clear, as illustrated in this case, that the transmission

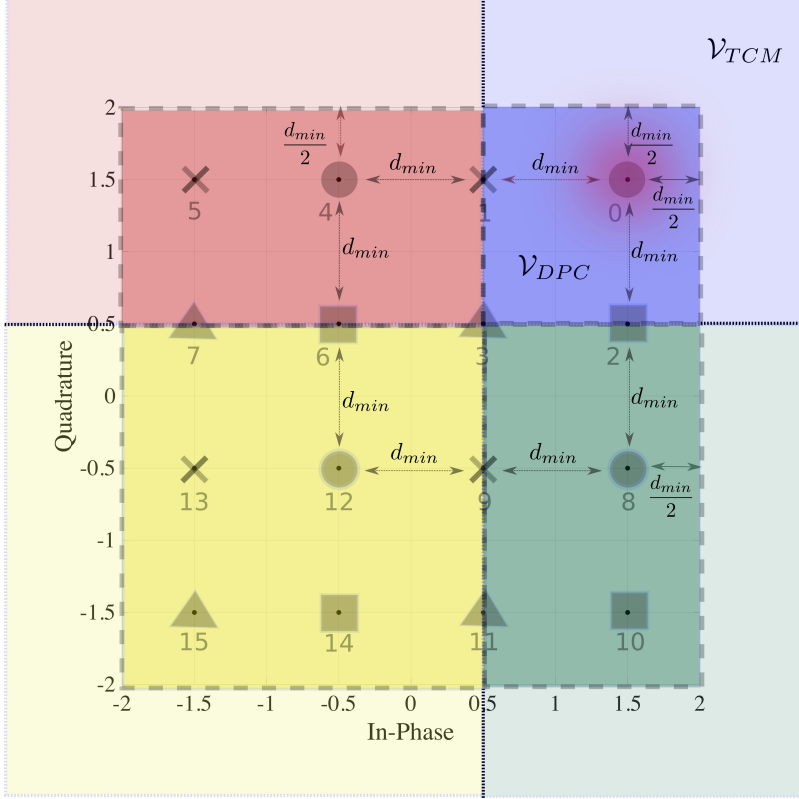


Figure 3-6: Representation of a received symbol from AWGN channel considering the proposed CU mapping impacted by modulo loss.

of the corner constellation points suffers a significant degradation when compared to the reference TCM.

In the same way, by considering the edges points "4" an "8", we also notice the reduction of the *Voronoi* region \mathcal{V}_{DPC} in respect to the reference \mathcal{V}_{TCM} . For this reason, it is also expected a degradation when comparing these schemes, especially in the typical intermediate SNR range assigned in our scenarios.

For the remaining inner point "12", we can infer that the performance is equivalent to the TCM, since the *Voronoi* region \mathcal{V}_{DPC} is delimited by the constellation point distance d_{min} in two directions and $3d_{min}/2$ in the other two directions.

It is worth noting that, due to the adopted mapping strategy, the same analysis is also valid to the others cosets. Roughly, also by inspection of the Fig. 3-6, we can observe that 25 % of the 16-QAM constellation points are located at the constellation corners, which have the smallest *Voronoi* region, 50 % in the edges, which also have reduced region, and just 25 % are inner points, which has no degradation in comparison with TCM. Based on this assumptions, even considering a scenario with no

interference disturbance, we can underline the impact of the boundaries points in the coded signal X_{cc} on the performance degradation (i.e. BER measurement). Thus, we highlight the importance to avoid the transmission of boundary constellation points.

Power Loss

Last but not least, we remark that the transmitted signal is a discrete constellation, since $\hat{X}_c = X_{cc}$. By this reason, in this scheme without interference presubtraction, the power loss is not present (as further explained in Section 2.6.1).

3.4.2 Qualitative Analysis for Interfering Scenarios

By following the same discussion and regarding the investigated scenarios, Fig. 3-7 presents the signals constellations involved by the described processing depicted in Fig. 3-1. The expanded constellation signal X_{cc}^n , from original 4-QAM to shaped 16-QAM, is shown in green marker X. The Gaussian distributed version of the scaled interference λS^n is superposed in red points and the transmitted signal \hat{X}_c^n , after presubtraction and modulo operation, is shown in blue dots.

In reference to the theory presented in [29], some important concepts may be extracted from this representation. We notice that in Fig. 3-7a, low interference power, almost all interference is confined within the expanded constellation. In this case, as it will be detailed in the following paragraphs, a significant part of the losses may be recovered. In the Fig. 3-7b, we notice that, even at medium interference, a considerable part remains inside the expanded constellation set, which lead us to expect that some loss could be recovered by the system. Finally, in Fig. 5c, we observe that the expansion is not sufficient for this strong amplitude of interference and a near-uniform distribution is expected for X_{cc}^n , i.e. little or almost none of the losses may be recovered.

Furthermore, as our previous definition and in contrast to [29] and [30], we are using the modulo operation at the transmitter output and the shaping metric is implemented taking that into account (see Eq. (3.1)). These design assumptions assure that the transmitted signal \hat{X}_c^n will be confined within the expanded constellation, independently of the channel interference, guaranteeing the condition $E[|\hat{X}_c^n|^2] \leq (1 - \alpha)P_c$,

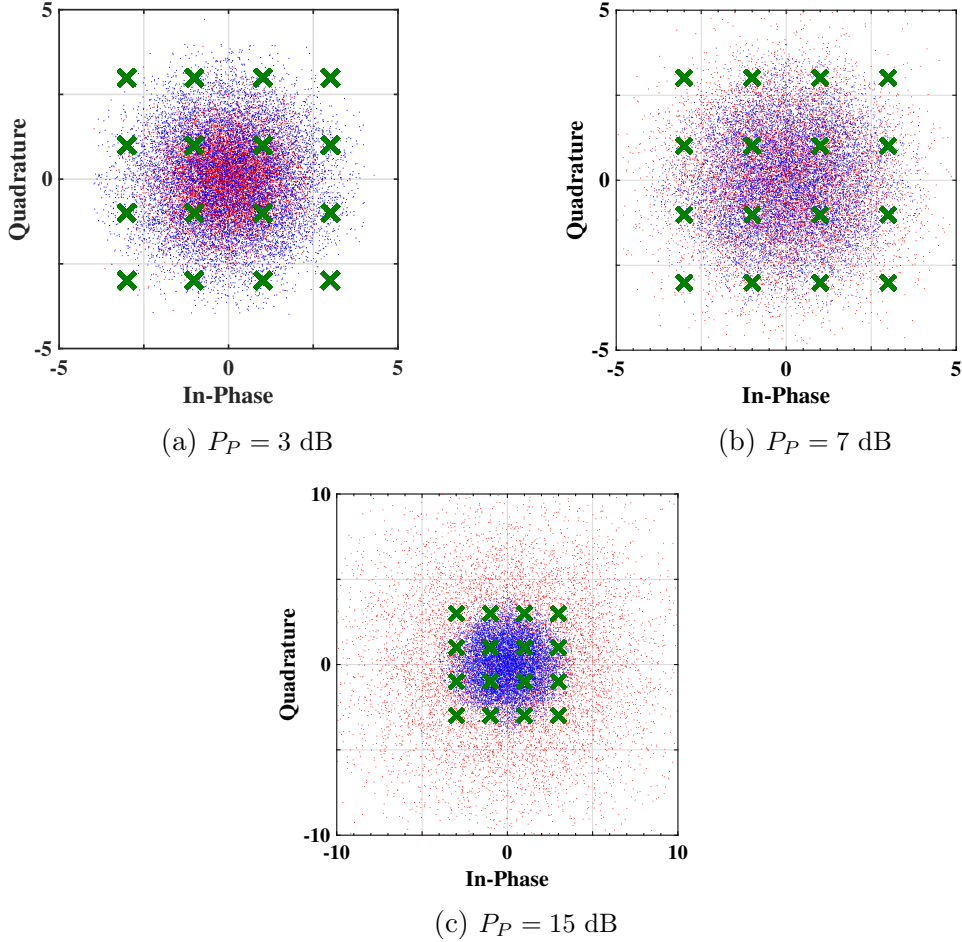


Figure 3-7: Scatter plots of signals constellations at different PU interfering powers.

which is a DPC requirement. By this design, in a clearly reference to the THP scheme, three important consequences are highlighted concerning its discriminated losses:

1. **Shaping loss:** according to the Trellis Shaping theory [28], we can realize that, by applying the modulo after the presubtracted signal without considering this operation in the *Viterbi* metric, the output signal is uniformly distributed inside the region delimited by the modulo boundaries Δ . However, when the shaping metric takes into account the modulo operation (see Eq. (3.1)), the shaping gain corresponding to C_s is also reached within the continuous region delimited by Δ , as the discrete TCM scheme (previously discussed in the Section 3.4.1). It is worth noting that the same shaping gain is achieved, independently of the channel interference power. This can be demonstrated by the following property:

$$[X_{cc}^n - \lambda S^n]_{\text{MOD}\Delta} = [X_{cc}^n - (\lambda S^n)_{\text{MOD}\Delta}]_{\text{MOD}\Delta}, \quad (3.2)$$

where we can conclude that the shaping minimization will be the same whether or not λS^n is confined within the modulo region.

This could be observed by the blue dots illustrated in the scatter plot, which provides the shaping gain equals to 0.97 dB for all scenarios, according to the implemented shaping code C_s (further details about the shaping evaluation is presented in [28]).

Another remarkable point concerning the shaping operation refers that, when the transmitted signal \hat{X}_c^n is Gaussian distributed, by means of the shaping operation, the usual decoding method by minimum Euclidean distance is optimum [29]. It could be realized directly by the overall distribution of the effective noise N' for DPC, given by Eq. (2.42) of the Chapter 2.

2. **Modulo loss:** based on the previous observation that the boundaries points should be avoided. This assumption has an ordinary impact in 16-QAM constellation since that, even in very low interfering regime, not all shaping selected points are chosen in the four central constellation points. The difference from the DPC analysis for the reference TS scheme is that: as the interference increases, the distribution of X_{cc}^n becomes closer to uniform. As a consequence, the assignments of boundary constellation points are increased and the modulo loss significantly degrades the performance.
3. **Power loss:** in the same way to the uniform case, the power loss is observed for the Gaussian distributed transmitted signal be \hat{X}_c^n . This is related to the power difference between the discrete and continuous transmission. As a consequence, the same degradation value evaluated for 16-QAM (in this case, equals to 0.28 dB), according to the presented result of Table 2.1 in Chapter 2, should be expected.

Complementary with the scatter plot, it is important take a deep look also into the distribution of these constellation points. The histogram of X_{cc}^n and \hat{X}_c^n signals are depicted in Fig. 3-8 and Fig. 3-9, respectively.

By inspecting the Fig. 3-8a and Fig. 3-8b, we have a new picture of the effect discussed in the previous Item 2 of the Section 3.4.2. In low interference condition, $P_p = 3$ dB, the constellation points are located with high probability within the 4 central points and with less probability at the boundary points. However, as the system experiences some transmissions at the boundaries, the modulo loss may be present. The possible solution for this case, since the interference is very low, would be to transmit without the output modulo. However, in this case, the control of the transmitted power would be lost. It is worth noting that, although small, the amount of interference increases the boundary transmission in comparison with the reference scheme (see Fig. 3-5).

On the other hand, when the interference increases $P_p = 7$ dB, we note that the points on the constellation boundaries are more selected than in the previous case. It relates to the interference presubtraction, according to the discussion concerning the Fig. 3-7b. In this case, due to the distribution of X_{cc}^n in Fig. 3-8c and Fig. 3-8d, the system performance is more degraded due to the modulo loss. We also noticed through simulations that, confirming the insight provided by the scatter plot, the transmitted power is increased for a system without output modulo at the transmitter, which do not satisfy the main DPC condition.

Finally, in the high interference regime, $P_p = 15$ dB, we observe that a nearly uniform distribution for X_{cc}^n is presented at Fig. 3-8e and Fig. 3-8f, the so-called *n-cube* distribution. We can infer that, considering the Gaussian distributed interference, this is the case that causes the worst degradation through the modulo operation (modulo loss).

In turn, regarding the transmitted signal \hat{X}_c^n , the distributions for all scenarios are depicted in the Fig. 3-9. It is worth noting, considering all points discussed, mainly corroborating with the Item 1 of the Section 3.4.2, that the signal is near-Gaussian distributed independently of the interference scenario. This is an important characteristics for system design, and it will be further developed in the next Chapter 4.

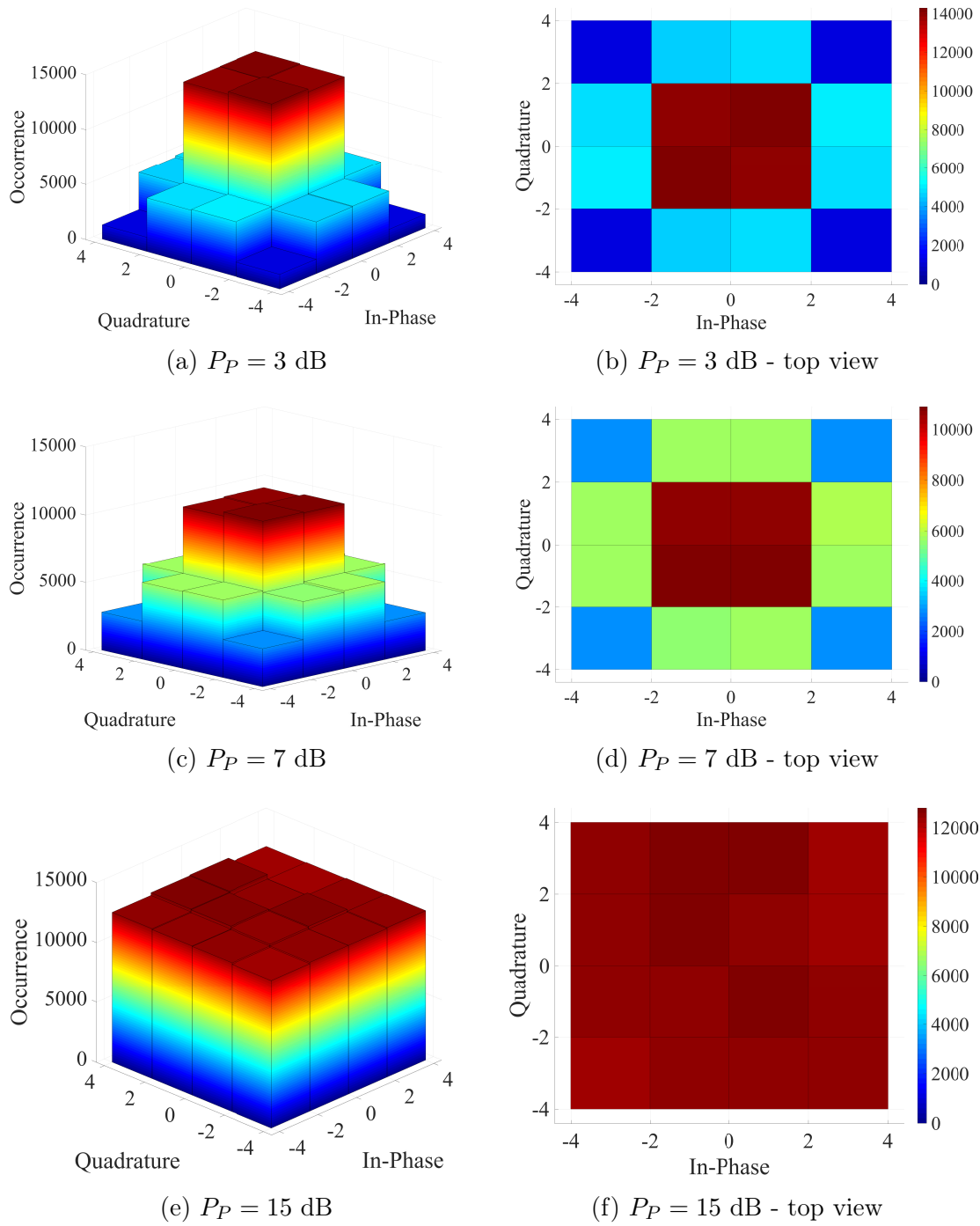
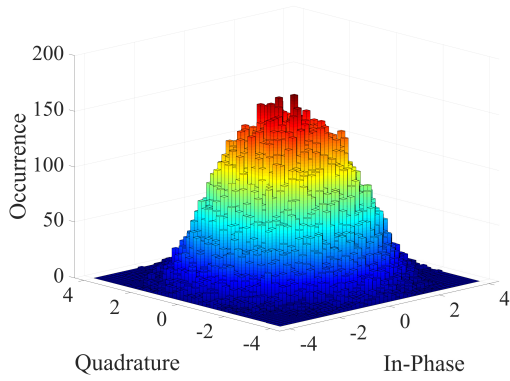
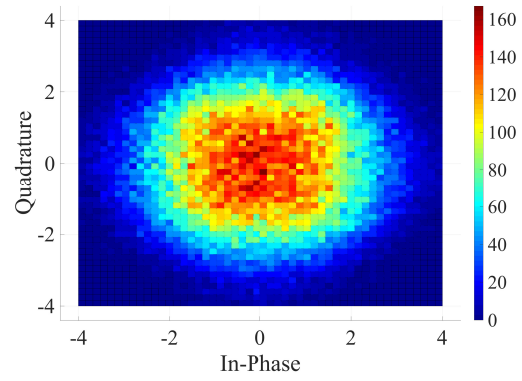


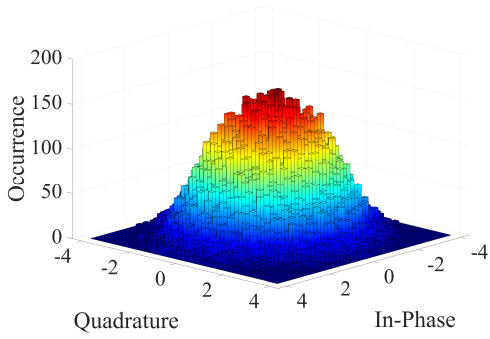
Figure 3-8: Histogram of the X_{cc}^n constellation at different PU interfering powers



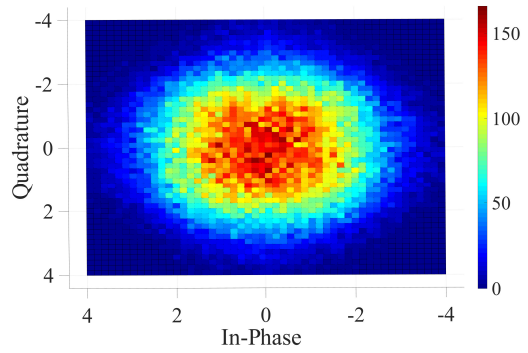
(a) $P_P = 3$ dB



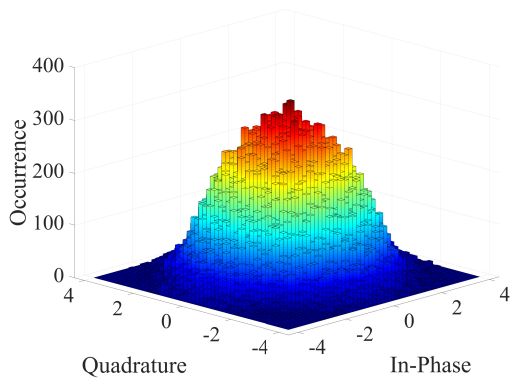
(b) $P_P = 3$ dB - top view



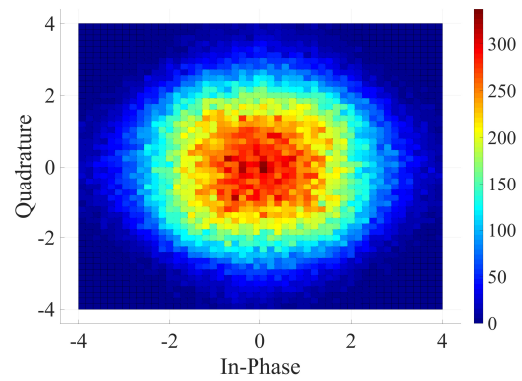
(c) $P_P = 7$ dB



(d) $P_P = 7$ dB - top view



(e) $P_P = 15$ dB



(f) $P_P = 15$ dB - top view

Figure 3-9: Histogram of the \hat{X}_c^n signal at different PU interfering powers

3.4.3 Quantitative Analysis for Interfering Scenarios

After this detailed analysis of the processing signals, as well as the relevant inferences to the system losses, this section quantitatively investigates the performance of both link transmissions by means of the Bit Error Rate (BER) examination.

Despite of the unquestionable importance and popularity of this measurement in communication systems, it is clear that, without previous study of the transmitted signal, it is quite difficult to identify the disturbance losses in a separated way.

Before a proper analysis and in order to set out a comparison among the reference scheme (corresponding to the TS scheme in AWGN channel) and the DPC curves, we define the SNR_{eff} per information bit in terms of:

$$\text{SNR}_{eff} = \frac{E_b}{P_{N'}}, \quad (3.3)$$

where $P_{N'}$ is the spectral power level of the effective noise N' , defined according Eq. (2.42), in the light of the discussion considering the correspondence between the MLAN and DPC channels (discussed in the Section 2.6). In addition, the energy per transmitted information bit E_b is given by:

$$E_b = \frac{P_{\hat{X}_c}}{kR}, \quad (3.4)$$

where $P_{\hat{X}_c}$ corresponds to the averaged power of the transmitted signal \hat{X}_c^n , k is the number of bits per transmitted symbol (in this case 4) and R is the system code rate (in this case 1/2). It is pointed out, for fair comparison, that we consider λ unitary for TS AWGN and equal to Eq. (2.34) for DPC schemes.

Once defined these parameters, Fig. 3-10 presents the BER curve for both primary and cognitive users.

We start our discussion about this figure by investigating the impact of the λ factor over the effective noise N' . According to Eq. (2.42) of the Chapter 2, as the SNR increases the AWGN noise component Z_s in the effective noise N' becomes more significant. By this reason, it is worth noting that, below the SNR of 5 dB, the degradation with respect to the TS AWGN is not so expressive (gap around 1 dB) between TS AWGN and DPC (PU=3 dB). In fact, in low SNR of 2 dB, we can

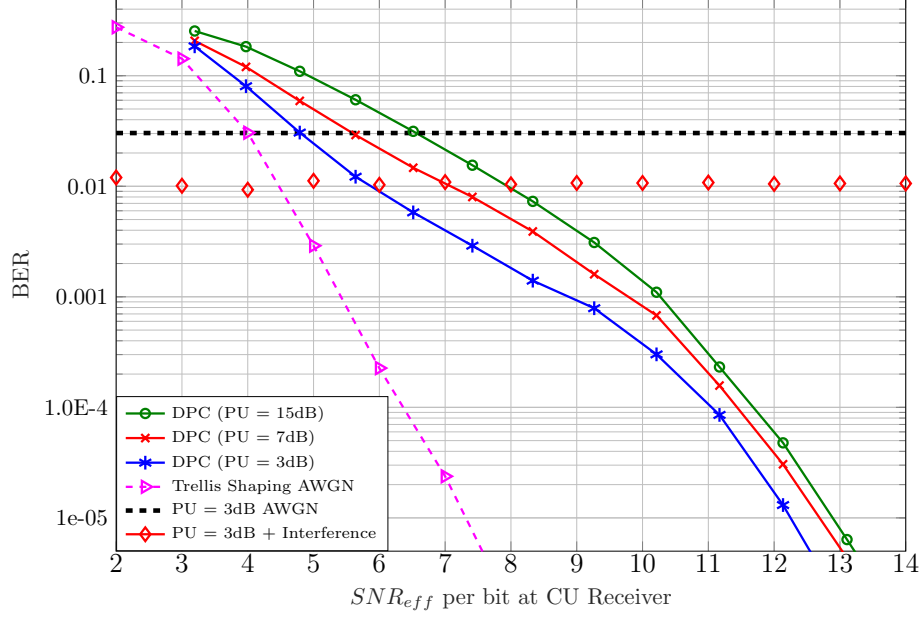


Figure 3-10: BER of the cognitive user

observe that the degradation is around 0.5 dB, mainly corresponding to the power loss (theoretically evaluated as 0.28 dB).

However, this gap increases, for all interfering cases, in the middle region of the operating SNR range (i.e. in a range from 5 to 10 dB). This effect is completely correlated to the λ increasing toward 1. In this condition, the system is highly affected by the modulo loss, as discussed by inspection of Fig. 3-8.

Moreover, it is quite interesting to observe, corroborating with our discussion in the Chapter 2 (see previous Fig. 2-10), that the degradation becomes less aggressive for SNR higher than 10 dB, when the modulo loss is clearly less disturbing. In this case, the AWGN is not sufficient high to cause the a large amount of shaping region errors in the decoding processing.

When the 3 scenarios are compared, it is noticed that the degradation increases as a function of the interference, where we can attest that the impact of the X_{cc}^n distribution in the boundary constellation points defines the system performance. It is observed that, for P_p of 3 and 7 dB, the losses can be partially recovered, resulting in gap around 1.0 and 0.5 dB respectively (considering a BER of 10^{-3} , typical for low data rate applications), when compared to P_p of 15 dB.

Furthermore, to verify that PU performance is not degraded, the simulated BER for PU at P_p of 3 dB is depicted in presence and absence of CU interference. Thus,

thanks to the superposition encoding strategy, the BER PU is not degraded. Interesting to observe that, in our case, the superposition even improves this BER. This can be explained by the fact that the superposition factor α was designed considering $E[|\hat{X}_c^n|^2] = (1 - \alpha)P_c$. However, because of the shaping gain obtained by the Trellis Precoding, the transmitted power is actually $E[|\hat{X}_c^n|^2] \leq (1 - \alpha)P_c$.

Finally, we remark that, for higher P_p of 7 and 15 dB, the maintenance of the PU service is evaluated by attesting the maintenance of the Eq. (2.22) lower bound, over the variation range of the SNR_{eff} at CU receiver. This way, as the previous case, the BER is also lower than specified.

The next section presents the main conclusions in light of the performed analysis.

3.4.4 Main Conclusions

First of all, we have highlighted that the adopted procedure for the superposition strategy, which is the technique responsible for PU link protection, could be further improved. The power reduction of the cognitive interference occasioned by the shaping gain on the transmitted \hat{X}_c^n , which is inherent to the precoder design, ultimately impacts both links of the overlay model.

Concerning the CU scheme, we have observed that the shaping gain is always reached, independently of the interference scenario, with the value defined by the implemented shaping code C_s . On the other hand, it was also suggested that the power loss slightly affects the performance, having its correspondence with the discrete 16-QAM constellation.

However, the main focus of the Chapter discussion was centering on the degradation caused by the modulo loss. It was pointed out the relation of this specific effect with the distribution of the X_{cc}^n signal, especially concerning the probabilities of boundaries symbols transmission. Moreover, we put some emphasis to the criticality of this effect when the hard decision strategy is employed for parallel transition in the TCM decoder, as chosen in our design in order to keep the low complexity.

Based on this assumption, some solutions could be investigated in order to minimize this specific degradation. The first approach could be to increase the modulo

boundaries Δ , which would make the system less susceptible to the modulo loss. In an extreme case, the system would approximate to the reference TCM performance and the degradation with respect to the modulo loss, would vanish. However, the power loss would be highly increased. On this direction, the work in [26] deals with inflated lattice concepts, discussing a slight boundary increase in respect to the λ factor.

A second approach, proposed by Wei in [29], deals with the higher expansion of the constellation in order to confine the whole interference. This solution may eliminate the modulo and its distortion. However, if all transmitted bits should be decoded, the SNR required to ensure standard BER would be higher than specified satellite operating range. Besides, the complexity of the transmitter would increase.

Another line of action, just considering the receiver, would be to propose another method of decoding to avoid the the parallel transition. This approach could be interesting since it keeps the same low complexity system at the transmitter, as proposed in this Chapter 3.

By continuing this discussion, the next Chapter 4 deals with these topics and proposes a design method to minimize this degradation.

3.5 Summary

This Chapter 3 proposed a low complexity transmission scheme using cognitive radio overlay paradigm towards satellite application, introducing some possible scenarios. The combination of Trellis Precoding and THP was implemented and the results present no PU degradation and a partial recovering of the precoding losses for CU signal.

In addition, a thorough analysis was carried out in such way to describe the degradation sources and to provide insights for improvements at the cognitive encoder design. The next chapters present some of these improvements, by considering the discussion presented here.

Chapter 4

A Design Method of Cognitive Overlay Links for Satellite Communications

Contents

4.1	Introduction	68
4.2	CU Practical Encoder Design for Dirty-Paper Channel	70
4.2.1	CU Transmitted Power Control	71
4.2.2	Constellation Expansion	72
4.2.3	Mapping Discussion	75
4.2.4	Simulation Approach	78
4.2.5	Results and Analysis	81
4.3	On the Modulo Loss Recovering at the Decoder	90
4.3.1	Method Description	90
4.3.2	Results and Analysis of the Proposed Metric	98
4.4	Discussion of the Chapter Results	102
4.5	Summary	102

Innovation and satellite are not always words that end up in the same sentence [1]. In a general sense, in the last decades, the technical advancements has been fairly slow

in satellite communications, especially due to the expensive nature, which implies a risk aversion by the main segment operators. As a consequence, the improvement of a satellite service suggests not only an increase in the available bandwidth, which is the focus of this thesis, but also the access to higher throughput, by augmenting the power efficiency, and low complexity design.

In this Chapter, we are dealing with the questions of the Chapter 3. By the previous discussion, we provide a new method to design cognitive overlay links for satellite communications, that allows the primary and the cognitive users to transmit concurrently while using efficiently the available power resources. Numerous schemes are investigated in various realistic scenarios, and different trade-offs between power efficiency *vs* complexity are obtained.

By simulations, we first show that we are able to design schemes where the primary user Bit Error Rate (BER) is exactly maintained as in the absence of the cognitive user interference.

Secondly, once the primary user link is properly designed, we demonstrate that the BER of the cognitive user can be made within 0.3 dB of corresponding the Gaussian channel BER. The implemented solution adopts the trellis precoding at the transmitter supported by appropriate constellation expansion, in consideration of the channel interference scenario.

In our third contribution, we present another design solution for the CU, however, only based on a slight change in the receiver decoding strategy. The same performance of the previous solution is reached, but, as an additional achievement, the low complexity implementation at the transmitter is preserved.

This Chapter summarizes the specific contributions of this thesis. A large part of the investigations presented here were published in [32]. Some novel results are part of a journal article in process of reviewing.

4.1 Introduction

In the last Chapter, we have proposed a low complexity scheme for cognitive user transmission over CR overlay paradigm, operating at the SNR range typically recom-

mended by satellite communications standards (for instance [6]). The performance of both users were investigated in two ways: (i) qualitatively, by interpretation of the histograms and scatter plots of the constellations involved in the signal processing, and (ii) quantitatively, by the scrutiny of the BER curve. Therefore, the impact of each THP loss was identified and compared in respect to the assumed reference TS-AWGN scheme. To sum up the analysis, some considerations towards system improvements were postulated.

By further detailing our previous highlights, we have observed that, due to the CU superposition encoding procedure, the SINR at PU receiver input (see Eq. (2.22)) is higher than specified for AWGN channel, impacting the system BER. We also pointed out that this occurs because the superposition factor α should be properly evaluated in Eq. (2.23), by taking the shaping gain of the transmitted signal \hat{X}_c^n into account.

Additionally, regarding the CU link, we have investigated the origins of the performance degradation caused by the modulo loss. It was pointed out the importance of controlling the probability distribution of the encoded signal X_{cc}^n , in order to avoid the selection of boundary constellation symbols (*i.e.* corner and edges constellation points). Also, it was underlined that the impact of this loss is more critical when the hard decision strategy for parallel transition decoding is implemented, typically adopted in TCM decoders.

All things considered, this Chapter proposes some improved solutions to overcome these identified impairments. The techniques are presented for both the encoder and decoder, taking into account the satellite scenarios and the trade-offs between power efficiency and complexity.

The first Chapter contribution introduces a method to control the CU transmitted power to conserve the same SINR at PU receiver as in the absence of interference. Consequently, the procedure for the superposition strategy is properly evaluated. Without going into details, such approach is accomplished by employing the shaping gain, provided by the shaping code C_s , as a scaling factor for the minimum distance d_{min} of the X_{cc}^n constellation. We remark that, with this design, besides solving the BER inconsistency in the PU link, the CU power resource is efficiently utilized.

Moreover, for the second contribution of this Chapter, regarding the amount of the channel interference, further constellation expansion along with the modulo quanti-

zation are implemented. The main purpose of this technique is to avoid the selection of boundaries constellation points for X_{cc} , as well discussed in the Chapter 3. To complement the scheme, we show that the control of CU transmitted signal power is ensured by a proper mapping design.

In our third contribution, a decoder based design is proposed. By using the same low complexity scheme of Chapter 3, regardless of the amount of channel interference, the proposed solution transfers an important part of the interference mitigation processing to the receiver side, which might be interesting for practical satellite missions. Basically, we show that, by slightly changing the *Viterbi* decoder metric for C_c implemented at the CU receiver (see Fig. 3-2), the system achieves the same performance as the previously proposed solution and, considering the defined SNR range, the modulo loss is recovered.

Following this introduction, the Section 4.2 presents the proposed CU encoding techniques, which address the control of the transmitted power (first contribution) and modulo loss mitigation (second contribution). Such techniques are evaluated in realistic scenarios, providing a detailed discussion about the results. In Section 4.3, the proposed decoder design (third contribution) is exposed. The simulation and results are also discussed, pointing out the existing trade-offs between the different analyzed solutions in Section 4.4. Finally, the main chapter conclusions are summarized in the Section 4.5.

4.2 CU Practical Encoder Design for Dirty-Paper Channel

In this Section, we describe our contributions based on some changes in the previous encoder presented in Chapter 3. Firstly, taking into account that the CU signal is Gaussian distributed due to the trellis shaping operation, we demonstrate a procedure that provides the appropriate output power for \hat{X}_c^n . As a consequence, the SINR_p of the PU (see Eq. (2.22)) is properly evaluated. Subsequently, we deal with the CU link by proposing further expansion in the X_{cc} constellation, jointly with an optimized mapping design. The results are analyzed as a function of the complexity involved in the transmitter implementation.

4.2.1 CU Transmitted Power Control

We have seen that the power reduction of \hat{X}_c^n , caused by the trellis precoding technique, impacts directly on both links performances (see Item 1 of Section 3.4.2), since the value of α , adopted for power sharing at the superposition strategy, is no longer exact (see Eq. (2.23)). It can be noted, as given by Eq. (2.22), that the SINR_p at the primary receiver is increased. As a result, the Fig. 3-10 showed that PU presents better BER performance than when operating in AWGN channel.

In addition, the exactly same shaping gain generated by a shaping code C_s is obtained for the multiuser precoding [29]. We have also investigated this concept and the Fig. 3-9 depicts the probability distribution of \hat{X}_c^n for different interfering scenarios.

By these demonstrations, we propose a method for controlling the CU output power such as $E[|X_c^n|^2] = P_c$, or, equivalently, $E[|\hat{X}_c^n|^2] = (1 - \alpha)P_c$. This is reached by proper scaling the minimum distance d_{min} of the coded constellation X_{cc}^n .

As a reference, we assume the power of the baseline, without considering the shaping operation, given by [55]:

$$P_{\oplus} = \frac{2^{R_c}}{6} d_{min}^2, \quad (4.1)$$

where R_c is the data rate in bits per two dimensions, without taking into account the shaping redundant bits. The scaled minimum distance is defined as d_{min}' . The shaping gain γ_s is then defined as:

$$\gamma_s = \frac{P_{\oplus}}{E[|\hat{X}_c^n|^2]} = \frac{P_{\oplus}}{(1 - \alpha)P_c}. \quad (4.2)$$

Thus, by combining Eq. (4.1) and Eq. (4.2) and rearranging the terms, the d_{min}' , such that the available power after the shaping operation is equal to $(1 - \alpha)P_c$, is given by:

$$d_{min}' = \sqrt{\frac{[(1 - \alpha)P_c]6\gamma_s}{2_c^R}}. \quad (4.3)$$

All things considered, some remarks are pointed out for this proposed procedure:

1. **Both links are properly adjusted.** Since the output power of the remaining CU transmission, after superposition, satisfies $E[|\hat{X}_c^n|^2] = (1 - \alpha)P_c$, the BER performance of PU in a interference channel is the same as AWGN channel. In addition, as the CU power is efficiently employed, the BER of cognitive link is improved or, equivalently, the secondary service data rate can be increased;
2. **CU modulo loss might be reduced.** We have observed that the performance degradation caused by modulo loss augments as a function of: (i) the selection probability of boundary symbols in the X_{cc}^n constellation and (ii) the reduction of the SNR_{eff} level. By these perceptions, it is worth noting that, by re-scaling the minimum distance of X_{cc}^n and considering the same Gaussian distributed interference S^n , this procedure might reduce the occurrence of boundary selected points for X_{cc}^n , since the constellation region is further enlarged. Clearly, because of this modulo loss reduction, this technique improves the cognitive system performance for the same fixed SNR_{eff} (see the discussion exposed in Section 3.4.2 for further clarification).
3. **Mapping of X_{cc}^n constellation should be optimized.** In order to obtain exactly the specified output power $(1 - \alpha)P_c$, the shaping operation should be performed over a defined continuous region delimited by Δ . In this sense, it is of utmost importance that the mapping be designed such that the interference presubtracted signal \hat{X}_c^n be confined within this delimited region. Otherwise, the previous procedure does not control the exact power. This specific issue, jointly considered with constellation expansion, is further discussed in the next section.

4.2.2 Constellation Expansion

The THP precoding works as the simplest solution for Multi-User Interference (MUI) presubtraction. By using the modulo operation, this technique satisfies the power constraint for application of dirty-paper encoder and results in almost negligible degradation in high SNR regimes [51, 52, 53].

However, our previous analysis have shown that, for low and intermediate SNR

regimes (for instance, below 14 dB), the degradation caused by THP losses becomes more significant, especially due to the modulo loss (see the Fig. 2-10 and the related discussion). Additionally, in the last Chapter 3, we demonstrated that the modulo loss increases as a function of the probability occurrence of the boundary constellation points in X_{cc}^n .

In order to recover part of the THP losses, some practical precoding techniques are proposed in [29]. Following, we present a short description of these implementations regarding the SNR regime, which could be seen as a starting point to introduce our contribution:

- **High-SNR regime:** By recalling of the Fig. 2-10, we notice that the THP on the dirty-paper channel causes a negligible degradation when operation on this SNR regime. In this sense, the adopted solution in [29] is an extension of the Trellis Precoding (TP) technique [53], usually developed for Inter-Symbol Interference (ISI) context, for MUI channel. The recommended shaping code rate is 5/6, in order to force greater expansion of X_{cc}^n , such that the interference lies entirely inside the expanded constellation (*i.e.* $|\text{Re}(S)|$ and $|\text{Im}(S)| < (\sqrt{M}/2).d_{min}$, where M is the constellation order of X_{cc}^n). It is worth noting, considering this scheme, that the modulo operation becomes useless. As a consequence, the modulo loss is eliminated, the shaping loss is partially recovered by the trellis shaping and the power loss can be assumed as negligible.
- **Low-SNR regime:** in this case, the system is affected by the power and modulo loss. In the same reference, Yu *et al.* proposes the employment of the Partial Interference Presubtraction for THP (PIP-THP).

However, as in this precoding configuration the trellis shaping is not implemented, the transmitted presubtracted signal \hat{X}_c^n has uniform distribution. As a consequence, the distribution of the effective noise N' (see Eq. (2.42)) is formed by the uniform part, derived from \hat{X}_c^n , and the Gaussian part, from the channel additive noise Z_s^n . The countermeasure adopted by Yu *et al.* adjusts the metric of the convolutional decoder, which takes the PIP into account, by capturing exactly the self-information of the effective noise. In fact, when λ is close to zero, the N' distribution is almost uniform. At the opposite, when λ approaches 1, as the additive Gaussian noise becomes more significant, the distribution is near Gaussian.

- **Intermediate-SNR regime:** This range is similar to our application scenario. The combination of TP and PIP techniques is proposed by [29]. The recommended shaping code, as the high interference regime, is also 5/6 in order to force the X_{cc}^n expansion, in such way to have the interference confined. Also, as the trellis shaping is implemented at the precoder, the transmitted presubtracted signal \hat{X}_c^n has Gaussian distribution.

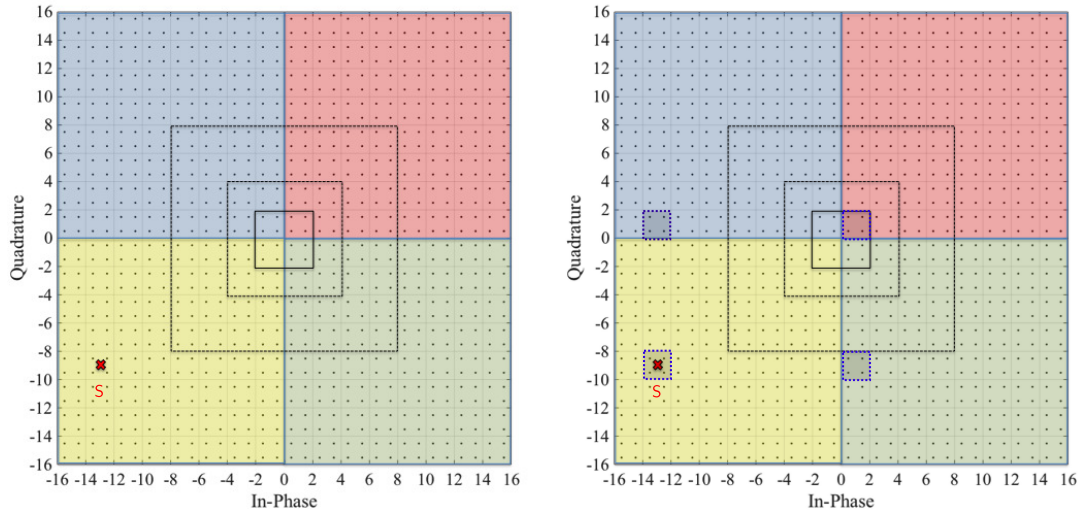
Interesting to observe that, as the modulo is not considered at the precoding, only the power and shaping losses are presented.

As a complement of the approach presented in [29], we consider in this Section realistic scenarios in the same way as in the Chapter 3, with modulo implemented at the transmitter output in all cases. The amount of the interference varies and, on the contrary of [29], different constellation expansions are considered. This assumption allows the analysis of the modulo loss impact. Also, the results could be evaluated considering the trade-off between complexity and power efficiency.

As an example for our proposed constellation expansion, and following the same notations as in previous Fig. 3-1, let us consider that the original DPC constellation is a 16-QAM. Each symbol is defined by the tuple $(z_1 z_2 y_{c_1} y_{c_2})$, where z_1 and z_2 are the sign bits while y_{c_1} and y_{c_2} are the coset bits (as proposed in our fixed design in the Chapter 3). This constellation can be expanded to, for instance, a 64-QAM by considering an additionally two information bits u_1 and u_2 or two 'auxiliary' bits (not information bits) z_{aux_1} and z_{aux_2} . Now, each symbol is defined by the tuple $(z_1 z_2 u_1 u_2 y_{c_1} y_{c_2})$ or $(z_1 z_2 z_{aux_1} z_{aux_2} y_{c_1} y_{c_2})$, respectively.

It is worth noting that, in this way, the signal constellation of X_{cc}^n can be expanded as necessary to confine the scaled interference (*i.e.* $|\text{Re}(\lambda S^n)|$ and $|\text{Im}(\lambda S^n)| < (\sqrt{M}/2)d_{min}$, where M is the constellation order of X_{cc}^n), in order to avoid the boundary points and mitigating the modulo loss. However, the transmitter design could be implemented with less constellation expansion, decreasing the complexity, and some modulo loss might be tolerated. Also, it is highlighted that the original rate could be maintained by expanding with 'auxiliary' bits instead of uncoded bits, preserving the desired SNR operating range.

For the transmitter, this operation could be seen as an extension of the trellis shaping procedure. The *Viterbi* decoder of the shaping operation acts as an usual



(a) Case 1 - 8 information bits per symbol \hat{X}_c (b) Case 2 - 2 information bits per symbol \hat{X}_c

Figure 4-1: Shaping regions mapping I

TCM decoder, where the 'auxiliary' shaping bits z_{aux} represent the parallel branches transitions, which are hard decided between consecutive state transitions in the trellis for C_s .

Furthermore, it is still necessary to design the optimal mapping of shaping regions, according to the information rate. The next section discusses this topic.

4.2.3 Mapping Discussion

Consider the implementation of the mapping I, depicted in the Fig. 4-1. We assume a shaping code C_s of rate 1/2, which provides four shaping regions, represented by the different colors. The convolutional code C_c of rate 1/2 is defined, which also provides four TCM cosets. In addition, the modulo regions are represented by dashed lines, according to the X_{cc} constellation expansion adopted in 16, 64, 256 and 1024-QAM.

The interference point is represented by the red "X", which is presubtracted by the X_{cc} constellation point, selected by C_s , to form the transmitted \hat{X}_c symbol. As we have discussed in the Section 4.2.1, by a proper mapping design, we confine the \hat{X}_c signal in a determined continuous region of the constellation. In this way, the control of the transmitted power is achieved. Following, two cases are analysed.

In the first case, depicted in the Fig. 4-1a, the uncoded information bits in the trellis precoding are considered. We define the mapping, according to the sign bit shaping strategy, proposed in [28], as $(z_1 z_2 u_1 u_2 u_3 u_4 u_5 u_6 y_{c_1} y_{c_2})$. In this way, we have 8 information bits transmitted by symbol, which require high SNR (unlike the operating range considered in this thesis). Thus, there is no shaping subregions in this scheme. Each 256-QAM constellation, divided in 4 cosets with 64 constellation points inside each coset, is repeated 4 times to form the outer shaping 4-QAM. Regardless of whether the interference S is confined within the 1024-QAM constellation of X_{cc} , the presubtracted signal \hat{X}_c , due to the modulo, is always restrict in its region. Based on this assumption, we observe the following:

- **The shaping loss is partially recovered.** This is achieved by the shaping gain γ_s , provided by the code C_s , and based on the fact that \hat{X}_c^n is continuous and shaped bounded by the squared region of $\Delta = 32$ (*i.e.* $|\text{Re}(\hat{X}_c)|$ and $|\text{Im}(\hat{X}_c)| < \Delta/2$, where Δ is the modulo boundary);
- **The modulo loss is assumed negligible.** In fact, even if there are some points selected at the boundaries of X_{cc}^n , since the system operates in high SNR regime (see Section 2.6.1 as well as the related discussion), the modulo loss only causes degradation in very low BER;
- **The power loss is close to zero.** By the continuous approximation, we obtain $\gamma_p = 1024/1023 \approx 0.0042$ dB for this 1024-QAM constellation (see Table 2.1).

In the second case, depicted in Fig. 4-1b, we transmit the rate of 2 information bits per \hat{X}_c symbol (suitable for the thesis scenario). The uncoded bits are replaced by the *auxiliary* shaping bits and the mapping is defined by $(z_1 z_2 z_{aux_1} z_{aux_2} z_{aux_3} z_{aux_4} z_{aux_5} z_{aux_6} y_{c_1} y_{c_2})$. The shaping operation selects the closest one of the 2^6 subregions (or equivalent, points inside each shaping cosets) of each one of the 4 region defined by C_s .

Considering this rate, as discussed in our proposed power control technique, the \hat{X}_c signal must be continuous, Gaussian shaped and bounded by the squared region of $\Delta = 4$ (*i.e.* $|\text{Re}(\hat{X}_c)|$ and $|\text{Im}(\hat{X}_c)| < \Delta/2$, where Δ is the modulo boundary). For the same interference S , represented also by the red "X", the only case that the presubtracted signal \hat{X}_c is confined in our region of interest occurs when the "yellow" region is selected by C_s . Intuitively, as the other shaping regions (*i.e.* colors) can

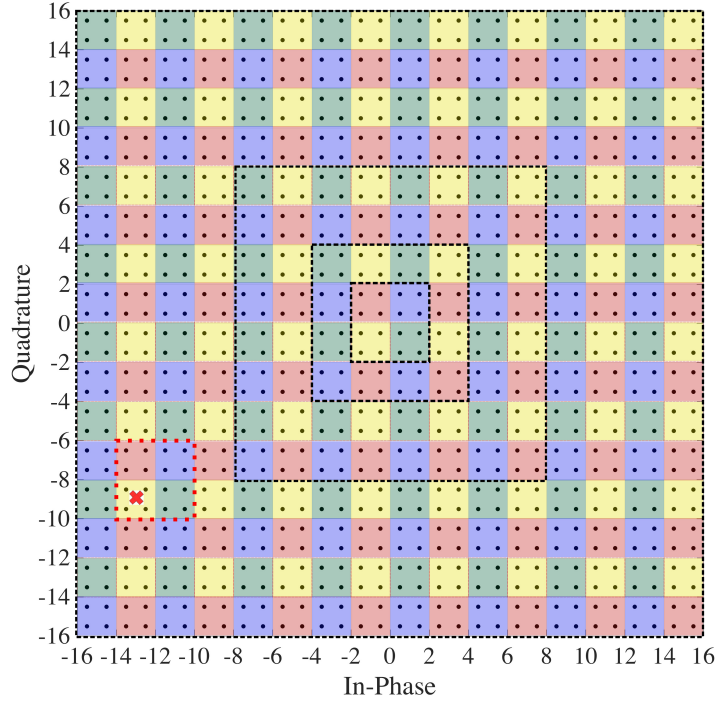


Figure 4-2: Shaping regions mapping II

also be selected by C_s , it is not guaranteed that the shaping gain γ_s , provided by this code, is achieved. As a result, the power control strategy, discussed in the last section, would not be effective in this case.

The following mapping, represented by the Fig. 4-2, is optimized for scenarios where 'auxiliary' bits are employed. In this case, the mapping is defined by $(z_{aux_1} z_{aux_2} z_{aux_3} z_{aux_4} z_{aux_5} z_{aux_6} z_1 z_2 y_{c_1} y_{c_2})$. The same four shaping cosets are represented by the four different colors and the 2^6 subregions (points inside each shaping coset) are spread over the expanded constellation.

The interference point is also represented by the red "X", which is presubtracted by the closest X_{cc} to provide the transmitted signal \hat{X}_c . It is worth noting that, considering the hard decision of the parallel branches for the C_s trellis, \hat{X}_c is always inside the smallest dashed square, which is our continuous region of interest ($\Delta = 4$). By this mapping design, we conclude that:

- **The shaping loss is partially recovered.** the shaping gain γ_s is reached according to the code C_s . As a consequence, the power control technique is

properly designed;

- **The modulo loss can be totally mitigated.** If the X_{cc} constellation is expanded enough such that the interference is confined and the boundary selected symbols are avoided, the modulo loss can be mitigated. However, we emphasize that, in some cases, a low modulo loss might be tolerated in order to reduce the transmitter complexity (this will be further discussed in the next section, by analyzing the simulated scenarios);
- **The power loss.** Considering this rate, this loss is evaluated by the approximation $\gamma_p = 16/15 \approx 0.28$ dB. It is important to recap, as discussed in the Section 3.4.2, that this loss represents the relation between continuous and discrete constellation transmission.

In summary, the previous discussions showed, by considering proper expansion of the DPC constellation, that the degradation can be made within 0.3 dB of the corresponding reference Trellis Shaping in AWGN channel. On the other hand, we have seen that the system complexity increases, which is a design drawback. Important to emphasize, at the opposite of the previous scheme presented in the Chapter 3, that the PU user maintains the same performance as in absence of the CU operation.

4.2.4 Simulation Approach

In this Section, the parameters implemented in the simulation framework are presented. We investigate the improvements produced by the introduced techniques in the system performance. The scenarios described are similar to that exposed in the Chapter 3¹.

The PU is implemented as a 4-QAM signal encoded by a 16-state, rate 1/2, convolutional code C_c , specified in the octal notation by the generators $g_1(D) = 31$ and $g_2(D) = 33$. The transmitted power is variable according to the specific scenario to be analyzed.

For the CU, unlike in Chapter 3, we specify the available transmitted power, to be shared in the superposition, as 10 W in all simulated cases. In addition, we maintain

¹In the same way as implemented in Chapter 3, without loss of generality, we assume the noise power N_s , at the input of PU receiver, as unitary in our analysis [23].

the same transmission rate as $R_c = 2$ bits/symbol, in line with the typical SNR range for satellite [6]. The same previously proposed DPC encoder, presented in the Fig. 3-1, is implemented for some configurations.

In the upper part of the encoder, for all cases, the systematic 64-state, rate 1/2, channel trellis convolutional code C_c , given by feedforward polynomial $h_1(D) = 54$ and the feedback polynomial $h_0(D) = 161$, is considered (as in the Chapter 3).

In the lower part of the encoder, for all cases, the same 4-state, rate 1/2, shaping code C_s , specified by generators $g_{s,1}(D) = 7$ and $g_{s,2}(D) = 5$ is assumed (as in the Chapter 3). We investigate the constellation expansion in 4, 16, 64, 256 regions, which represents $n_s = 2, 4, 6, 8$ (where, in case of $n_s > 2$, the remaining $n_s - 2$ are auxiliary bits). It is important to point out that the minimum distance d_{min} , evaluated by scaling method previously exposed in Section 4.2.1, is implemented in all simulated schemes. Additionally, the impact of modulo operation in the system is also considered.

We have seen in the last section that the proper choice of the shaping regions mapping is of crucial importance for the combination of constellation expansion and power controlling. In this implementation, since we are employing $R_{cu} = 2$ bits/symbol, the transmitted signal should be confined within the region defined by the 16-QAM constellation (*i.e.* $|\text{Re}(\hat{X}_c)|$ and $|\text{Im}(\hat{X}_c)| < 2d_{min}$). Having this in mind, we are assuming the previously discussed Mapping II (see Fig. 4-2) for all considered scenarios.

The following example, depicted in the Fig. 4-3, clarifies the mapping strategy. In this case, the constellation is expanded from 16 to 64 regions, where the X_{cc} symbol is defined by $(z_{aux1}, z_{aux2}, z_1, z_2, y_{c1}, y_{c2})$. Consequently we have the middle bits z_1 and z_2 as the shaping coset bits, which assign the shaping regions (represented by colors) and z_{aux1} and z_{aux2} as a points within each shaping coset, which define the shaping subregions. Finally, the convolutional coded bits y_{c1} and y_{c2} select a point (represented by the markers \circ , \times , \square and \triangle) inside each shaping subregion.

Consider that the pair of bits (y_{c1}, y_{c2}) are mapped to $(0, 0)$ by the channel trellis convolutional code C_c , represented in the figure by the marker \circ . In this case, Fig. 4-4 elucidates the *Viterbi* decoder for the shaping operation located at the transmitter. By observing this example, the trellis transition from the state σ_j^n to the state σ_j^{n+1} provides (z_1, z_2) mapped to $(0, 0)$, which is represented by the "yellow" color regions

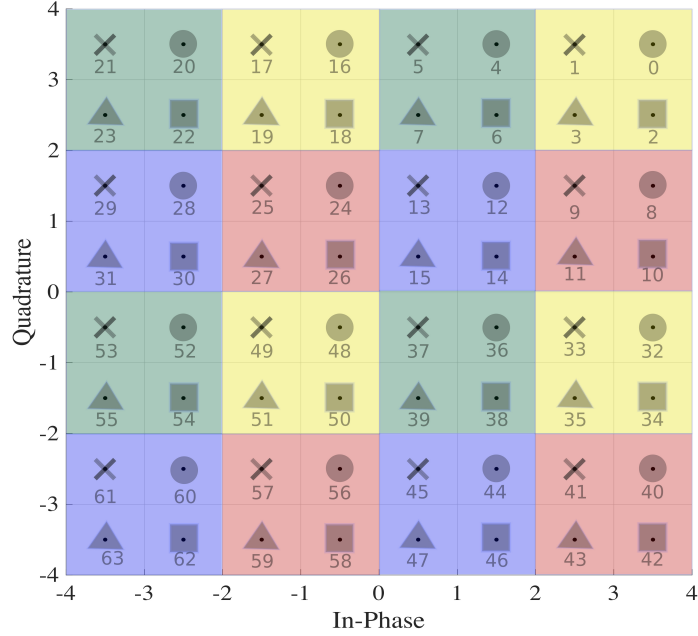


Figure 4-3: Shaping regions mapping II for 64-QAM

according to the assigned mapping. Thus, the decoder will perform a hard decision among the four constellation symbols (0, 16, 32, 48), representing the points within the assigned shaping region coset, in turn, each defined by the pair of bits (z_{aux1}, z_{aux2}) . In the same way, the transition from the state σ_j^n to σ_{j+1}^{n+1} provides (z_1, z_2) mapped to (0, 1), represented by the "green" color regions, which decide among the parallel transitions (4, 20, 36, 52).

We can notice that, thanks to this mapping strategy, regardless the interference S^n , the presubtracted signal \hat{X}_c^n is confined within the 16-QAM region, assuring that the power control is established. In our analyzed scenarios, when required to mitigate the modulo loss, further expansions are implemented following the same presented procedure.

Regarding the scenarios, as considered in the last chapter and without loss of generality, the interfering path gains a and b are assumed real values and equal to 0.2, which represent the attenuation factors. The following scenarios, with respect of the PU power P_p , are evaluated at (i) $P_p = 3$ dB; (ii) $P_p = 7$ dB; (iii) $P_p = 15$ dB and (iv) $P_p = 20$ dB.

Since the P_p changes, a different value of the superposition factor α is computed

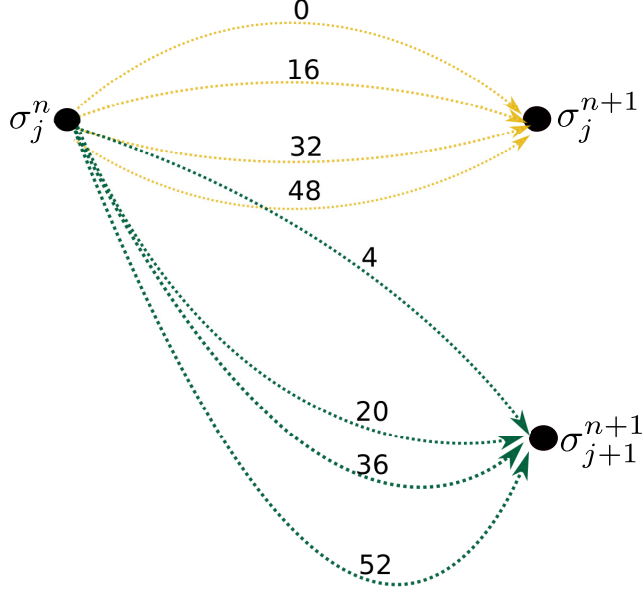


Figure 4-4: Example of parallel transitions for *Viterbi* decoder of trellis shaping at the transmitter, according to mapping of Fig. 4-3.

at the CU design for each scenario, according to Eq. (2.23). As a consequence, the remaining power of the signal \hat{X}_c^n as well as the amount of interference S^n at CU receiver vary from case to case.

4.2.5 Results and Analysis

The system performance is analysed in both qualitative and quantitative approaches. The main objective is to provide a comparative study regarding the different expansions of X_{cc}^n , emphasizing the trade-off between power efficiency *vs* complexity.

To support the analysis, for all scenarios, the scatter plot of the signal constellations that are part of the partial interference pre-subtraction processing is interpreted. The expanded constellation signal X_{cc}^n is shown in green "x". The Gaussian distributed version of the scaled interference λS^n is superposed in red points and the transmitted signal \hat{X}_c^n is shown in blue dots.

Additionally, we depict the histogram of X_{cc}^n in order to study the probability of the boundary symbols, since that it is determinant for the degradation caused by modulo loss. Connected with this qualitative investigation, the BER of both PU and CU is shown for quantitative performance evaluation.

(i) Low Interference Scenario - $P_p = 3$ dB

The results and analysis of the first scenario, for PU transmitted power P_p of 3 dB, are presented in Fig. 4-5. The scheme with slight constellation expansion of 16-QAM has proved effective. The CU output power remains constant (10 W), which implies an accurate superposition strategy thanks to the minimum distance scaling $d_{min}!$. By inspection of the Fig. 4-5a, we notice that the interference is confined within the expanded constellation X_{cc}^n . In this case, we may infer that the shaping gain provided by the shaping code C_s is reached.

However, unlike the work presented in [29], we are always considering the THP in our systems (modulo operation at the transmitter output). This implies, as we have seen in the Chapter 3, in modulo loss when the boundaries symbols are assigned for X_{cc}^n . The correspondent histogram in Fig. 4-5c highlights this effect. Similarly to our reference scheme TS AWGN, investigated in the last Chapter 3 (see Fig. 3-5), we notice that the occurrence is highly concentrated in the four inner constellation points, while the four corners points are practically avoided. But, as we also have some transmission of edges constellation points, the system is degraded by modulo loss. We notice the similarity between the two representations (TS AWGN and this 16-QAM histograms), since the interference is very low with respect to the expanded constellation.

In order to eliminate this modulo loss, we expand the constellation for 64-QAM, as represented in the Fig. 4-5b. In this scheme, it is worth noting, by the histogram in Fig. 4-5d, that the boundary points are avoided due to the expansion. Moreover, we realize, by comparing both histograms of 16 and 64-QAM, that exactly same 16-QAM constellation points are going to be selected by the trellis shaping operation for both schemes. Thus, we conclude that further constellation expansion would not improve the system performance, besides increase the complexity (more branches in the shaping code).

The performance can be expressed, in a quantitative way, by the BER curves shown in Fig. 4-5e. We can detect the same behaviour discussed in the previous Fig. 3-10 for the 16-QAM scheme. The same effect of λ in low SNR is also noticed in this configuration. However, due to the re-scaling of the minimum distance $d_{min}!$, which reduces the occurrences of boundaries assigned points, we notice that the performance

presented here is improved. By comparing the curves, for a BER of 10^{-3} , the SNR_{eff} is about 7.5 dB in this scheme while 9 dB in the previous one. In addition, by considering low data rate services, a gap around 2 dB is observed when compared with the reference TS-AWGN considering this BER.

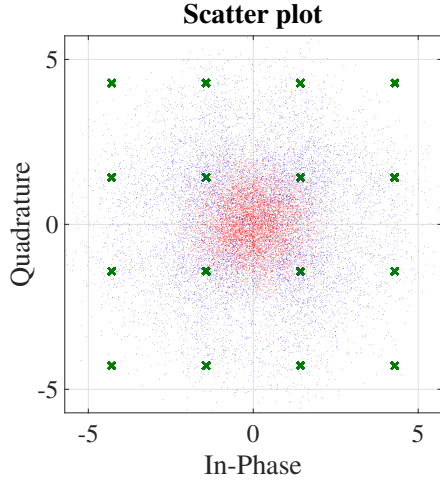
The main result of this technique is obtained when the expansion for 64-QAM is implemented. As the modulo loss is recovered, by avoiding the boundary symbol transmission, and the shaping gain is reached, by the combination of the trellis shaping and the mapping design, a gap less than 0.3 dB from the TS-AWGN curve is obtained. This degradation corresponds to the power loss, computed as 0.28 dB for 16-QAM (see Section 2.6.1 for further details). We recall that this specific loss is due to the fact that our reference TS-AWGN scheme is discrete while the DPC, due to the presubtraction, is continuous. By these considerations, we attest that our design reaches our performance limit by some complexity increase.

Furthermore, in order to verify that the PU operates properly, the simulated BER for PU at P_p of 3 dB is depicted in the presence and in the absence of CU interference, *i.e.* 16-QAM scheme. Thanks to the superposition and to the method of d'_{min} scaling, the BER of the PU, in the presence of CU interference, remains exactly the same as in the case of no CU interference.

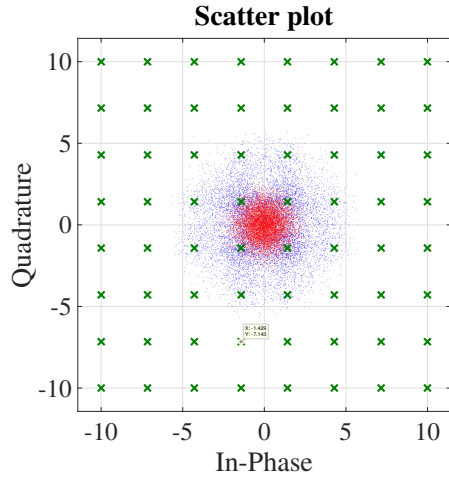
(ii) Intermediate Interference Scenario - $P_p = 7$ dB

The Fig. 4-6 presents the results and analysis of the second scenario, for P_p of 7 dB. The interference can not be confined within the 16-QAM scheme (see Fig. 4-6a). In this case, after the presubtraction, the CU output power is increased and the DPC condition is not satisfied. As a consequence, the modulo has to be applied. In Fig. 4-6b, we note that, by adopting the solution with 64-QAM, the interference remains inside of the expanded constellation region of X_{cc}^n and the boundary points are avoided, as depicted by the corresponding histogram in Fig. 4-6d. In this sense, we expect that the modulo loss could be recovered by the system.

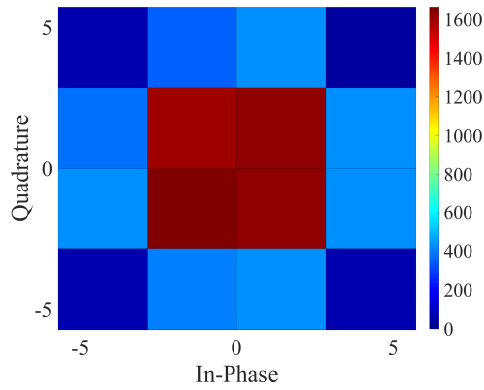
The Fig. 4-6e presents the BER performance for this scenario. The results for 16-QAM scheme and 64-QAM are exposed. The 16-QAM scheme has a similar behaviour in relation to the previous scenario, except by the increase of the modulo loss due to the greater occurrence of boundary points transmission in X_{cc}^n . We observe that



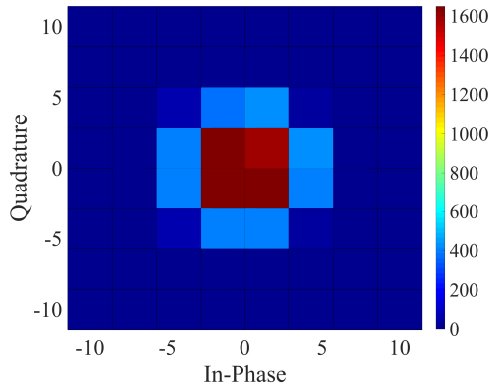
(a) Scatterplot for $P_P = 3$ dB and X_{cc}^n as 16-QAM



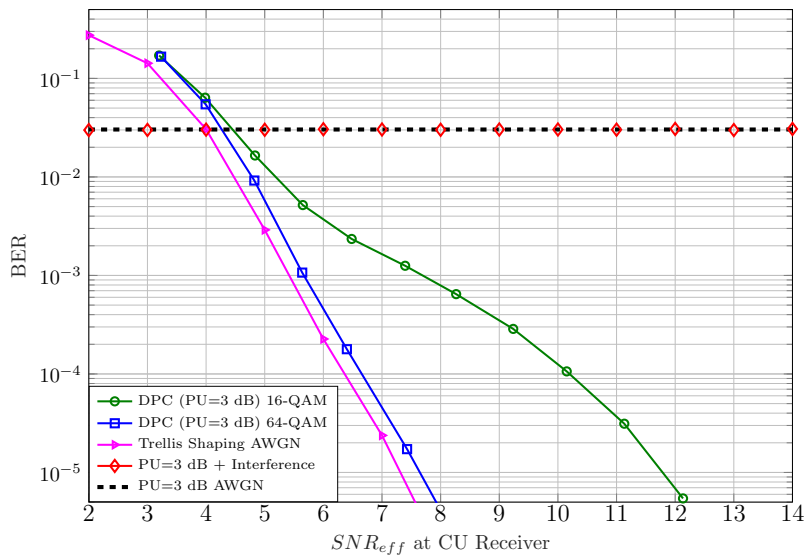
(b) Scatterplot for $P_P = 3$ dB and X_{cc}^n as 64-QAM



(c) Histogram of X_{cc}^n as 16-QAM for $P_P = 3$ dB



(d) Histogram of X_{cc}^n as 64-QAM for $P_P = 3$ dB



(e) BER of the Cognitive User at $P_P = 3$ dB

Figure 4-5: Results and analysis for $P_P = 3$ dB

64-QAM scheme performs within 0.3 dB to the AWGN trellis shaping BER curve, reaching the same performance as our previous analysis (see Fig. 4-5e), limited by the small power loss degradation. In addition, as in the previous case, by using the 16-QAM signal as an CU interfering signal, the BER of the PU remains the same in comparison with the interference-free PU channel.

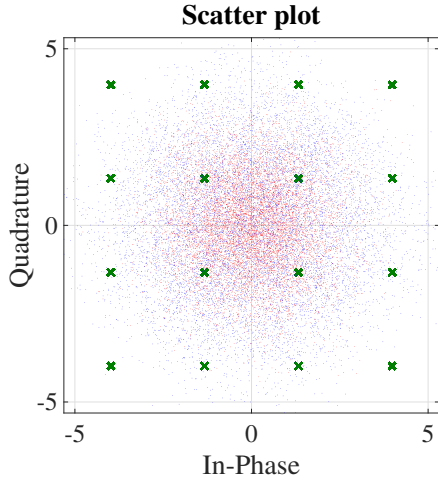
(iii) High Interference Scenario - $P_P = 15$ dB

Regarding the high interference scenario, *i.e.* P_P of 15 dB, investigated in Fig. 4-7, we can observe in Fig. 4-7a that a higher constellation expansion is necessary in order to accommodate the strong amount of interference ($n_s = 6$, which means 64 shaping regions). By this way, the expanded constellation X_{cc}^n will be a 256-QAM scheme. The histograms in Fig. 4-7b, Fig. 4-7c and Fig. 4-7d show the occurrence of boundaries constellation points decreasing as further constellation expansion is considered.

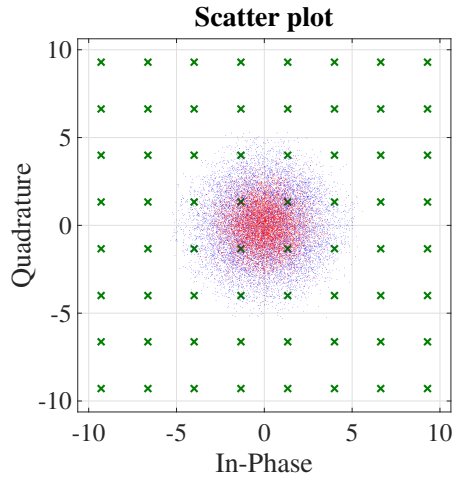
The Fig. 4-7e presents the BER curves for this scenario. We observe that the modulo loss is not significantly high for the 64-QAM scheme, especially when the BER of 10^{-3} is considered, providing a gap less than 1 dB when compared with the reference TS-AWGN scheme. This could be important for the communication design, since the complexity is decreased by using less expanded expansion at the transmitter. As the previous cases, when 256-QAM is implemented, the same performance limit (gap less than 0.3 dB) is obtained. Finally, we remark that the maintenance of the PU service, in this case, is evaluated by attesting the exact same SINR_P at the primary receiver input as in AWGN channel. This is accomplished thanks to the proposed power control technique for CU encoder (see Section 4.2.1).

(iv) Extremely High Interference Scenario - $P_P = 20$ dB

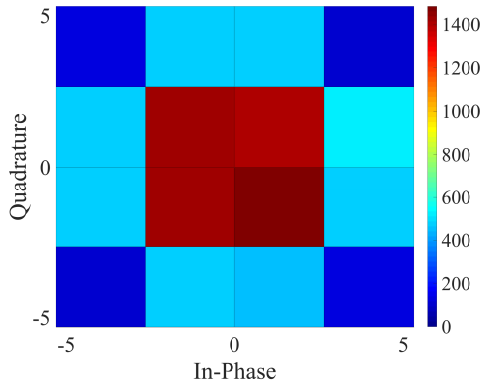
In the last scenario presented in Fig. 4-8, *i.e.* P_P of 20 dB, we expand the constellation up to 1024-QAM, as depicted in the Fig. 4-8a, in order to confine the amount of interference (n_s about 8, which means 256 shaping regions). By inspection of Fig. 4-8b, we observe that for 16-QAM the X_{cc}^n constellation is uniformly distributed (*i.e.* the so-called *n-cube* distribution). We also notice, by inspecting the histograms of 256-QAM and 1024-QAM (presented in Fig. 4-8c and Fig. 4-8d), that the occurrence



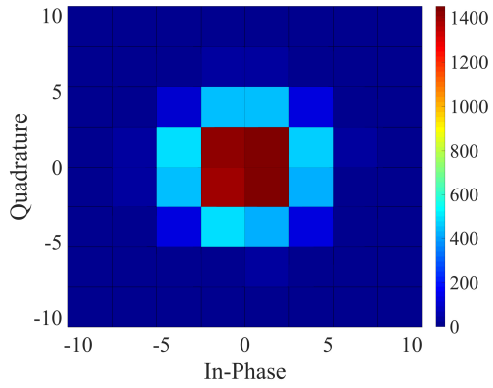
(a) Scatterplot for $P_P = 7$ dB and X_{cc}^n as 16-QAM



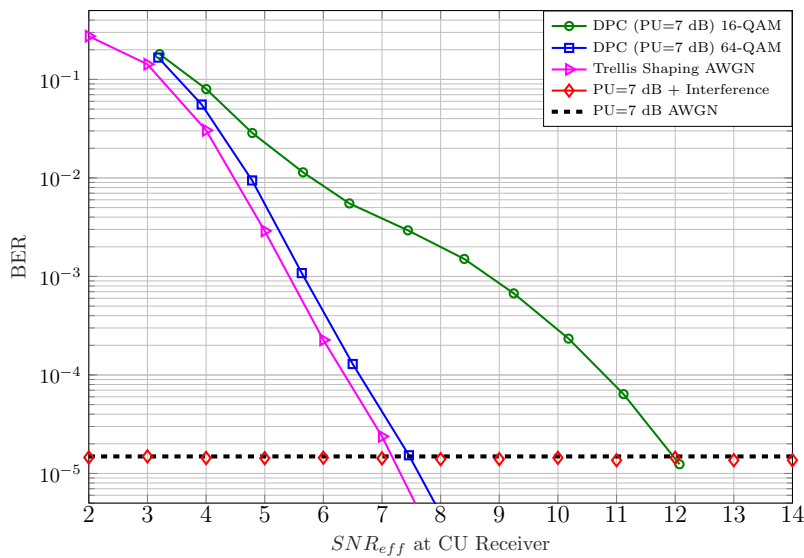
(b) Scatterplot for $P_P = 7$ dB and X_{cc}^n as 64-QAM



(c) Histogram of X_{cc}^n as 16-QAM for $P_P = 7$ dB

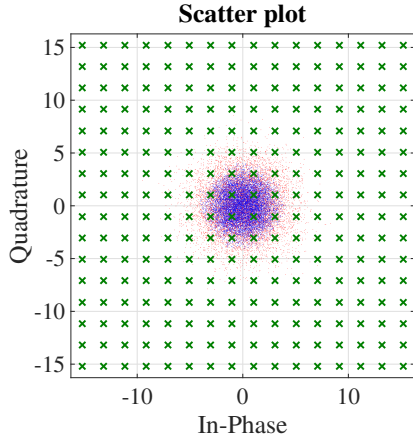


(d) Histogram of X_{cc}^n as 64-QAM for $P_P = 7$ dB

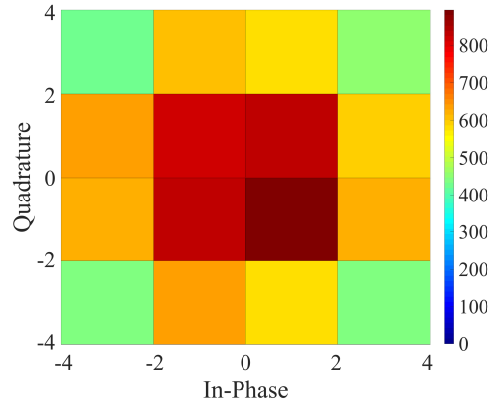


(e) BER of the Cognitive User at $P_P = 7$ dB

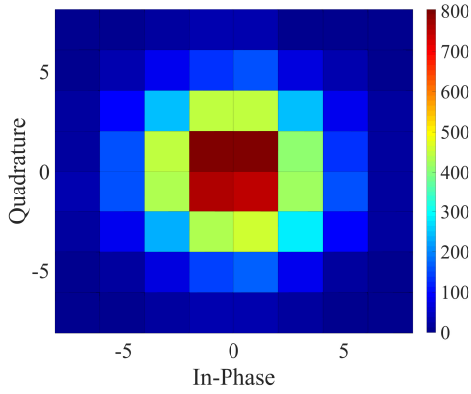
Figure 4-6: Results and analysis for $P_P = 7$ dB



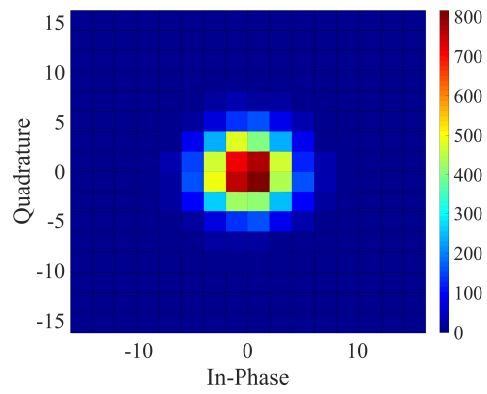
(a) Scatterplot for $P_P = 15$ dB and X_{cc}^n as 256-QAM



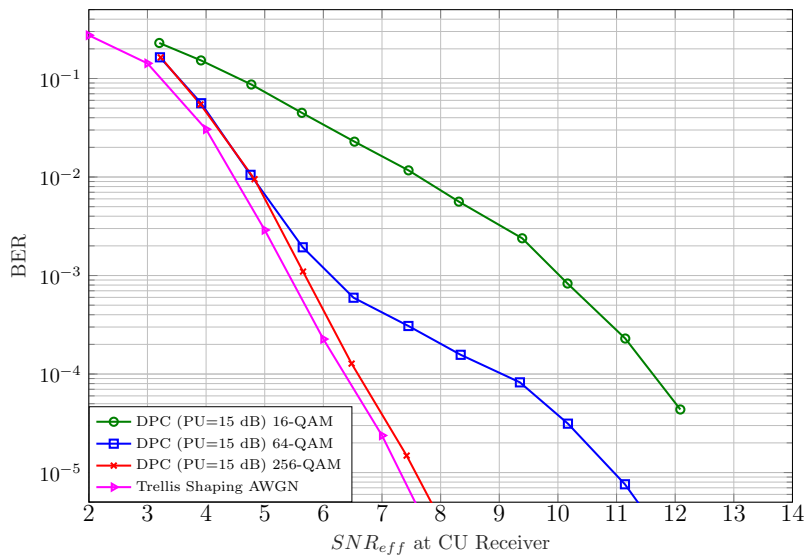
(b) Histogram of X_{cc}^n as 16-QAM for $P_P = 15$ dB



(c) Histogram of X_{cc}^n as 64-QAM for $P_P = 15$ dB



(d) Histogram of X_{cc}^n as 256-QAM for $P_P = 15$ dB



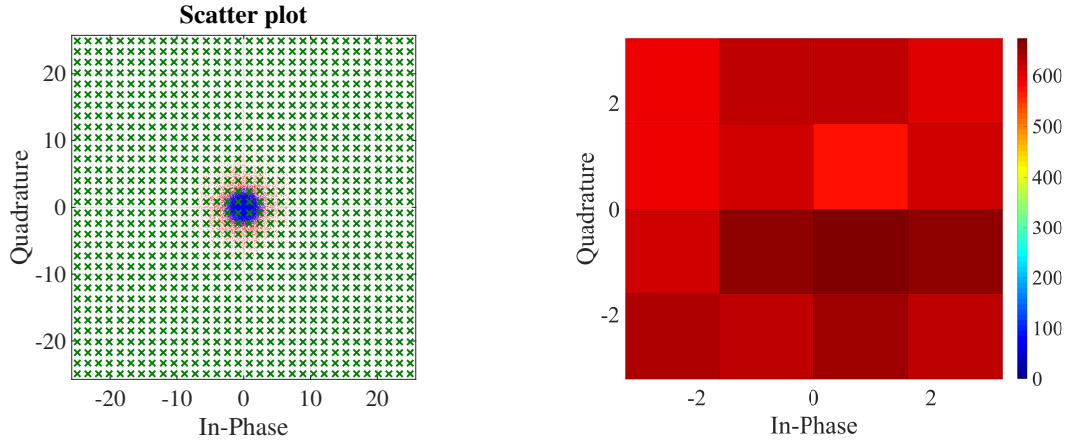
(e) BER of the Cognitive User at $P_P = 15$ dB

Figure 4-7: Results and analysis for $P_P = 15$ dB

of boundary constellation points decrease as further expansion is considered.

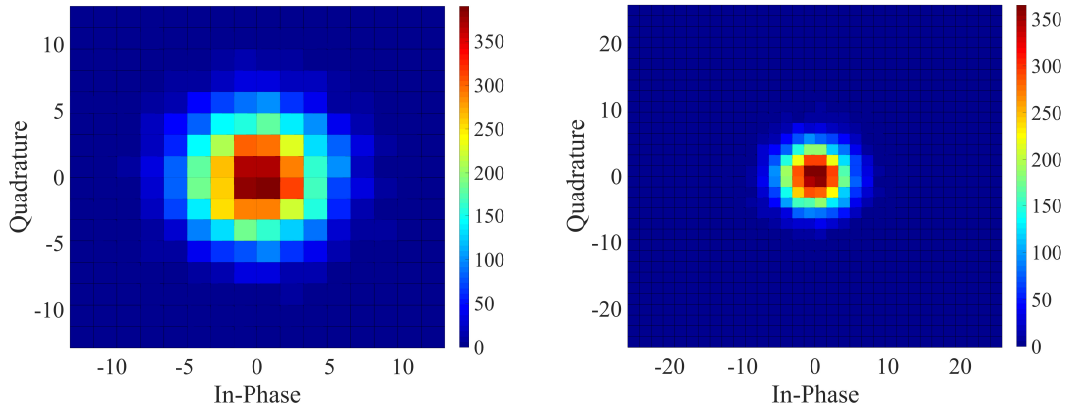
The Fig. 4-8e presents the BER curves for this scenario. We observe that the modulo loss is significantly high for the 16-QAM and 64-QAM schemes. However, when 256-QAM is considered, the degradation just becomes present after 7 dB of SNR, displaying a gap less than 1 dB when compared with the reference TS-AWGN scheme for a BER of 10^{-5} . This could be inferred by the increase of λ in this SNR region. When 1024-QAM is implemented, the same performance limit (gap less than 0.3 dB) is reached. Once again, the maintenance of the PU service is evaluated by attesting the exact specified SINR_P at the primary receiver.

The implementation of 1024-QAM at the transmitter side could be seen as prohibitive in reference to satellite communications. However, we emphasize that the impact is only on the increase of the system complexity, since more comparisons should be performed by the shaping operation. As we have discussed in Section 4.2.3, the \hat{X}_c^n signal is continuous within the squared region bounded by $\Delta = 4d_{min}$ (*i.e.* $|\text{Re}(\hat{X}_c)|$ and $|\text{Im}(\hat{X}_c)| < \Delta/2$, where Δ is the modulo boundary). Thus, the transmitted power (*i.e.* $E[|\hat{X}_c^n|^2]$) as well as the Peak-to-Average Power Ratio (PAPR) remain in the same order, regardless the constellation expansion.



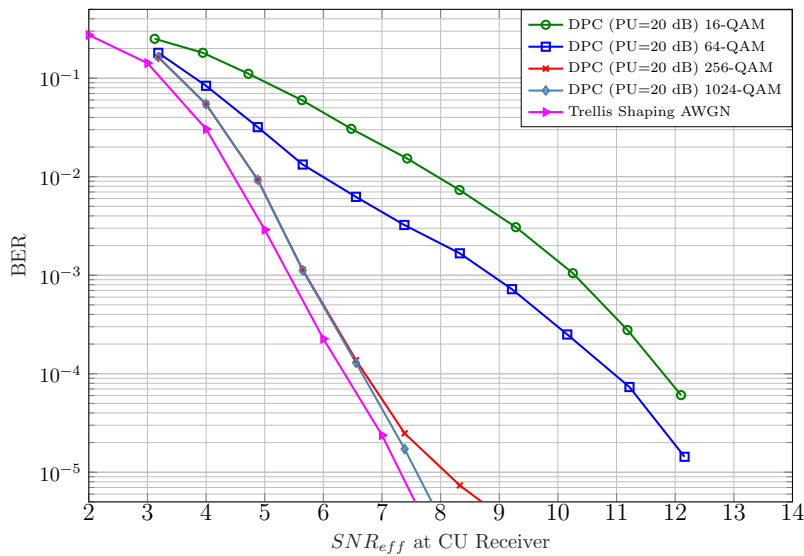
(a) Scatterplot for $P_P = 20$ dB and X_{cc}^n as 1024-QAM

(b) Histogram of X_{cc}^n for $P_P = 20$ dB and 16-QAM



(c) Histogram of X_{cc}^n for $P_P = 20$ dB and 256-QAM

(d) Histogram of X_{cc}^n for $P_P = 20$ dB and 1024-QAM



(e) BER of the Cognitive User at $P_P = 20$ dB

Figure 4-8: Results and analysis for $P_P = 20$ dB

4.3 On the Modulo Loss Recovering at the Decoder

In the Chapter 3, we have proposed a scheme with slight constellation expansion to recover part of the shaping loss (our assigned shaping code C_s reaches a gain of 0.97 dB of maximum achievable of 1.53). On the other hand, we have demonstrated that this simple solution suffers a significant degradation due to the THP losses, which are separated as: (i) the modulo loss (about 4 – 5 dB) and the power loss (about 0.3 dB). Furthermore, our discussions pointed out the relation of this degradation with the X_{cc}^n distribution and the decoding process (see Section 3.4.4 for further details).

To recover the modulo loss, the last section proposed a method that gradually expands the X_{cc}^n constellation, avoiding the boundary point selection according to the amount of interference present in the channel. As a consequence, we analysed a trade-off between the power efficiency and complexity.

Although the last results have presented an almost full recovering of the THP losses, with total mitigation of the modulo loss and limited only by the small power loss existing in the system, the proposed high constellation expansion (also considered in [29, 30, 53]) might not be encouraged in some practical satellite transmitters, where the low complexity is many times adopted as the most decisive factor. Thus, according to the service application, it is convenient for satellite communications systems that the complexity be settled at the receiver side.

With regard to the above, we present in this section a solution that implements a slightly different decoding process at the receiver. The metric for the convolutional decoder C_c also captures the modulo operation, mitigating the modulo loss at our SNR of interest. In this sense, the DPC decoder reaches a performance of a sub-optimal TCM, by increasing the decision region of the parallel transitions branches in the trellis for C_c .

4.3.1 Method Description

The Fig. 4-9 represents the reception of a DPC communication system without modulo (as considered in [29]) and with modulo (as our proposed DPC scheme). Two cases are illustrated: for intermediate and low SNR regimes (Fig. 4-9a and Fig. 4-9b,

respectively). In this example, at the transmitter, the symbol "0" (corner point) is assigned at the X_{cc}^n constellation and the interference presubtracted signal \hat{X}_c^n is transmitted. Assuming for simplicity that λ is unitary and that the channel interference is totally canceled at the receiver input, the received signal Y_s^n is formed by X_{cc}^n corrupted by the additive Gaussian noise Z^n , as represented by the red dots. By continuing the DPC receiver chain (Fig. 3-2), the modulo operation is performed, resulting in the \hat{Y}_s^n signal at the decoder input.

By implementing the same decoding strategy used during this thesis, a hard decision among the parallel transition is performed (see Fig. 3-4). Thus, in our example, the decision should be performed among the symbols "0" (transmitted symbol), "4", "8" and "12", corresponding to the marker "○". We investigate the following metrics to selected the estimated symbol \hat{X}_{cc} :

$$d_A^k = \|Y_s - X_{cc,k}\|^2; \quad (4.4)$$

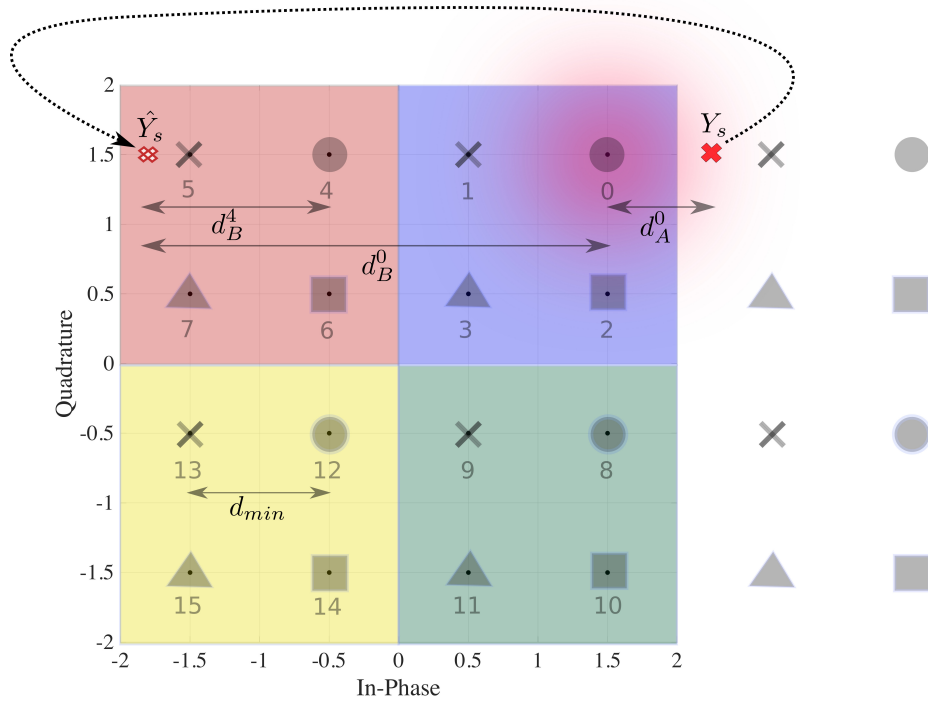
$$d_B^k = \|\hat{Y}_s - X_{cc,k}\|^2; \quad (4.5)$$

$$d_C^k = \|[\hat{Y}_s - X_{cc,k}]_{\text{MOD}_\Delta}\|^2 = \|[Y_s - X_{cc,k}]_{\text{MOD}_\Delta}\|^2, \quad (4.6)$$

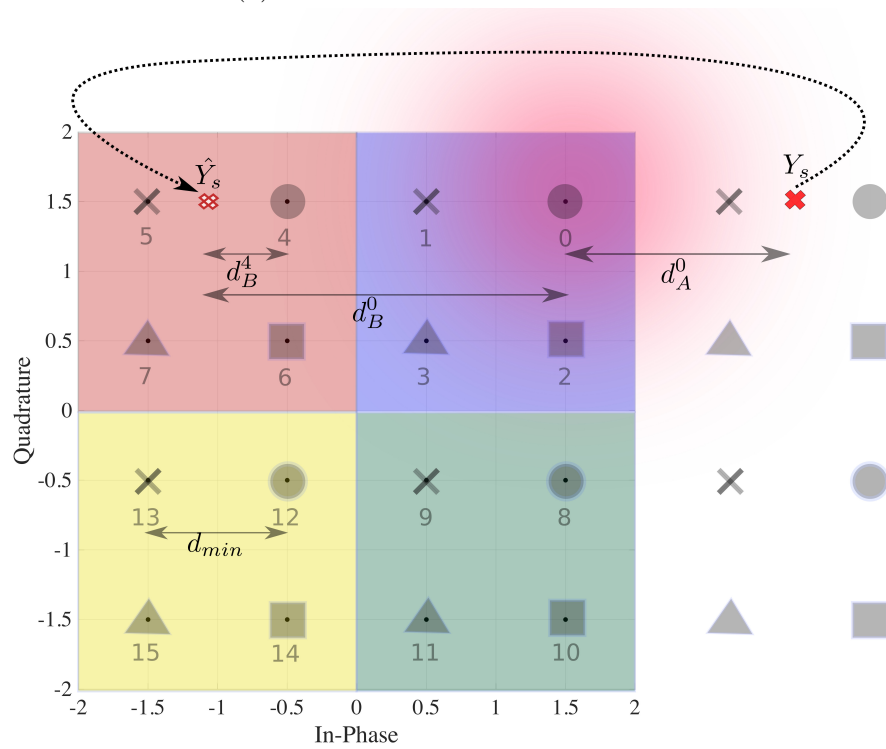
where the index k is related to the X_{cc}^n constellation symbol.

The metric d_A^k is implemented for system without modulo operation at both the transmitter and receiver. This is the case when the interference is totally confined within the expanded constellation X_{cc}^n . As a consequence, the modulo becomes non-functional and can be removed [29]. Moreover, this is the metric employed in the usual TCM decoders (as in our reference TCM scheme with TS).

In turn, the metric d_B^k is implemented in our previous DPC schemes, further discussed in the last section. The modulo is deployed at the transmitter, to limit the transmitted output power, and at the receiver, to mitigate the interference. As a consequence, the hard decision is performed considering the \hat{Y}_s signal, since the previous Y_s^n information is irrecoverable after the receiver modulo processing. Thus, we have observed that, if the constellation is not properly expanded, the modulo loss



(a) Case 1 - Intermediate SNR



(b) Case 2 - Low SNR

Figure 4-9: Modulo loss recovering at the receiver side

degrades the system performance.

Finally, the metric d_C^k is proposed in this section. The hard decision is also performed in respect to \hat{Y}_s signal, but the slight difference is that the modulo operation is also captured by the metric. The intuition behind this assumptions lies in the application of the same procedure previously adopted in the shaping *Viterbi* minimization at the transmitter side (see Eq. (3.1)). By implementing the equivalent concept at the receiver, we envisage to find the minimization that the most likely results according the noised observation \hat{Y}_s .

Next, we exemplify these metric decisions. Two cases are considered, regarding the SNR regimes:

Case 1: Intermediate SNR ($|\operatorname{Re}(Z)|$ and $|\operatorname{Im}(Z)| < d_{min}$).

In this first case, depicted in the Fig. 4-9a, the additive noise Z is bounded in both in-phase and quadrature components by the constellation minimum distance d_{min} .

As a numerical example, we attribute the receiver and decoder input signals, respectively, as:

$$Y_s = 2.25 + j1.5;$$

$$\hat{Y}_s = [Y_s]_{\text{MOD}_\Delta} = -1.75 + j1.5.$$

In addition, the X_{cc} constellation points, corresponding to the trellis parallel paths, are defined as:

$$X_{cc,0} = 1.5 + j1.5;$$

$$X_{cc,4} = -0.5 + j1.5;$$

$$X_{cc,8} = 1.5 - j0.5;$$

$$X_{cc,12} = -0.5 - j0.5.$$

Following the metric computations for estimation of \hat{X}_{cc} :

(A) For DPC decoding without modulo operation at the transmitter and receiver,

we have:

$$\hat{X}_{cc} = \arg \min_{k \in \{0,4,8,12\}} d_A^k$$

$$d_A^0 = 0.5625 ;$$

$$d_A^4 = 7.5625 ;$$

$$d_A^8 = 4.5625 ;$$

$$d_A^{12} = 11.5625.$$

Thus, the estimation is correctly performed. The symbol "0" along with its respective metric are assigned to the corresponding trellis transition (cf. Fig. 3-4):

$$\hat{X}_{cc} = X_{cc,0}.$$

(B) Considering now the second DPC decoding metrics d_B^k :

$$\hat{X}_{cc} = \arg \min_{k \in \{0,4,8,12\}} d_B^k$$

$$d_B^0 = 10.5625 ;$$

$$d_B^4 = 1.5625 ;$$

$$d_B^8 = 14.5625 ;$$

$$d_B^{12} = 5.5625.$$

As we observe, the estimation is incorrectly performed, since the symbol "4" along with its respective metric are assigned in the *Viterbi* decoder:

$$\hat{X}_{cc} = X_{cc,4}.$$

(C) We consider now our slight modified metric, which captures the modulo operation:

$$\hat{X}_{cc} = \arg \min_{k \in \{0,4,8,12\}} d_C^k$$

$$d_C^0 = 0.5625 ;$$

$$d_C^4 = 1.5625 ;$$

$$d_C^8 = 4.5625 ;$$

$$d_C^{12} = 5.5625.$$

We notice, by implementing this adaptation in the decision metric, that the symbol "0" is also correctly decided in DPC schemes with modulo. Furthermore, we realize that the same distance in both DPC decoding is obtained:

$$\hat{X}_{cc} = X_{cc,0},$$

$$d_A^0 = d_C^0.$$

Case 2: Low SNR ($|\operatorname{Re}(Z)|$ or $|\operatorname{Im}(Z)| > d_{min}$).

In our second case, depicted in the Fig. 4-9b, we investigate the same decision metrics in the low-SNR regime.

For this example, the signals at receiver and decoder inputs are assumed as:

$$Y_s = 3 + j1.5;$$

$$\hat{Y}_s = [Y_s]_{\text{MOD}_\Delta} = -1 + j1.5.$$

The same attributed X_{cc} constellation points in the previous case are considered. In the same way, we compute the metrics:

(A) For DPC decoding, without modulo operation at both the transmitter and the receiver, we have:

$$\hat{X}_{cc} = \arg \min_{k \in \{0,4,8,12\}} d_A^k$$

$$d_A^0 = 2.25 ;$$

$$d_A^4 = 12.25 ;$$

$$d_A^8 = 6.25 ;$$

$$d_A^{12} = 16.25.$$

Thus, the correct decision is performed. $\hat{X}_{cc} = X_{cc,0}$.

(B) For our previous decoding DPC metric, given by d_B^k :

$$\hat{X}_{cc} = \arg \min_{k \in \{0,4,8,12\}} d_B^k$$

$$d_B^0 = 6.25 ;$$

$$d_B^4 = 0.25 ;$$

$$d_B^8 = 10.25 ;$$

$$d_B^{12} = 4.25.$$

Thus, the wrong decision is made:

$$\hat{X}_{cc} = X_{cc,4}.$$

(C) For DPC decoding with the proposed metric:

$$\hat{X}_{cc} = \arg \min_{k \in \{0,4,8,12\}} d_C^k$$

$$d_C^0 = 2.25 ;$$

$$d_C^4 = 0.25 ;$$

$$d_C^8 = 6.25 ;$$

$$d_C^{12} = 4.25.$$

Thus, on the contrary to the case 1, the symbol decision is incorrect. We observe that the proposed metric is not effective in low-SNR regime:

$$\hat{X}_{cc} = X_{cc,4}.$$

Fig. 4-10 summarizes the effect of the proposed metric d_C^k in the *Voronoi* region \mathcal{V}_C^k (represented in dark colors) still considering the same example. All constellation symbols have the same decision region, delimited by d_{min} . As a consequence, we can infer that the modulo loss may be recovered in intermediate and high SNR regimes. Also, by extending this region, we have \mathcal{V}_A^k (represented in pale colors), that represents the system without modulo at both the transmitter and the receiver, determined by the metric d_A^k . Finally, the modulo region \mathcal{R}_Δ is illustrated by the dashed line and the *Voronoi* region \mathcal{V}_B^k , corresponding to the metric d_B^k , is given as:

$$\mathcal{V}_B^k = \mathcal{V}_A^k \cap \mathcal{R}_\Delta; \tag{4.7}$$

It is worth noting that the regions are further increased when d_C^k is implemented instead of d_B^k . By inspection of the same figure, we compute the decisions regions for each decoding metric discussed in this section:

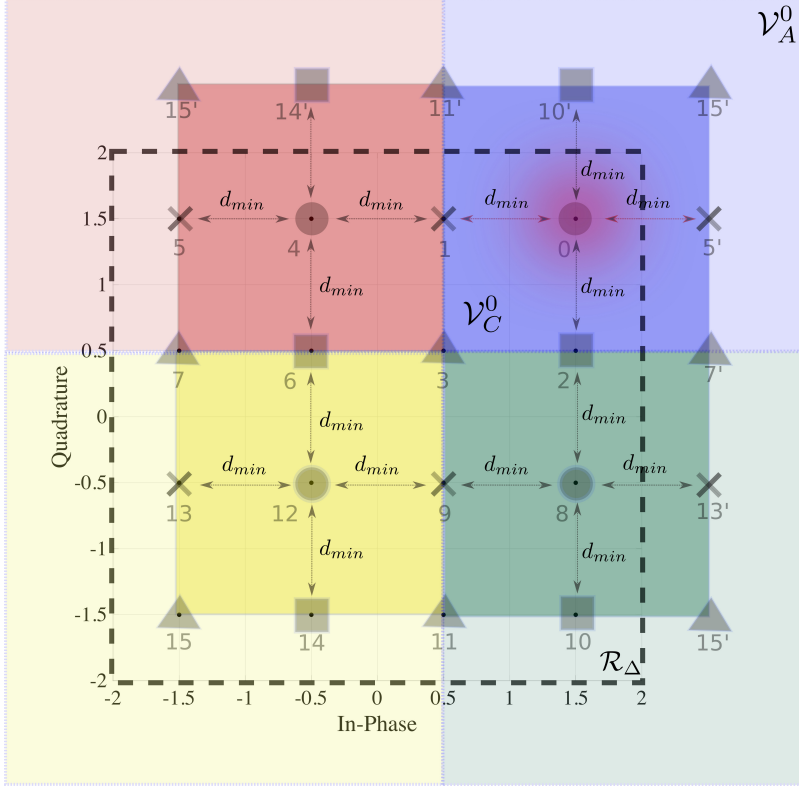


Figure 4-10: Decision regions of the investigated metrics.

- Considering the TCM region, or metric d_A^k :

$$\mathcal{V}_A^0 = \text{Re}(Z) > -d_{min} \text{ and } \text{Im}(Z) > -d_{min};$$

$$\mathcal{V}_A^4 = \text{Re}(Z) < d_{min} \text{ and } \text{Im}(Z) > -d_{min};$$

$$\mathcal{V}_A^8 = \text{Re}(Z) > -d_{min} \text{ and } \text{Im}(Z) < d_{min};$$

$$\mathcal{V}_A^{12} = \text{Re}(Z) < d_{min} \text{ and } \text{Im}(Z) < d_{min}.$$

- Considering the DPC region and metric d_B^k :

$$\mathcal{V}_B^0 = -d_{min} < \text{Re}(Z) < \frac{d_{min}}{2} \text{ and } -d_{min} < \text{Im}(Z) < \frac{d_{min}}{2};$$

$$\mathcal{V}_B^4 = -\frac{3d_{min}}{2} < \text{Re}(Z) < d_{min} \text{ and } -d_{min} < \text{Im}(Z) < \frac{d_{min}}{2};$$

$$\mathcal{V}_B^8 = -d_{min} < \text{Re}(Z) < \frac{d_{min}}{2} \text{ and } -\frac{3d_{min}}{2} < \text{Im}(Z) < d_{min};$$

$$\mathcal{V}_B^{12} = -\frac{3d_{min}}{2} < \text{Re}(Z) < d_{min} \text{ and } -\frac{3d_{min}}{2} < \text{Im}(Z) < d_{min}.$$

- Considering the DPC region and proposed metric d_C^k :

$$\mathcal{V}_C^0 = \mathcal{V}_C^4 = \mathcal{V}_C^8 = \mathcal{V}_C^{12} = |\text{Re}(Z)| \text{ and } |\text{Im}(Z)| < d_{min}.$$

4.3.2 Results and Analysis of the Proposed Metric

To evaluate the proposed scheme, the Fig. 4-11 and Fig. 4-12 present the BER curve for low ($P_P = 3$ dB) and extremely high ($P_P = 20$ dB) interference scenarios. At the transmitter, a low complexity scheme is considered, which implements a slight constellation expansion of $n_s = 2$ (as in the Chapter 3). We investigate the performance in respect to the discussed metrics d_A^k , d_B^k and d_C^k for the *Viterbi* decoder at the reception.

Firstly, we analyze the BER performance for low interference scenario ($P_P = 3$ dB), presented in Fig. 4-11. We point out that, as the interference is totally confined within the expanded 16-QAM constellation (previously analysed in the Fig. 4-5a), the power of the transmitted signal \hat{X}_c^n is not increased after the presubtraction operation. This satisfies the main DPC requirement and, in this sense, the modulo becomes unnecessary for the system (at the transmitter and, consequently, at the receiver). Due to this fact, the receiver metric d_A^k can be implemented. and the system is only degraded by the shaping and power losses [29]. As the shaping gain is the same as reached by our reference TS-AWGN scheme, the degradation is only within 0.3 dB, uniquely due to the power loss. We can compare this result with our previous analysis that utilized the modulo and, consequently, the receiver metric d_B^k . By inspection of the figure, we notice that the degradation is about 4 dB for a BER of 10^{-5} , characterizing the modulo loss disturbance.

Remarkably, we observe that, even preserving the modulo in the system, but slightly modifying the receiver by implementing our proposed metric d_C^k , the exactly same performance as the system without modulo is obtained (d_A^k). In other words, by capturing the modulo operation in the metric, the modulo loss is totally recovered in this intermediate SNR regime. In addition, we can infer that the condition $|\text{Re}(Z)|$ or $|\text{Im}(Z)| < d_{min}$ is also maintained by the employment of the PIP technique, which decreases λ in low SNR. In summary, by this BER results, we quantitatively assimilate the favorable impact of the *Voronoi* region expansion of \mathcal{V}_C^k in respect to \mathcal{V}_B^k , underlined in Fig. 4-10.

Regarding the extremely high interference scenario ($P_P = 20$ dB), we realize that it is not possible to implement a DPC scheme without modulo due to the increase of the transmitted power after the presubtraction. By analyzing the schemes with modulo

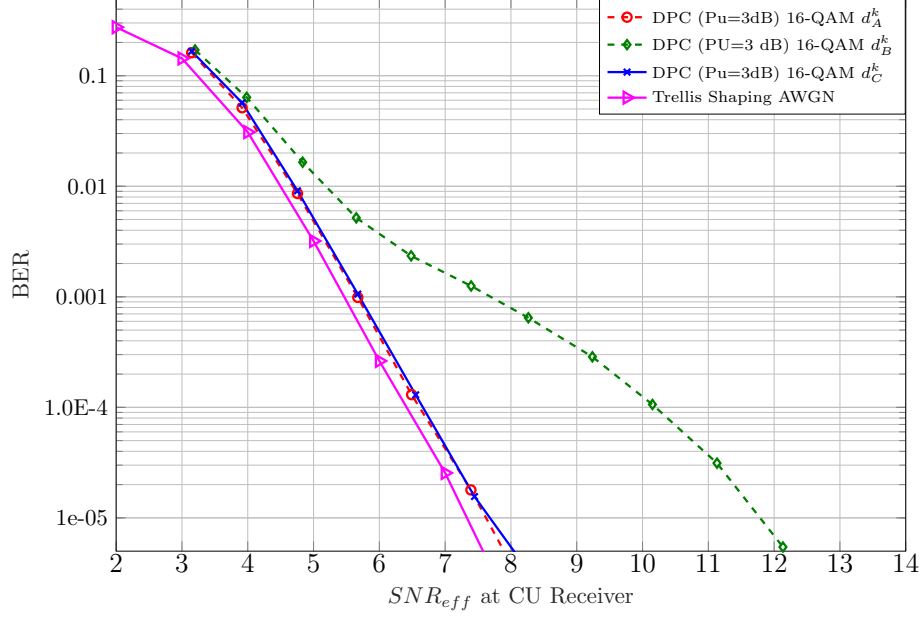


Figure 4-11: BER of cognitive user considering different TCM decoder metrics at receiver for $P_P = 3$ dB.

to limit the transmitted power, we observe in the Fig. 4-12 that a high degradation is obtained when the metric d_B^k is employed, since we have a n -cube X_{cc} distribution in this case (see Fig. 4-8b). However, when the proposed metric d_C^k is employed, even for this extremely high amount of interference, the degradation is also within 0.3 dB, exclusively limited by the power loss.

Finally, we underline that the same performance is reached for both interfering scenarios. It means that, for this SNR operation range, the modulo loss is totally recovered by this method, regardless the interference amount. The main contribution of this result is the achievement of almost full THP losses recovery without high constellation expansion (as presented in the Section 5.3.2 and in [29, 30]). When considering the satellite application, it may be an important solution to guarantees low complexity transmitter design.

The Table 4.1 summarizes the impact of the investigated metrics on the DPC system:

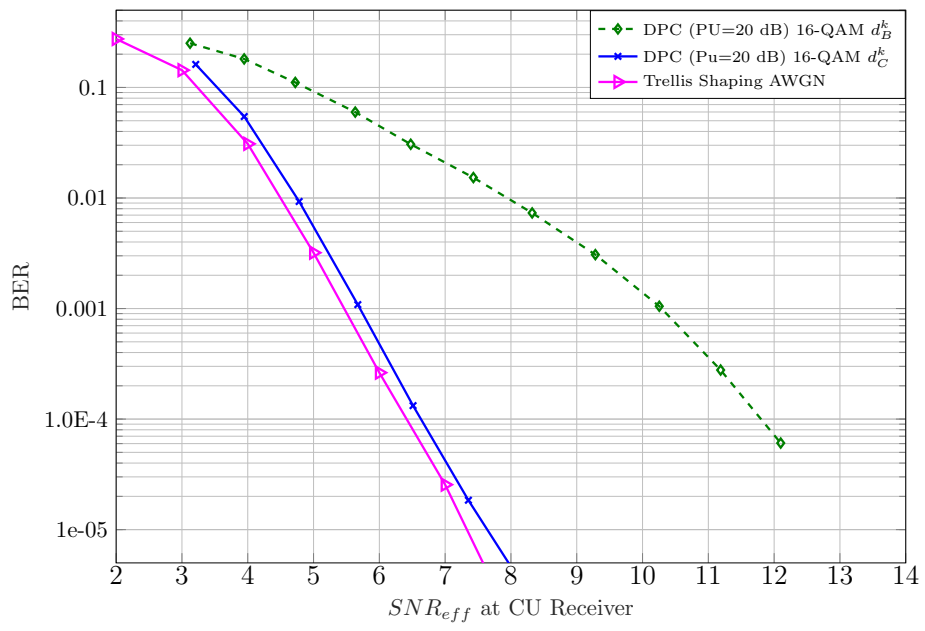


Figure 4-12: BER of cognitive user considering different TCM decoder metrics at receiver for $P_P = 20$ dB.

Table 4.1: Summary of the investigated receiver metrics on DPC schemes.

d_i^k	\mathcal{V}_i^0	\mathcal{V}_i^4	\mathcal{V}_i^8	\mathcal{V}_i^{12}	+	-
A	$\text{Re}(Z) > -d_{min} \cap$ $\text{Im}(Z) > -d_{min}$	$\text{Re}(Z) < d_{min} \cap$ $\text{Im}(Z) > -d_{min}$	$\text{Re}(Z) > -d_{min} \cap$ $\text{Im}(Z) < d_{min}$	$\text{Re}(Z) < d_{min} \cap$ $\text{Im}(Z) < d_{min}$	No mod loss Rx complexity	> Tx power Power loss (0.28 dB)
B	$-d_{min} < \text{Re}(Z) < \frac{d_{min}}{2} \cap$ $-d_{min} < \text{Im}(Z) < \frac{d_{min}}{2}$	$-\frac{3d_{min}}{2} < \text{Re}(Z) < d_{min} \cap$ $-d_{min} < \text{Im}(Z) < \frac{d_{min}}{2}$	$-d_{min} < \text{Re}(Z) < \frac{d_{min}}{2} \cap$ $-\frac{3d_{min}}{2} < \text{Im}(Z) < d_{min}$	$-\frac{3d_{min}}{2} < \text{Re}(Z) < d_{min} \cap$ $-\frac{3d_{min}}{2} < \text{Im}(Z) < d_{min}$	Tx power control Rx complexity	Mod loss (> 4 dB) Power loss (0.28 dB)
C	$ \text{Re}(Z) < d_{min} \cap$ $ \text{Im}(Z) < d_{min}$	$ \text{Re}(Z) < d_{min} \cap$ $ \text{Im}(Z) < d_{min}$	$ \text{Re}(Z) < d_{min} \cap$ $ \text{Im}(Z) < d_{min}$	$ \text{Re}(Z) < d_{min} \cap$ $ \text{Im}(Z) < d_{min}$	Tx power control Mod loss recover	> Rx complexity Power loss (0.28 dB)

4.4 Discussion of the Chapter Results

The main objective of this Chapter was to propose solutions for the open points identified in the Chapter 3.

Firstly, the exact PU performance was guaranteed by a method which uses the shaping gain, provided by the shaping code C_s , to scale the minimum distance d_{min} of the coded constellation X_{cc}^n . We demonstrated that both links are affected by this strategy.

After that, we focused the investigation on the modulo loss recovering. Two different methods were considered: (i) a X_{cc}^n constellation expansion at the transmitter, in order to avoid selected boundaries points and (ii) a slight modification in the metric of the convolutional decoder at the receiver.

For the first approach, we also emphasized the importance of mapping design, that must properly assign the *auxiliary* shaping bits. Also, we analyzed the proposed solution, providing a trade-off between complexity *vs* power efficiency. In the second approach, we transferred the moderate complexity from the transmitter to the receiver. We investigate the proposed scheme as a function of the channel interference.

Both solutions presented the same BER performance, limited by the THP power loss (theoretically evaluated as 0.28 dB) and were validated by simulations.

4.5 Summary

This Chapter presents a design method of cognitive overlay links for satellite communications. Different schemes were implemented in different realistic scenarios. The results presented the exactly same bit error rate for the primary user when compared with its performance on the corresponding AWGN channel. By proposing two different approaches, the cognitive user presented a gap within 0.3 dB in comparison to the reference trellis shaping scheme over the AWGN channel.

In the next Chapter 5, we will analyse the exposed techniques in a realistic satellite scenario, focusing on the feasibility of low data rate secondary service transmission.

Chapter 5

On the Feasibility of a Secondary Service Transmission Over an Existent Satellite Infrastructure

Contents

5.1	Introduction	104
5.2	Practical System Analysis	106
5.2.1	System Engineering Design	106
5.2.2	Techniques Design	106
5.3	Realistic Use Case	107
5.3.1	Primary Service Transmission Analysis	107
5.3.2	Secondary Service Transmission Analysis	109
5.4	Conclusion	113

In this Chapter, we present a realistic use case in order to investigate the feasibility of a secondary service transmission over an existent satellite infrastructure. By employing the overlay cognitive radio paradigm towards satellite communications, and by adopting the techniques previously developed in the last two chapters, we compute the theoretical achievable data rate. This later varies in the range of around 16 (minimum) and 90 (maximum) kbps for the secondary service, which are suitable for most of Machine-to-Machine (M2M) applications [1, 63, 64]. In this sense, the

previously discussed tradeoff between power efficiency (*i.e.* higher data rate) and complexity is considered in a practical scenario. Using simulation results and link budget computations, we also show that this can be achieved while preserving the primary service performance. In addition, a system design framework is discussed in order to dimension such systems by considering practical implementation.

A large part of this contribution was presented in [34] and had its extended version published in *EURASIP Journal on Wireless Communications and Networking*, in the special issue *New application domains for the cognitive-based solutions in the context of 5G and beyond*. Furthermore, by using the simplest scheme (*i.e.* with lowest achievable bit rate), we proposed the application of these techniques for the watermarking transmission scheme for CubeSat. This latter study was presented in 10th *European CubeSat Symposium* [35].

5.1 Introduction

In the manuscript opening, we emphasized the opportunistic spectrum sharing strategy. A significant amount of this perception is highly related to the increase of CubeSat missions. In a historical approach, by the early of 2000s, the CubeSat design was conceptually standardized and emerged as a low cost alternative for space access. This fact allowed the implementation, for instance, of store and forward payload systems (S&F), which have been able to connect two arbitrary points on the Earth by a non-real time transmission at moderate data rates. On other hand, due to the limited processing and physical constraints, the satellite should be conceived in a quite low complexity way employing, whenever possible, Commercial Off-The-Shelf (COTS) components [65]. Based on the above and supported by the increasingly higher reliability of the components and materials available, CubeSats have been attracting much-deserved attention, not only for academic proposals but also for professional applications.

Also accentuated in our context description, the employment of the satellite-based Machine-to-Machine (M2M) communications allows the data global access [1]. Moreover, the satellite transmission is safer, harder to disrupt, and easier to deploy in remote area than terrestrial networks [64]. Due to the superposition strategy, the

remaining power for secondary service transmission is quite limited, which leads to low supported bit rate. In this sense, considering the required bit rate of most M2M applications (< 100 kbps), the use of the Cognitive User (CU) transmission is suitable for this service.

As another application to the scheme introduced in this thesis, also regarding the range of bit rate, is the need of the confidentiality as well as the integrity and authentication of the received data by the Earth terminals. In this way, a scheme that transmits a watermarking like signal using Dirty-Paper Coding (DPC) technique could be proposed for data validation, as presented in [35]. In this context, adopting CR nomenclature, the Primary User (PU) represents the original transmitted signal and the CU carries the watermarking information. Both signals are summed and transmitted by the same satellite antenna, respecting the power constraints and without degrading the performance of the primary service. The reception is realized either by one single terminal equipped with two decoders or two physically separated decoders, one for the original signal and the another for the watermarking.

This Chapter presents a practical scenario for the techniques previously exposed in the last chapters, which concern the design of the overlay paradigm transmission towards satellite communication systems. By using the concepts and the framework detailed in the last Chapter 3 and Chapter 4, we extend the previous analysis focusing on the feasibility of a low data rate transmission. As we have discussed, the superposition strategy reduces the power utilized for secondary service transmission. Therefore, it is necessary to investigate how the proposed solutions fit in a realistic scenario.

In this sense, a practical use case is investigated, which considers a CubeSat designed with COTS parts [66] and assumes realistic link budget parameters in its evaluation. The discussions and results contained herein could be seen as part of a "preliminary phase" of an engineering process plan [67].

Following this introduction, Section 5.2 points out some practical issues concerning the scenarios and techniques. Subsequently, in Section 5.3, a realistic scenario is investigated and a feasibility analysis is presented for both users. Finally, Section 5.4 is dedicated to the conclusions.

5.2 Practical System Analysis

This section intends to point out some practical issues concerning the techniques exposed and its application in the satellite scenario.

5.2.1 System Engineering Design

As a matter of system engineering, the design for the CU payload could either be a standalone system (implemented by a dedicated transmission chain and antenna) or a shared transmitter (by using the same transponder and antenna as the PU). In this latter configuration, notice that more caution should be taken into account when the transmission of both signals inputs the same High Power Amplifier (HPA). In fact, this practice should be avoided since this implementation may induce higher nonlinear distortions, particularly in terms of AM/AM and AM/PM conversions [68].

Moreover, at the receiver side (PU and CU), two scenarios could be encountered: (i) by the deployment of geographically separated receiving sites for each user, and thus reducing the interference due to the attenuation at the interfering paths, or (ii) by using the same receiving station with two dedicated demodulators and decoders. In this last case, the attenuation of the interfering and direct paths are the same (i.e. $|h| = |h_{pp,i}| = |h_{cc}| = |h_{pc,i}| = |h_{cp,i}|$). In fact, this increases the interference of both links and, as a consequence, requires higher value of the superposition factor α .

5.2.2 Techniques Design

Deepening our vision on the techniques described, we point out that, due to the superposition, the bit rate of the secondary service might be very low with respect to the primary. However, this practice generates two implementation problems: (i) in the presubtraction operation of the DPC technique (see Eq. (2.39)), the same symbol rate for both signals is considered for the coded signal X_{cc} and the interference S and (ii) in the superposition technique, the interference generated by the CU signal would appear as spikes in the PU bandwidth, which makes the usual interference model [69] unrealistic in this case. In order to avoid both constraints, we can think of the implementation of the chirp spread spectrum technique [41] at CU transmission. In

this sense, the DPC encoder can correctly perform its operation and the CU receiver can demodulate at a more flexible transmitted data rate.

To improve the whole system performance, the channel estimation techniques could be realized at the terminals end through a feedback link, for instance, according to the DVB-S2X standard [6]. By these features, the superposition factor α , which depends directly on the channels conditions, as well as the λ , which depends on SNR, can be periodically updated, changing the achievable secondary service data rate and, as consequence, optimizing CU performance.

5.3 Realistic Use Case

In order to investigate the system feasibility, we adopt a scenario where a Cubesat is at a altitude of 600 km with the same orbital parameters as [70]. In addition, the design considers COTS parts and transmits both signals (primary and cognitive) from the same satellite antenna towards a single Earth station, which is equipped with two dedicated demodulators. In this sense, the channel attenuations are the same and defined as $|h|$. In this study, without loss of generality, just the downlink is considered.

The next sections describe the design procedure by separately analyzing both transmissions. The evaluation of the parameters as well as the practical notes concerning the implemented assumptions are detailed in Appendix B.

5.3.1 Primary Service Transmission Analysis

The main specification for the PU signal are: output power of 1 W [66], operating frequency of 2200 MHz (the downlink band for Earth Exploration Satellite Service - EESS [5]), bit rate of 3.4 Mbps, BER specified to 10^{-5} and coded QPSK modulation with Forward Error Correction (FEC) ($R = 1/2$). The following Table 5.1 presents the link budget of PU, without secondary service addition (see Appendix B for details):

It is worth noting that a conservative margin for demodulation losses of 6 dB is assumed in order to cover the impairments of the communication chain (nonlinear

Table 5.1: Primary User link budget (QPSK coded FEC R=1/2).

Frequency (MHz)	2200
Throughput rate (Mbps)	3.4
Transmitted power (mW)	1000
Satellite carrier EIRP (dBm)	38.3
Free space loss (dB)	-162.2
Depointing loss (dB)	-10
E. S. Antenna max gain - 5m, eff 50 % (dBi)	38.2
System noise temperature (K)	130
C/N0 (dB-Hz)	81.8
Eb/N0 (dB)	16.5
Demodulation losses (dB)	-6
Eb/N0 required (dB) – for BER = 1E-5	7
Margin (dB)	3.5

distortion (AM/AM and AM/PM), filter mismatches, modulator/demodulator imbalances, phase noise, residual AM etc.). The overall link margin is about 3.5 dB, as required by the targeted BER.

The principle behind this design strategy is to use part of the power remaining in this link margin to transmit the CU signal. Therefore, we defined that 900 mW are allocated for PU transmission (which meets the recommended link margin of 3 dB [71]) and 100 mW are assign for CU. Fig. 5-1 presents the overlay model considering this use case.

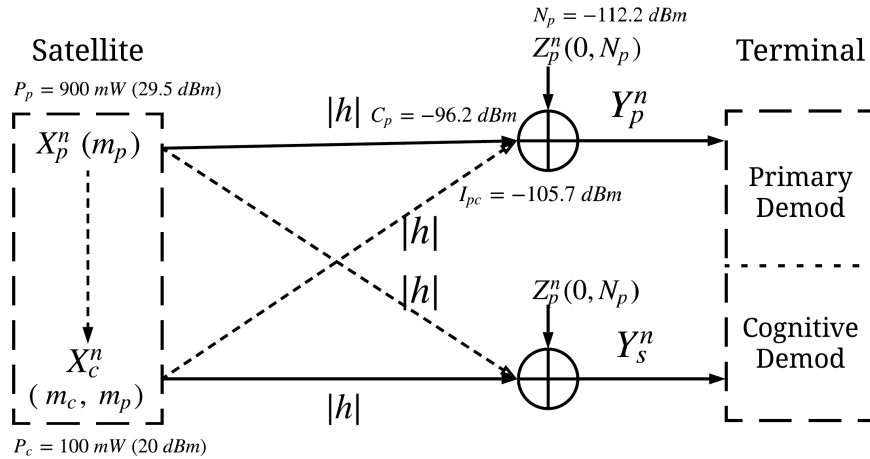


Figure 5-1: Overlay model considering realistic satellite link budget.

The transmitted and received powers are provided considering an example of a realistic link budget parameters. By computations according to the Table 5.1, the channel attenuations equal $\|h\|_{dB}^2 = -125.7$ dB. In this condition, the Interference-to-Noise Ratio (INR_p) and the PU link degradation D_p , due to the CU interference, are given by:

$$\text{INR}_p = \frac{I_{pc}}{N_p} = 4.47; \quad (5.1)$$

$$D_p(dB) = 10 \cdot \log_{10}(1 + \text{INR}) = 7.38 \text{ dB}. \quad (5.2)$$

Considering all parameters, the CU performs the superposition strategy and, by the Eq. (2.18), the factor $\alpha \approx 0.85$ is evaluated. This value guarantees a SINR of 16 dB at the input of PU receiver. We highlight that, thanks to the superposition strategy and the power controlling design of the DPC encoder (see results in Chapter 4), the PU maintains the same performance as in absence of the CU interference.

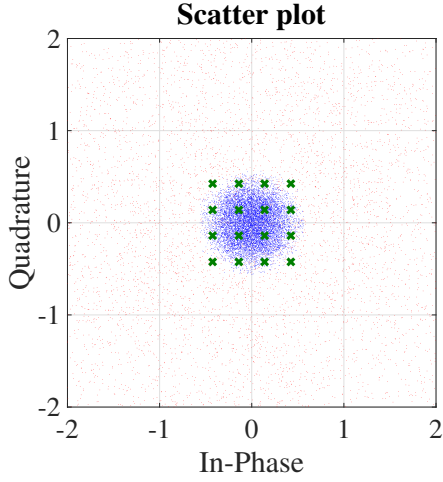
5.3.2 Secondary Service Transmission Analysis

Once the PU performance is guaranteed, from this point, a simulation for CU link is performed considering the whole CU channel interference, which is composed by the PU signal and the CU shared power in the superposition.

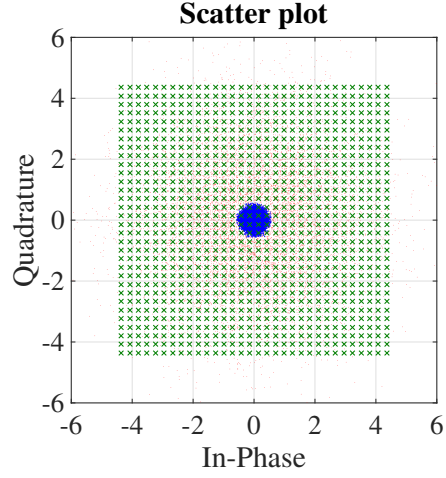
CU Results and Analysis

The system performance is analyzed for the scenario depicted Fig. 5-1. The main objective is to provide a comparative study regarding the different expansions of X_{cc}^n , emphasizing the trade-off between power efficiency *vs* complexity. Fig. 5-2 presents the main results.

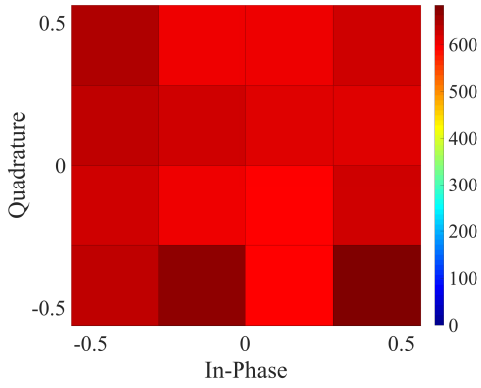
The scatter plot of the signal constellations, in the same way as the previous Chapters, are interpreted (represented in Fig. 5-2a and Fig. 5-2b). We recap that the expanded constellation signal X_{cc}^n is shown in green X. The Gaussian distributed version of the scaled interference λS^n is superposed in red points and the transmitted signal \hat{X}_c^n is shown in blue dots.



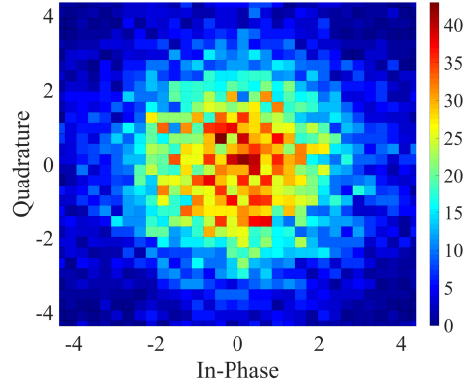
(a) Scatterplot for X_{cc}^n as 16-QAM.



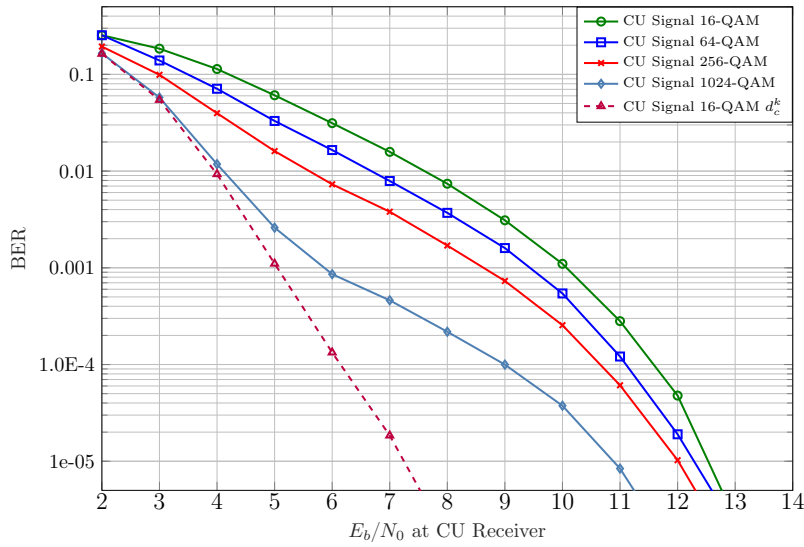
(b) Scatterplot for X_{cc}^n as 1024-QAM.



(c) Histogram of X_{cc}^n as 16-QAM.



(d) Histogram of X_{cc}^n as 1024-QAM.



(e) BER of the Cognitive User.

Figure 5-2: Results and analysis for CU, considering $10.\log_{10}(P_p/P_c) = 9.5$ dB and $\alpha = 0.85$, according to different constellation expansion.

Additionally, we also present the histogram of X_{cc}^n (resp. Fig. 5-2c and Fig. 5-2d) in order to inspect the probability of assignment for corner and edges constellation points.

We observe that, in this realistic scenario, the interference entering in the CU decoder is quite high. The scatter plots of minimum and maximum constellations expansion (resp. 16-QAM and 1024-QAM) are depicted in Fig. 5-2a and Fig. 5-2b. Also, the respective histograms Fig. 5-2c and Fig. 5-2d are shown. Without going into further details, since we have already discussed these concepts, we can notice by the representations that even the 1024-QAM is not expanded enough to avoid boundaries points. In this sense, the modulo loss degrades the system performance.

In addition, we consider the same 16-QAM scheme with the modified metric at the decoder, as explained in Section 4.3.

The Fig. 5-2e presents the BER curves for this scenario. Firstly, on the contrary of the previous BER results (for example, presented in Fig. 3-10 or Fig. 4-8e), in this case the BER is plotted as a function of the E_b/N_0 ratio instead of the defined SNR_{eff} (see Eq. (3.3)). This approach is classically considered in practical satellite designs [68], since only the white Gaussian noise Z^n is sensed at the receiver input, instead of the effective noise N' (given by Eq. (2.42)).

We observe in the Fig. 5-2e that the modulo loss is significantly high for the 16-QAM, 64-QAM and 256-QAM schemes. This occurs due to the near uniform (*n-cube*) distribution for X_{cc}^n in such schemes. We have discussed that the more boundary constellation points are selected, more degradation is experienced. Thus, by increasing the constellation order, the ratio between the number of boundary and inner constellation points is reduced, which proportionally improves the performance. As a example, for a fixed $E_b/N_0 = 7$ dB, we observe a BER of 1.6×10^{-2} , 8×10^{-3} and 4×10^{-3} for 16-QAM, 64-QAM and 256-QAM, respectively.

When 1024-QAM is considered, the distribution is near-Gaussian and degradation only becomes more significant at SNR higher than 5 dB. This could be inferred by the increase of λ as a function of SNR (see Eq. (2.34)). Consequently, this causes the modulo loss. When comparing minimum and maximum X_{cc}^n constellation expansion (resp. 16-QAM and 1024-QAM), we detected a gap around 4 dB considering a BER of 10^{-3} and 1.5 dB considering a BER of 10^{-5} . This defines the supported bit rate for

the secondary service. As a result, we point out the tradeoff between power efficiency (or, alternatively, the supported bit rate) and complexity.

Therefore, the main point to be highlighted in this analysis is the efficiency of the proposed solution by changing the decoding *Viterbi* metric at the receiver. As we can observe in the Fig. 5-2e for 16-QAM with metric d_c^k , the performance is improved of about 1 dB for a BER of 10^{-3} and almost 4 dB for a BER of 10^{-5} , in respect to the maximum adopted extension 1024-QAM. This performance gain is traduced as higher supported bit rate at the expense of moderate complexity at the receiver terminal.

Finally, the maintenance of the PU service is evaluated by attesting the exact specified SINR_P at the primary receiver, thanks to the superposition strategy, computed in the last section.

CU Link Budget

By taking the link parameters and the CU BER curve presented in Fig. 5-2e, we can now evaluate the link budget, presented at Table 5.2 (see Appendix B for further details). It is important to note that, by reason of superposition, just 15 % of the power originally allocated for CU is used for its own transmission. However, despite of the received low power, the sensitivity of the receiver is in line with the specifications usually attributed for small satellites links (*i.e.* sensitivity threshold of -118 dBm [72]). We emphasize that all conservative margins are still being considered in order to guarantee the performance.

It is worth noting, as we have discussed in Section 4.2.3, that the \hat{X}_c^n signal is continuous within the squared region bounded by $\Delta = 4d_{min}$ (*i.e.* $|\text{Re}(\hat{X}_c)|$ and $|\text{Im}(\hat{X}_c)| < \Delta/2$, where Δ is the modulo boundary). Thus, the transmitted power (*i.e.* $E[|\hat{X}_c^n|^2]$) as well as the Peak to Average Power Ratio (PAPR) remain in the same order (around 5, or equivalently, around 7 dB), regardless the constellation expansion.

As the main result of this feasibility analysis, we fulfill the minimum supported bit rate of 16 and 28 kbps (*w.r.t.* BER of 10^{-5} and 10^{-3} , respectively) and the maximum of 55 and 91 kbps (*w.r.t.* BER of 10^{-5} and 10^{-3} , respectively) for the secondary service. This range is suitable for most of M2M applications [1, 63, 64].

Table 5.2: Cognitive User link budget.

Transmitted power (mW)	100*0.15
Satellite carrier EIRP (dBm)	20.1
Free space loss (dB)	-162.2
Depointing loss (dB)	-10
Ground Station Antenna max gain - 5m, eff 50 % (dBi)	38.2
System noise temperature (K)	130
C (dBm)	-113.9
C/N0 (dB-Hz)	63.6
Demodulation losses (dB)	-6
Eb/N0 required (dB) – for BER = 1E-3	
DPC 16-QAM	10
DPC 64-QAM	9.4
DPC 256-QAM	8.5
DPC 1024-QAM	5.9
DPC 16-QAM d_c^k	5
Eb/N0 required (dB) – for BER = 1E-5	
DPC 16-QAM	12.5
DPC 64-QAM	12.25
DPC 256-QAM	12
DPC 1024-QAM	11
DPC 16-QAM d_c^k	7.2
Margin (dB)	3
Minimum Bit Rate (kbps) – DPC 16-QAM	
BER = 1E-3	28.8
BER = 1E-5	16.2
Maximum Bit Rate (kbps) – DPC 16-QAM d_c^k	
BER = 1E-3	91.2
BER = 1E-5	55.0
PAPR	
DPC 16-QAM	5.0
DPC 64-QAM	4.67
DPC 256-QAM	4.79
DPC 1024-QAM	4.91

5.4 Conclusion

This Chapter investigated the feasibility of a low data rate secondary service transmission over a primary user infrastructure. A realistic scenario was presented and different techniques were implemented to resolve the interference of both links. As a result, we obtained the same performance for the PU as in absence of the CU oper-

ation (AWGN channel). Concerning the secondary service, we have reached a data rate in the range suitable for most of M2M applications.

However, as a drawback, we point out an increase of the output power of the satellite due to the intrinsic signal correlation presented at the superposition technique. In the described scenario, the total power transmitted is about 32 dBm instead of 30 dBm specified. In this case, the transmitted antenna should be properly designed in order to consider this output power (see Appendix B).

Chapter 6

Conclusion and Future Work

This Chapter summarizes the results of this doctoral thesis and, based on the previous discussions, suggests topics for future research.

6.1 Discussion and Summary of Results

The motivation behind the theme of this doctoral thesis lies in the trend to reconsider the regulation procedure for spectrum allocation, as well as to stimulate the development of techniques which enable the coexistence of different networks. In this view, the terrestrial cognitive radio techniques have also been employed in the satellite communication context. A step forward is presented in this manuscript, where the coexistence among primaries and cognitive users is investigated by using *overlay* paradigm. We have seen (cf. Chapter 2) that, in this specific paradigm, the Cognitive User (CU) has noncausal knowledge about the message and encoding strategy of the Primary User (PU). By this assumption, we have shown that the optimum CU encoding strategy consists in: the superposition and dirty paper coding techniques. We have discussed the main concepts of these techniques, pointing out implementation aspects.

In this line, given that the PU should operate as in the absence of interference, with no performance degradation, we propose (cf. Chapter 3) a scheme based on the Trellis Shaped Dirty-Paper Coding (DPC) encoder for CU. In this first approach, a slight constellation expansion combined with Tomlinson-Harashima Precoding (THP)

is implemented. In addition, we consider the modulo operation as part of our transmission system, assuring the required power limitation for the transmitter. The results present no PU performance degradation and, regarding the CU performance, the precoding losses are identified and quantitatively evaluated.

Thereafter (cf. Chapter 4), we propose some improvements in the CU encoder design to overcome these underlined precoding losses. Techniques are presented for both the encoder and decoder, taking into account the satellite scenarios and the trade-offs between power efficiency and complexity.

We first show that we are able to design schemes where the PU Bit Error Rate (BER) is maintained as in the absence of the cognitive user interference (AWGN channel). Secondly, thanks to trellis precoding and an appropriate constellation expansion, we show that the BER of the cognitive user can be made within 0.3 dB of corresponding the Gaussian channel BER, recovering almost all precoding loss.

Furthermore, we discuss a receiver based design. By employing the slight constellation expansion, which means low complexity scheme, the proposed solution transfers an important part of the interference mitigation processing to the receiver side. We underline that this practice might be interesting for practical satellite missions. Basically, we show that, by changing the *Viterbi* decoder metric, implemented at the CU receiver, the system achieves the same performance as the previously proposed solution (within 0.3 dB of performance loss).

Finally, we investigate the feasibility of a low data rate secondary service transmission over a primary user infrastructure. A realistic scenario was presented and different techniques were implemented to resolve the interference of both links. As a result, we obtained the same performance for the PU as in absence of the CU operation (AWGN channel). Concerning the feasibility analysis, we fulfill the minimum supported bit rate of 16 and 28 kbps (*w.r.t.* BER of 10^{-5} and 10^{-3} , respectively) and the maximum of 55 and 91 kbps (*w.r.t.* BER of 10^{-5} and 10^{-3} , respectively) for the secondary service, where this range is suitable for most of M2M applications.

In light of the present results, this doctoral thesis intends to provide a further step in considering coexistence of secondary user in a existent primary user infrastructure. We introduced, analyzed, proposed techniques and evaluated the results in this context. The next section provides some suggestions to further investigations based on

work introduced in this thesis.

6.2 Outlook of Future Work

The concepts and results presented in this manuscript might be helpful for new research development concerning overlay paradigm. In this way, this section points out same topics of interest that could be further explored:

1. **Investigation of the feasibility of a secondary service transmission for GEO multibeam satellite scenario.**

Fig. 2-1b depicts a multibeam scheme where the CR overlay paradigm might be applied. In addition, due to the superposition strategy (see Eq. (2.16) for further clarification), we highlighted that the secondary service data rate is decreased as aggressive frequency reuse scenario is employed.

In this way, we recommend a detailed investigation, by considering the practical advances in flexible payload techniques, about the feasibility of a secondary transmission for typical multibeam satellite scenario. Different reuse configurations can be explored and performance limits could be evaluated, adopting, for instance, the M2M transmission context.

Besides, practical issues could be further discussed assuming different payloads architecture and commercial components. Also, realistic geographical use cases can be adopted, where these techniques would highly improving the service connectivity.

2. **Study of the Trellis Shaped based DPC encoder concepts for nonlinear modulations.**

In this thesis, we have characterized Trellis Shaped DPC encoder by considering linear modulations (QAM modulation), according to the main references on this subject.

However, it is well-known, in the space communications context, that the power amplifier at the transmitter usually operates in saturation region. By this rea-

son, constant envelope modulations (*i.e.* nonlinear modulation), are recommended for satellite system.

In this way, modulation schemes such as Phase-Shift Keying (PSK), Amplitude and Phase-Shift Keying (APSK), Continuous Phase Modulation (CPM) or even (if low data rate is considered) Frequency-Shift Keying (FSK) should be also investigated in DPC applications. We underline that the TS technique have been explored in PSK schemes (for instance in [73]), however, the DPC context is not addressed. Hence, the analysis of the performance of this thesis approach for nonlinear modulation could be seen as a promising research work.

3. Analysis of the satellite impairments effects on DPC schemes.

We also purpose a further investigation concerning the effects of unwanted impairments, typical on satellite communication. Beside of these impairments are well characterized in the literature, there is no unique reference that address all distortions.

Furthermore, we might infer that these distortions would impact the interference presubtraction at the DPC encoder. As a result, the interference would not be properly eliminated at the receiver decoder, which would degrades the cognitive user performance.

Considering the communication chain, as examples of these impairments, we could point out: nonlinear distortions (AM/AM and AM/PM conversions)[74], jitter [75], amplitude and phase imbalances [76, 77] and phase noise[78, 79, 80], filtering distortion [81, 82] etc.

We suggest both qualitative and quantitative analysis concerning these distortions on the DPC scenario, focusing in the analytical model and evaluating the results by simulations.

4. On the Peak to Average Power Ratio (PAPR) reduction for DPC schemes based on presubtraction.

Among the related distortions of the last topic, special attention should be done to the nonlinear distortion present in the satellite channel. Corroborating with this, we have experienced the increase of PAPR caused by the presubtraction performed at DPC (see cf. Section 5.3.2).

In this sense, a further investigation should be performed to countermeasure this effect. This subject remains an open problem regarding the DPC context.

5. Development of a proof of concept by SDR implementation.

Finally, we strongly encourage the implementation of a real test bench (composed of primary users, secondary user, predistortion procedure) in an SDR environment for laboratory experiments and real signal validation.

By using the concepts discussed in this thesis, this challenging approach will deal with practical problems such as: (i) channel estimation, to properly assign the value α and λ ; (ii) the accurate synchronization of primary and cognitive users, in order to guarantee proper interference mitigation; and (iii) implementation of the primary and cognitive decoders.

Chapter 7

Résumé de la Thèse

7.1 Contexte de la Thèse

On peut affirmer avec conviction que l'accès à l'espace est plus facile, moins cher et plus rapide que jamais. C'est le point de vue largement diffusé parmi les principaux acteurs du secteur des satellites en ce qui concerne le temps opportun et unique que traversent actuellement les activités spatiales. Même si l'on tient compte de l'évolution technologique continue des réseaux terrestres, les systèmes de communication par satellite restent plus valables que jamais et jouent un rôle crucial dans le monde moderne des télécommunications.

En termes d'applications, les projections favorables pour ce segment pourraient être maintenues, surtout aujourd'hui, puisque la demande de nouveaux services a considérablement augmenté, ce qui est justifié par les caractéristiques uniques des satellites, telles que la capacité de multidiffusion et de transmission, les aspects liés à la mobilité, la portée mondiale et la capacité de couvrir et de connecter les espaces verts et les environnements hostiles [1].

Un exemple typique dans ce contexte serait l'utilisation du satellite pour soutenir les communications de machine à machine (M2M), en fournissant une connectivité aux utilisateurs finaux à tout moment, en tout lieu, pour tous les types de médias et de dispositifs [2]. Les communications M2M sont l'un des principaux cas d'utilisation dans le nouveau réseau mobile de cinquième génération (5G) [3], puisque ces communications jouent un rôle majeur dans l'Internet des objets (IoT). En fait, il est

prévu dans [4] le déploiement d'environ 1 million de dispositifs par km² comme des capteurs/actionneurs, des véhicules etc.

En ce qui concerne les avancées technologiques, cette consolidation de l'ère des satellites pourrait être renforcée (mais pas seulement) par la maturité récente atteinte dans le processus de fabrication, qui conduit finalement à des coûts plus bas et des délais de livraison plus courts, ainsi que par les avancées sur les capacités des charges utiles concevables, également stimulées par la nouvelle tendance vers les expériences nouvelles qui dépasse les frontières du risque.

Néanmoins, en contrepartie, pour répondre à ces exigences de plus en plus strictes et maintenir la compétitivité face aux technologies terrestres, les systèmes de communication par satellite doivent repousser les limites vers des solutions techniques de plus en plus efficaces. Dans cette optique, la recherche de l'efficacité en matière de puissance et de largeur de bande, combinée à la tendance actuelle vers des systèmes moins complexes, doivent être une priorité pour les développeurs de systèmes, car, en raison des compromis existants, l'assimilation de ces facteurs devient souvent un défi majeur.

Pour un service délivré aux utilisateurs finaux, les exigences de conception du système de communication sont en général réglées par (i) la disponibilité du service, qui spécifie ultimement le taux d'erreur sur les bits (BER) requis ; (ii) la bande spectrale attribuée, qui est assignée par le règlement des radiocommunications de l'Union internationale des télécommunications (ITU-RR) [5], et (iii) la gamme du rapport porteuse/bruit (CNR) reçu, mesuré dans la largeur de bande occupée, qui est limitée l'atténuation de la liaison, ainsi que par le comportement non linéaire du canal satellite. Par exemple, on pourrait lui attribuer une gamme dynamique de CNR entre -3 et 20 dB, conformément à l'extension récemment présentée à la norme DVB-S2X (Digital Video Broadcasting -Satellite - Second Generation Extension) [6].

Essentiellement, en ce qui concerne ces limites, le système peut être conçu de manière efficace en puissance, en diminuant la puissance reçue (ou de manière équivalente la CNR) nécessaire pour atteindre le BER spécifié, par exemple en ajoutant des bits de redondance dans un système de codage numérique, ou efficace sur le plan spectral, en augmentant le nombre de bits par hertz dans la largeur de bande occupée, ce qui augmente finalement le débit de données transmis. Enfin, la complexité

du système doit être attentivement évaluée afin de réduire le plus possible le nombre d'opérations de traitement sans dégrader les performances globales, en particulier lorsque des systèmes embarqués sont considérés. L'objectif principal est d'équilibrer le compromis en fonction des ressources disponibles de la mission.

En plus des défis mentionnés ci-dessus, le spectre radioélectrique disponible est aujourd'hui une ressource limitée (cf. [7] par exemple). Par conséquent, un autre challenge consiste à développer des techniques qui permettent une meilleure coordination entre les services existants et futurs, notamment en vue de ce nouvel environnement de communication de type machine et de sa mise en œuvre à grande échelle. La nécessité de reconsidérer l'exclusivité statique à long terme du spectre par le biais de procédures de régulation sous licence, ainsi que l'encouragement des techniques permettant la coexistence de différents réseaux, deviennent un élément important pour permettre une expansion adéquate de ces nouveaux services [8].

C'est dans ce cadre que les techniques de radio cognitive (CR), qui visent à réduire la rareté croissante du spectre, sont également devenues attractives pour les applications spatiales [9]. Avec les récents développements de la radio logicielle (SDR) qualifiée pour l'espace [10] et l'acceptation de concepts tels que les charges utiles flexibles [11], [12], les techniques de CR ont été développées ces dernières années, ce qui a permis une exploitation plus efficace du spectre. En outre, des recherches pionnières et de grande valeur [13] ont été menées sur la conscience spectrale et les techniques d'exploitation spectrale, ce qui a conduit les communications cognitives par satellite vers une approche prometteuse afin d'améliorer l'accès à un service secondaire.

Pour résumer cette description du contexte, le thème principal de ce manuscrit concerne la coexistence d'une transmission de service secondaire sur l'infrastructure d'utilisateur primaire. Nous proposons une solution technique générale en mettant en évidence les résultats de certaines contributions de recherche spécifiques.

7.2 Présentation de la Problématique

À la lumière du thème précédemment exposé, ce travail examine les concepts du CR et les techniques qui y sont associées. En ce sens, nous proposons une solution pour une coexistence de services secondaires en accédant au réseau de services primaires dans

le contexte des communications par satellite, en respectant les contraintes strictes du système. Dans cette section, le problème est décrit dans une approche séquentielle de manière à introduire la nouveauté ainsi que les contributions de recherche spécifiques de cette thèse. Par conséquent, Nous présentons donc brièvement la nomenclature et les paradigmes.

Premièrement, en adoptant la nomenclature usuelle dans la grande majorité des références, l'utilisateur primaire (PU) est défini comme l'utilisateur licencié pour opérer dans la bande de fréquences en question. D'autre part, l'utilisateur cognitif (CU) est défini comme l'utilisateur non licencié, qui transmet de manière opportuniste ou même simultanément dans cette même bande attribuée au PU, tout en garantissant les mêmes performances à ce dernier.

Conformément à cette définition, l'opération cognitive est réalisée par la CR, introduite originellement par Mitola en [14]. Cette radio particulière est formellement définie par la Commission fédérale des communications (FCC) comme «une radio ou un système qui perçoit son environnement électromagnétique en étant capable, de manière autonome et dynamique, de fixer ses paramètres afin de: optimiser le débit de transmission, contrôler l'atténuation des interférences, l'interopérabilité et l'accès aux marchés secondaires [15]». De cette façon, il peut envisager deux opérations radio fondamentales qui peuvent être séparées comme: la conscience spectrale et l'exploitation du spectre.

Pour résumer, la première activité (conscience spectrale) pourrait être réalisée par des techniques comme: la détection spectrale, la base de données coopérative, l'estimation du rapport signal/bruit, la cicle-stationnarité etc [16]. La seconde activité (exploitation du spectre), se réfère à l'adaptation des paramètres du signal pour atteindre des schémas de transmission efficaces. Cette activité est généralement réalisée par des techniques telles que: le contrôle adaptatif des ressources (puissance, fréquence, espace), les techniques de *beamforming*, l'adaptation de la modulation et du codage etc [17].

Au niveau du système, trois paradigmes classifient l'opération radio [18]:

- *interweave*, qui repose sur l'idée de communication opportuniste. En bref, le CU recherche les espaces blancs qui ne sont pas utilisés par la transmission du PU, qui peut être dimensionnée dans l'espace, le temps ou la fréquence, et

ajuste ses paramètres de fonctionnement. On en conclut que, idéalement, il n'y a pas de coexistence entre les utilisateurs et, par conséquent, aucun contrôle de puissance de la transmission du CU n'est nécessaire;

- *underlay*, dénommé espace de spectre gris, où le CU, grâce à une compréhension partielle des caractéristiques du signal PU et du canal, ajuste ses paramètres de manière à respecter un niveau d'interférence établi (par exemple, un masque spectral préalablement requis). Contrairement à l'opération de *interweave*, dans ce paradigme, deux utilisateurs peuvent transmettre simultanément. Cependant, comme la compréhension du signal PU est nécessaire, des techniques de détection spectrale plus complexes doivent être employées, comme les algorithmes d'estimation du rapport signal/bruit (SNR). Quelques exemples de techniques que l'on trouve dans la littérature sont: le contrôle dynamique des ressources (puissance et fréquence), *beamforming* avec plusieurs antennes et *spectral spreading* [17];
- *overlay*, dans lequel le CU, à partir des informations complètes et non causales sur la forme d'onde, le message et le canal du PU, utilise des stratégies de codage et de modulation avancées pour transmettre simultanément tout en mitigant l'interférence. L'espace spectral utilisé par le CR dans ce dernier paradigme est appelé noir, car il est occupé par les signaux interférants et le bruit, et n'est pas limité en puissance.

Il faut noter que le choix du paradigme à utiliser par le CU dépend fortement des informations disponibles du signal du PU. Brièvement, si l'information disponible n'est que la présence (ou l'absence) du PU, on utilise le *interweave*. D'autre part, si en plus de l'activité, les états des canaux sont également connus, le CU peut opérer sous le paradigme de *underlay*. Enfin, si les stratégies de codage et les données transmises par la PU sont entièrement connues, le CU peut fonctionner en *overlay*, contribuant aux deux liaisons.

La présente thèse de doctorat, avec le soutien de l'Institut national de recherche spatiale (INPE/Brésil) et du Conseil national pour le développement scientifique et technologique (CNPq/Brésil), développée à l'IMT-Atlantique (site de Toulouse), étudie la faisabilité d'une transmission de service secondaire sur l'infrastructure utilisateur primaire en utilisant le paradigme de *overlay* des techniques de CR. À la

connaissance de l’auteur, aucun travail n’a encore été réalisé sur le paradigme de *overlay* dans le contexte des communications par satellite. En considérant l’objectif général de cette thèse, nous démontrons que cette nouvelle approche est bien adaptée aux applications M2M à faible débit de données.

La principale raison de proposer le paradigme de *overlay* pour les communications par satellite réside dans la possibilité de transmettre simultanément des services licenciés et non licenciés à partir du même satellite vers leurs terminaux respectifs. Nous soulignons, en raison de la priorité accordée par les utilisateurs, que la stratégie de codage par superposition est nécessaire [23] pour relayer la transmission PU, contrairement aux solutions techniques adoptées pour la chaîne de diffusion [24]. De plus, le *dirty-paper coding* (DPC) [25], est mis en œuvre pour adapter le signal cognitif à la direction de l’interférence du PU.

Le DPC est une technique de communication qui permet de mitiger l’interférence si cette dernière est connue de manière non causale dans l’émetteur. Cette technique a été introduite par Costa [25] en 1983. Néanmoins, la première idée de schéma pratique a été proposée par Erez, Shamai et Zamir [26]. Ils soulignaient le précodage Tomlinson Harashima (THP) pour l’annulation de l’interférence intersymbole (ISI), qui peut être vue comme une application DPC pour le canal sélectif en fréquence. Dans cette technique, l’opération modulo est utilisée pour pré-soustraire l’interférence par une augmentation minimale de la puissance. Dans ce travail également, les pertes de précodage, c’est-à-dire la perte de mise en forme dans un régime de SNR élevé et les pertes combinées de modulo et de puissance dans des régimes de SNR intermédiaire/faible, ont été bien caractérisées. De plus, Eyuboglu et Forney, dans leur article précurseur [27], ont généralisé la combinaison de la technique de *Trellis Shaping* (TS) [28], de la technique de *Trellis Coded Modulation* (TCM) et du THP pour les canaux ISI gaussiens. Le *Trellis Precoding* (TP) effectue une pré-soustraction des interférences et permet de récupérer la perte de mise en forme. Également, un peu plus proche de notre application, une extension du TP pour l’interférence multi-utilisateur a été proposée pour récupérer la perte de mise en forme avec une expansion de constellation suffisamment élevée dans [29] et [30], où la technique TS agit comme une quantification vectorielle, remplaçant l’opérateur modulo.

À la lumière de ce qui précède, les contributions spécifiques de cette thèse présentent des variations visant à la conception de liaisons dans le paradigme *overlay*, en con-

sidérant des scénarios d'interférence réalistes. Un codeur DPC est proposé, utilisant les concepts TS et TCM ainsi qu'une expansion de constellation adéquate combinée avec la THP. Les discussions conduisent à un compromis entre l'efficacité en puissance (réduction de la perte modulo) et la complexité, éléments clés pour le traitement à bord des satellites et des terminaux.

7.3 Discussion et Synthèse des Résultats

Cette thèse de doctorat est motivée par la tendance à reconsidérer la procédure de régulation de l'allocation du spectre, ainsi que par la stimulation du développement de techniques qui permettent la coexistence de différents réseaux. Dans cette optique, les techniques de radio cognitive terrestre ont également été utilisées dans le contexte des communications par satellite. Un pas en avant est présenté dans ce manuscrit, où la coexistence entre les utilisateurs primaires et cognitifs est étudiée en utilisant le paradigme de *overlay*.

En effet, le Chapitre 2 nous a rappelé que, dans ce paradigme spécifique, l'utilisateur cognitif (CU) a une connaissance non causale du message et de la stratégie d'encodage de l'utilisateur primaire (PU). Par cette hypothèse, nous avons montré que la stratégie d'encodage optimale du CU consiste en: la superposition et les techniques de *dirty-paper coding* (DPC). Nous avons discuté des principaux concepts de ces techniques, en soulignant les aspects de mise en œuvre.

Dans cette perspective, considérant que le PU doit fonctionner de manière à ce qu'il n'y ait pas d'interférences, sans dégradation des performances, nous proposons (cf. Chapitre 3), dans notre première contribution, un schéma basé sur le codeur DPC en forme de treillis pour CU. Dans cette première approche, une petite expansion de la constellation combinée au précodage Tomlinson-Harashima (THP) est mise en œuvre. En outre, nous considérons le fonctionnement modulo comme faisant partie de notre système de transmission, assurant la limitation de puissance obligatoire pour l'émetteur. Les résultats ne présentent aucune dégradation de la performance du PU et, en ce qui concerne la performance du CU, les pertes de précodage sont identifiées et évaluées quantitativement.

Ensuite (cf. Chapitre 4), dans notre deuxième contribution, nous proposons

quelques innovations dans le codeur CU pour surmonter ces pertes de précodage soulignées. Les techniques sont présentées pour tant le codeur que le décodeur, considérant les scénarios de satellite et les compromis entre l'efficacité de la puissance et la complexité.

Premièrement, nous démontrons la possibilité de concevoir des schémas qui maintiennent le taux d'erreur sur les bits (BER) du PU comme en l'absence d'interférence de l'utilisateur cognitif (canal AWGN). Dans un deuxième temps, grâce au précodage en treillis et à une expansion appropriée de la constellation, nous démontrons que le TEB de l'utilisateur cognitif peut être obtenu à moins de 0,3 dB du TEB correspondant du canal gaussien, ce qui permet de récupérer presque toute la perte de précodage.

Dans notre troisième contribution, nous discutons d'une conception basée sur le récepteur. En utilisant une petite expansion de la constellation, qui signifie un schéma peu complexe, la solution proposée transfère une partie importante du traitement de mitigation des interférences vers le côté récepteur. Nous soulignons que cette pratique pourrait être intéressante pour les missions satellitaires. Essentiellement, nous montrons qu'en changeant la métrique du décodeur de Viterbi, mis en œuvre au niveau du récepteur du CU, le système atteint les mêmes performances que la solution proposée précédemment (dans une limite de 0,3 dB de perte de performance).

Finalement, nous étudions la faisabilité d'un service secondaire de transmission de données à faible débit sur une infrastructure d'utilisateur primaire. Un scénario réaliste est présenté et différentes techniques sont mises en œuvre pour résoudre l'interférence des deux liaisons. Nous obtenons ainsi les mêmes performances pour la PU qu'en l'absence de l'opération CU (canal AWGN). En ce qui concerne l'analyse de faisabilité, nous respectons le débit minimum supporté de 16 et 28 kbps (concernant les BER de 10^{-5} et 10^{-3} , respectivement) et le maximum de 55 et 91 kbps (concernant les BER de 10^{-5} et 10^{-3} , respectivement) pour le service secondaire, pour lequel cette gamme convient à la majorité des applications M2M.

Appendix A

Alternative Proof of the DPC Capacity

In the development presented in Section 2.5.2, we have seen that the DPC capacity reaches the AWGN capacity by properly introducing the auxiliary random variable $X_{cc} = \hat{X}_c + \lambda S$, where the value of λ is optimized and given by Eq. (2.34). In fact, this factor is usually coined as "Wiener coefficient" and is key element for linear Minimum Mean-Square Error (MMSE) estimation of \hat{X}_c given $Y_s = \hat{X}_c + Z_s$ (see [83, 84, 54] for further details).

In this alternative proof, we use this connection between the MMSE estimation and DPC in order to generalize the previous result for non Gaussian interference S .

Firstly, we compute the mutual information in a zero interference channel (or standard Gaussian channel), by considering the channel output $Y_s = \hat{X}_c + Z_s$ and employing the MMSE estimation:

$$\begin{aligned}
C_{AWGN} &= I(\hat{X}_c; Y_s) \\
&= h(\hat{X}_c) - h(\hat{X}_c | Y_s) \\
&= h(\hat{X}_c) - h(\hat{X}_c | \hat{X}_c + Z_s) \\
&= h(\hat{X}_c) - h(\hat{X}_c - \lambda^*(\hat{X}_c + Z_s) | \hat{X}_c + Z_s) \\
&= h(\hat{X}_c) - h(\hat{X}_c - \lambda^*(\hat{X}_c + Z_s)) \\
&= h(\hat{X}_c) - h((1 - \lambda^*)\hat{X}_c - \lambda^*Z_s) \\
&= \frac{1}{2} \ln \left(\frac{P_{\hat{X}_c}}{(1 - \lambda^*)^2 P_{\hat{X}_c} + \lambda^{*2} N_s} \right) \\
&= \frac{1}{2} \ln \left(\frac{P_{\hat{X}_c}}{P_{\hat{X}_c} N_s / (P_{\hat{X}_c} + N_s)} \right) \\
&= \frac{1}{2} \ln \left(1 + \frac{P_{\hat{X}_c}}{N_s} \right), \tag{A.1}
\end{aligned}$$

where the fourth step comes from the fact that $(\hat{X}_c - \lambda(\hat{X}_c + Z_s))$ and $(\hat{X}_c + Z_s)$ are orthogonal and independent, since \hat{X}_c and $\hat{X}_c + Z_s$ are jointly Gaussian [39]¹. In addition, we define the linear MMSE estimation error \mathbf{E} as:

$$\mathbf{E} = \hat{X}_c - \lambda^*(Y_s) = (1 - \lambda^*)\hat{X}_c - \lambda^*Z_s, \tag{A.2}$$

where the second moment of \mathbf{E} is given by:

$$E \left[\|\mathbf{E}\|^2 \right] = (1 - \lambda^*)^2 P_{\hat{X}_c} + \lambda^{*2} N_s = \frac{P_{\hat{X}_c} N_s}{P_{\hat{X}_c} + N_s} = \lambda^* N_s \tag{A.3}$$

In the presence of interference, we once again recall to the *Gelfand-Pinsker* theorem (see Eq. (2.30)) in order to compute the DPC capacity. By considering the MMSE estimation and further developing, we have:

$$\begin{aligned}
C_{DPC} &= (I(X_{cc}^*; Y_s) - I(X_{cc}^*; S)) \\
&= h(X_{cc}^*) - h(X_{cc}^* | Y_s) - (h(X_{cc}^*) - h(X_{cc}^* | S)) \\
&= h(X_{cc}^* | S) - h(X_{cc}^* | Y_s). \tag{A.4}
\end{aligned}$$

¹The complete proof and further explanation can be met in [83]

By evaluating each term of Eq. (A.4):

$$\begin{aligned}
h(X_{cc}^*|S) &= h(\hat{X}_c + \lambda^*S|S) \\
&= h(\hat{X}_c|S) \\
&= h(\hat{X}_c).
\end{aligned} \tag{A.5}$$

$$\begin{aligned}
h(X_{cc}^*|Y_s) &= h(\hat{X}_c + \lambda^*S|Y_s) \\
&= h(\hat{X}_c + \lambda^*S - \lambda^*Y_s|Y_s) \\
&= h(\hat{X}_c - \lambda^*(\hat{X}_c + Z_s)|Y_s) \\
&= h(\hat{X}_c - \lambda^*(\hat{X}_c + Z_s)).
\end{aligned} \tag{A.6}$$

Therefore, by substituting Eq. (A.5) and Eq. (A.6) in Eq. (A.4), we obtain:

$$\begin{aligned}
C_{DPC} &= h(\hat{X}_c) - \overbrace{h(\hat{X}_c - \lambda^*(\hat{X}_c + Z_s))}^{\text{E}} \\
&= \frac{1}{2} \ln \left(1 + \frac{P_{\hat{X}_c}}{N_s} \right) = C_{AWGN},
\end{aligned} \tag{A.7}$$

Thus, the proof is completed regardless the distribution of S .

Appendix B

Design Computations for Analysis of the Feasibility of a Secondary Service Transmission

In this Appendix, we present the main computations employed in the investigation of feasibility exposed in Chapter 5.

The purpose is to underline the main equations as well as the adopted concepts. Nonetheless, this Section does not intend to provide an in-depth study about the link budget topic, recommending to the reader the supported references [85, 68] for further clarifications.

B.1 Primary Service Feasibility

B.1.1 Main Specifications for Primary User

For ease of notation, in the following, $X \stackrel{dB}{=} Y$ means $Y = 10\text{LOG}_{10}(X)$ and $X \stackrel{dBm}{=} Y$ means $Y = 10\text{LOG}_{10}(X) + 30$.

- Transmitter power P_P : according to the COTS transmitter [66], adopted for this design (specification: P_P variable, in the range (27-33) dBm in steps of 0.5 dBm), we assign

$$P_P = 1W \stackrel{dBm}{=} 30 \text{ dBm};$$

- Operating frequency: according to the attributed downlink band for Earth Exploration Satellite Service (EESS) (*i.e.* 2200-2290 MHz) [5], we select

$$f_c = 2200 \text{ MHz};$$

- Orbit parameters: as an example of application, we adopted a scenario based on the work presented in [70]

$$R_E = 6378 \text{ km};$$

$$h_{ES} = 120 \text{ m};$$

$$h_s = 600 \text{ km};$$

$$\mathcal{E} = 20^\circ,$$

where R_E is the Earth radius, h_{ES} is the Earth station height, h_s is the satellite height and \mathcal{E} is the minimum elevation angle.

Based on these assumptions, the farthest distance $d_{s,ES}$, considering the position of the satellite and the ground station, is represented in Fig. B-1 and given by (based on [85]):

$$d_{s,ES} = -(R_E + h_{ES})\sin(\mathcal{E}) + \left[(R_E + h_{ES})^2 \sin^2(\mathcal{E}) + 2(R_E + h_{ES})(h_s - h_{ES}) + (h_s - h_{ES})^2 \right]^{1/2} = 1392.2 \text{ km}.$$

- Throughput rate: according to the maximum supported bit rate R_b of the transmitter [66], which is typical for remote sensing applications, we attribute $R_b = 3.4 \text{ Mbps}$.

In addition, by considering a QPSK signal ($k_p = 2$) encoded by a code rate ($R_{FEC} = 1/2$) convolutional code, the symbol rate R_s , is given by:

$$R_s = \frac{R_b}{k_p \cdot R_{FEC}} = 3.4 \text{ Msps}. \quad (\text{B.1})$$

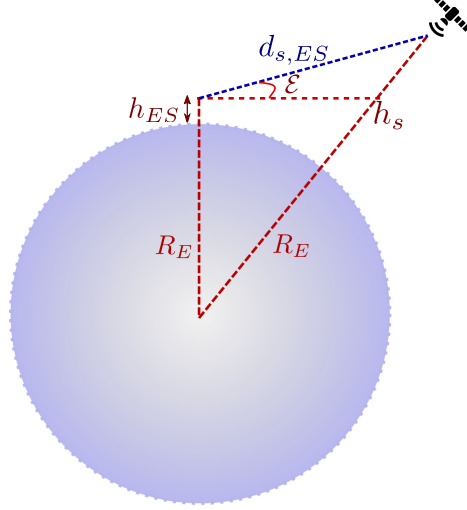


Figure B-1: Relative position of the satellite and the ground station at the farthest communicative distance.

B.1.2 Link Budget for Primary User

In compliance with the proposed overall specification, we present the main points of the PU link budget.

1. Satellite Transmitter Parameters

- Transmitter power P_P :

$$P_P = 1 \text{ W} \stackrel{\text{dBm}}{=} 30 \text{ dBm} \text{ (from COTS adopted transmitter [66])}.$$

- Maximum gain of satellite antenna G_S :

$$G_S \stackrel{\text{dB}}{=} 8.3 \text{ dBi} \text{ (by considering the COTS S-Band antenna [86])}^1.$$

- *Effective Isotropic Radiated Power* (EIRP), which characterizes the transmitter field, is given by:

$$\text{EIRP} = P_P G_S \stackrel{\text{dBm}}{=} 38.3 \text{ dBm}, \quad (\text{B.2})$$

where we disregarded the attenuation losses caused by cables as well as internal elements at the transmitter. In fact, this loss could be inferred as

¹We highlight, by closely inspecting the data sheet of our adopted antenna [86], that the return loss is not well adjusted for the specified operating frequency (2200 MHz). However, as in our analysis we are mainly interested in the maximum gain and in the RF output power (spec. up to 36 dBm), we consider this equipment. We underline that other COTS antennas could be employed in the design, although with less gain, such as [87, 88].

very low considering S-Band operation.

2. Channel Attenuation and Propagation Effects

- Free space loss ²:

$$L_{FS} = \left(\frac{c}{4\pi f_c d_{s,ES}} \right)^2 \stackrel{dB}{=} -162.2 \text{ dB}; \quad (\text{B.3})$$

- Polarization loss: since the circularly polarized antenna is implemented, the Faraday rotation will not disturb the transmission. Thus, this loss is mitigated;
- Depointing loss: value typically attributed in CubeSats link budgets due to the commonly implemented attitude control system [70].

$$L_{Dep} \stackrel{dB}{=} -10 \text{ dB};$$

3. Earth Station Parameters:

- maximum gain of the Earth Station parabolic antenna G_{ES} :

$$G_{ES} = \eta \left(\frac{\pi D}{\lambda} \right)^2 \stackrel{dB}{=} 38.2 \text{ dBi}, \quad (\text{B.4})$$

where the antenna efficiency factor is assumed as $\eta = 50\%$ and the cross-sectional diameter as $D = 5$ meters.

- Receiver noise temperature: according to the scenario presented in [70], we assign as:³

$$T = 130 \text{ K} \stackrel{dB}{=} 21.1 \text{ dBK}.$$

- Receiver figure of merit:

$$\left(\frac{G_{ES}}{T} \right) \stackrel{dB}{=} 17.1 \text{ dB}. \quad (\text{B.5})$$

²In this analysis the rain fall effect is not considered. In addition, since the system operates in S-band, both the atmospheric and the ionospheric scintillation effects are assumed to be negligible [85]

³The receiver noise temperature may be controlled by both: (i) the antenna background (elevation angle, site positioning, etc) and (ii) receiver electronic components [85]. Without loss of generality, we adopted the value presented in [70] as typical earth station. However, by a slight change in the aperture field intensity distribution over the antenna dish, we can drive $\eta = 65\%$ (also typically considered) [85], which ultimately increases the gain $G_{ES} = 39.4$ dBi.

- Received carrier power:

$$C_p = \text{EIRP} L_{FS} L_{Dep} G_{ES} \stackrel{\text{dBm}}{=} -95.7 \text{ dBm}. \quad (\text{B.6})$$

- Received bit energy:

$$E_b = \left(\frac{C_p}{R_b} \right) \stackrel{\text{dBm}}{=} -161 \text{ dBm-Hz}. \quad (\text{B.7})$$

- Noise spectral level entering the receiver:

$$N_{0p} = k.T \stackrel{\text{dBm}}{=} -177.5 \text{ dBm-Hz}. \quad (\text{B.8})$$

- Noise power entering the receiver:

$$N_p = k.T.B_{RF} \stackrel{\text{dBm}}{=} -112.2 \text{ dBm}, \quad (\text{B.9})$$

where k is the *Boltzmann's* constant ($k \approx -228.6 \text{ dB W/K-Hz}$) and B_{RF} is the receiver bandwidth.⁴

4. Ratios:

$$\left(\frac{C_p}{N_p} \right) \stackrel{\text{dB}}{=} 16.5 \text{ dB}; \quad (\text{B.10})$$

$$\left(\frac{C_p}{N_{0p}} \right) \stackrel{\text{dB}}{=} 81.8 \text{ dB}; \quad (\text{B.11})$$

$$\left(\frac{E_b}{N_{0p}} \right) \stackrel{\text{dB}}{=} 16.5 \text{ dB}. \quad (\text{B.12})$$

5. Link Margin

- Demodulation Losses: related to the impairments disturbing the signal at demodulator input. Several sources of distortion, located at the transmitter and receiver, should be considered, such as: nonlinear distortion

⁴Without loss of generality, we assume that the receiver uses the minimum possible bandwidth. This assumption is often considered in practical system and recommended in [72].

(AM/AM and AM/PM), filter mismatches, modulator/demodulator imbalances, phase noise, residual AM etc.⁵

$$L_{Dem} \stackrel{dB}{=} -6 \text{ dB.}$$

- Required E_b/N_0 ratio: by considering the proposed scenario and the simulation results for a targeted BER of 10^{-5} , we define:

$$\left(\frac{E_b}{N_{0p}}\right)_{req} \stackrel{dB}{=} 7 \text{ dB.} \quad (\text{B.13})$$

- Link margin: is given by

$$M = \left[\left(\frac{E_b}{N_{0p}}\right)\right]_{dB} - \left[\left(\frac{E_b}{N_{0p}}\right)_{req}\right]_{dB} - [L_{Dem}]_{dB} = 3.5 \text{ dB} \quad (\text{B.14})$$

B.1.3 Primary User Transmission on the Interfering Scenario

By using 0.5 dB from the margin of the PU link budget for secondary service transmission, and considering the interference scenario described in Fig. 5-1, we have:

- PU Transmitted Power P_P :

$$P_P = 900 \text{ mW} \stackrel{dBm}{=} 29.5 \text{ dBm}$$

- CU Transmitted Power P_C :

$$P_C = 100 \text{ mW} \stackrel{dBm}{=} 20 \text{ dBm}$$

- the channel attenuation, by considering that the same Earth station receives both signals:

$$\|h\|^2 = (G_S L_{FS} L_{Dep} G_{ES}) \stackrel{dB}{=} -125.7 \text{ dB}, \quad (\text{B.15})$$

Thus, by inspection of Fig. 5-1, we evaluate the following ratios at the receiver input:

⁵The adopted value is conservative in order to take account, especially, the nonlinear distortions that might be occasioned by the PAPR provided at the DPC technique. This value is also recommended in [71].

$$\left(\frac{C_p}{N_p}\right) \stackrel{dB}{=} 16 \text{ dB}; \quad (\text{B.16})$$

$$\left(\frac{C_p}{I_{pc}}\right) \stackrel{dB}{=} 9.5 \text{ dB}; \quad (\text{B.17})$$

$$\text{INR} = \left(\frac{I_{pc}}{N_p}\right) = 4.47 \stackrel{dB}{=} 6.5 \text{ dB}; \quad (\text{B.18})$$

$$\left(\frac{C_p}{N_p + I_{pc}}\right) = \left(\frac{C_p/N_p}{1 + \text{INR}}\right) = 7.28 \stackrel{dB}{=} 8.62 \text{ dB}. \quad (\text{B.19})$$

Thus, the degradation in the PU link due to the cognitive user interference is quantified by [69]:

$$D_p = 1 + \text{INR} = 5.47 \stackrel{dB}{=} 7.38 \text{ dB}. \quad (\text{B.20})$$

Superposition Strategy Computation

In order to overcome the degradation presented in Eq. (B.20), the CU implements the superposition encoding strategy. By using the Eq. (2.18) in the described scenario, the superposition factor α is given by:

$$\alpha = \left(\frac{|h| \sqrt{P_p} \left(\sqrt{N_p^2 + \|h\|^2 P_c (N_p + \|h\|^2 P_p)} - N_p \right)}{|h| \sqrt{P_c} (N_p + \|h\|^2 P_p)} \right)^2 = 0.8413. \quad (\text{B.21})$$

B.2 Secondary Service Feasibility

Based on the previous computations, a summary of the power sharing is illustrated in Fig. B-2.

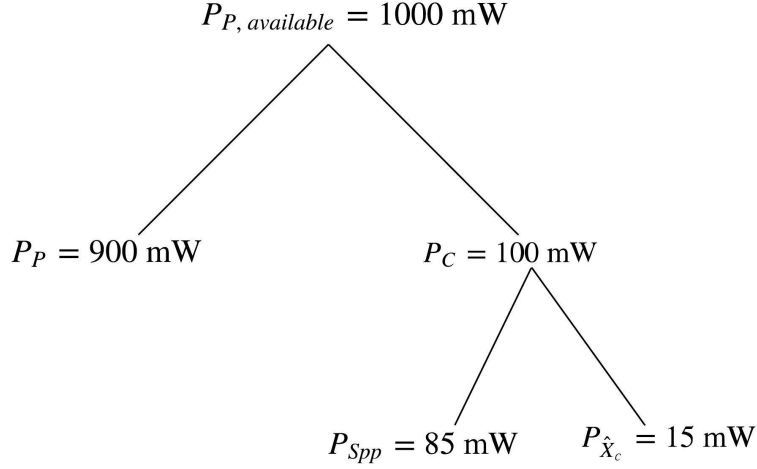


Figure B-2: Summary of the power sharing assignment in this design.

B.2.1 Link Budget for Cognitive User

We present the main points of the link budget for the secondary service transmission, considering the remaining CU power after the superposition strategy. By assuming the factor $\alpha \approx 0.85$, we have:

1. CU Transmitter Parameters:

- CU Transmitted Power $P_{\hat{x}_c}$:
 $P_{\hat{x}_c} = P_c(1 - \alpha) = 15 \text{ mW} \stackrel{dBm}{=} 11.8 \text{ dBm}$.
- Maximum gain of satellite antenna G_S :
 $G_S \stackrel{dB}{=} 8.3 \text{ dBi}$ (both signals are transmitted by the same antenna).⁶
- *Effective isotropic radiated power* (EIRP):

$$\text{EIRP}_c = P_{\hat{x}_c} G_S \stackrel{dBm}{=} 20.1 \text{ dBm}, \quad (\text{B.22})$$

2. Channel attenuation and propagation effects: the same as considered in PU link budget.

3. Earth Station Parameters: the same as considered in Pu link budget.

⁶According to the antenna data sheet [86], the output transmitted power, which is composed by both users, is in line with the specification ($P_{X_T} < 4\text{W}$).

4. Ratios:

- Received carrier power:⁷

$$C_c = \text{EIRP}_c L_{FS} L_{Dep} G_{ES} \stackrel{dBm}{=} -113.9 \text{ dBm}. \quad (\text{B.23})$$

- Receiver noise power: The same as computed for PU (same Earth station).
- Receiver noise spectral level: The same as computed for PU (same Earth station).

Thus, we compute the following ratio for CU at the receiver input:

$$\left(\frac{C_c}{N_{0p}} \right) \stackrel{dB}{=} 63.6 \text{ dB}. \quad (\text{B.24})$$

- Link Margin: assumed as 3 dB (according to [71]).
- Demodulation Losses: The same as assumed for PU (equal to 6 dB assuming the same impairments)

5. Bit Rate R_{bc} :

$$R_{bc} = \frac{(C_c/N_0)_p}{(E_{bc}/N_0)_{req} ML_{Dem}} \text{ bps} \quad (\text{B.25})$$

Where the results are presented in Table B.1:

Table B.1: Bit rate (kbps) supported by each DPC scheme of Fig. 5-2e

BER	10^{-3}	10^{-5}
16-QAM	28.8	16.2
64-QAM	33.1	17.2
256-QAM	40.7	18.2
1024-QAM	74.1	22.9
16-QAM d_c^k	91.2	55

⁷It is worth noting that this parameter complies with typical specification sensitivity adopted in COTS receivers (*i.e.* $C > -118$ dBm) [72].

B.3 Transmitted Output Power

As an important drawback of the proposed scheme, the output power at the antenna input is increased when the CU signal is added in the system. This occurs due to the superposition strategy. In practice, the antenna should be designed in order to handle with this issue (as emphasized in this design). However, particular attention should be paid to avoid that these two different signals pass through the same power amplifier, which would generate an intermodulation distortion as well as the AM/AM and AM/PM effects, degrading both signal performance.

The signal X_T , composed by both PU and CU signals (resp. X_p and X_c) at the antenna input is given by:

$$\begin{aligned}
 X_T &= X_c + X_p \\
 &= \hat{X}_c + \sqrt{\alpha \frac{P_c}{P_p}} X_p + X_p \\
 &= \hat{X}_c + \left(1 + \sqrt{\alpha \frac{P_c}{P_p}}\right) X_p.
 \end{aligned} \tag{B.26}$$

Assuming that X_p and \hat{X}_c are uncorrelated, the power of X_T is evaluated as:

$$\begin{aligned}
 P_{X_T} &= E[\|X_T\|^2] \\
 &= E[\|\hat{X}_c + \left(1 + \sqrt{\alpha \frac{P_c}{P_p}}\right) X_p\|^2] \\
 &= E[\|\hat{X}_c\|^2] + \left(1 + \sqrt{\alpha \frac{P_c}{P_p}}\right)^2 E[\|X_p\|^2] \\
 &= (1 - \alpha)P_c + \left(1 + \sqrt{\alpha \frac{P_c}{P_p}}\right)^2 P_p.
 \end{aligned} \tag{B.27}$$

By considering the assumed values $\alpha = 0.85$, $P_p = 900$ mW and $P_c = 100$ mW, the total power at the antenna input is:

$$P_{X_T} = 1553.2 \text{ mW} \stackrel{dBm}{=} 31.9 \text{ dBm}. \tag{B.28}$$

Bibliography

- [1] D. Minoli, *Innovations in Satellite Communications and Satellite Technology: The Industry Implications of DVB-S2X, High Throughput Satellites, Ultra HD, M2M, and IP*. John Wiley & Sons, 2015.
- [2] Z. Qu, G. Zhang, H. Cao, and J. Xie, “LEO satellite constellation for internet of things,” *IEEE Access*, vol. 5, pp. 18 391–18 401, 2017.
- [3] ITU-R, “Emerging trends in 5G/IMT2020,” *Geneva Mission Briefing Series*, September 2016.
- [4] Huawei, “5G network architecture - a high-level perspective,” *White paper*, December 2016.
- [5] R. Regulations ITU, “Article 5,” *Frequency allocations*, September 2016.
- [6] DVB, “Doc A-172 - white paper on the use of DVB-S2X for DTH applications DSNG & professional services broadband interactive services and VL-SNR applications,” 2015.
- [7] United States Department of Commerce, “United States radio spectrum frequency allocations chart,” <https://www.ntia.doc.gov/files/ntia/publications/january-2016-spectrum-wall>, (Online); accessed 27 January 2020.
- [8] Y. Han, E. Ekici, H. Kremo, and O. Altintas, “Spectrum sharing methods for the coexistence of multiple rf systems: A survey,” *Ad Hoc Networks*, vol. 53, pp. 53–78, 2016.
- [9] K. Patil, K. Skouby, A. Chandra, and R. Prasad, “Spectrum occupancy statistics in the context of cognitive radio,” in *IEEE 14th International Symposium on Wireless Personal Multimedia Communications (WPMC)*, 2011, pp. 1–5.
- [10] M. R. Maheshwarappa, M. Bowyer, and C. P. Bridges, “Software defined radio (SDR) architecture to support multi-satellite communications,” in *IEEE Aerospace Conference, 2015*, pp. 1–10.
- [11] G. Cocco, T. De Cola, M. Angelone, Z. Katona, and S. Erl, “Radio resource management optimization of flexible satellite payloads for DVB-S2 systems,” *IEEE Transactions on Broadcasting*, 2017.

- [12] N. Porecki, G. Thomas, A. Warburton, N. Wheatley, and N. Metzger, “Flexible payload technologies for optimising Ka-band payloads to meet future business needs,” in *Proc. 19th Ka Broadband Commun., Navigat. Earth Observat. Conf.*, 2013, pp. 1–7.
- [13] S. K. Sharma, S. Chatzinotas, and B. Ottersten, “Cognitive radio techniques for satellite communication systems,” in *IEEE 78th Vehicular Technology Conference (VTC Fall), 2013*, pp. 1–5.
- [14] J. Mitola, “Cognitive radio,” Ph.D. dissertation, Institutionen för teleinformatik, 2000.
- [15] F. C. Commission *et al.*, “Notice of proposed rule making and order: Facilitating opportunities for flexible, efficient, and reliable spectrum use employing cognitive radio technologies,” *ET docket*, no. 03-108, p. 73, 2005.
- [16] T. Yucek and H. Arslan, “A survey of spectrum sensing algorithms for cognitive radio applications,” *IEEE communications surveys & tutorials*, vol. 11, no. 1, pp. 116–130, 2009.
- [17] S. K. Sharma, T. E. Bogale, S. Chatzinotas, B. Ottersten, L. B. Le, and X. Wang, “Cognitive radio techniques under practical imperfections: A survey,” *IEEE Communications Surveys & Tutorials*, vol. 17, no. 4, pp. 1858–1884, 2015.
- [18] E. Biglieri, “An overview of cognitive radio for satellite communications,” in *IEEE First AESS European Conference on Satellite Telecommunications (ES-TEL), 2012*, 2012, pp. 1–3.
- [19] A. Vanelli-Coralli, A. Guidotti, D. Tarchi, S. Chatzinotas, S. Maleki, S. K. Sharma, N. Chuberre, B. Evans, M. Lopez-Benitez, W. Tang *et al.*, “Cognitive radio scenarios for satellite communications: the CoRaSat project,” in *Cooperative and Cognitive Satellite Systems*. Elsevier, 2015, pp. 303–336.
- [20] B. Evans, P. Thompson, E. Lagunas, S. K. Sharma, D. Tarchi, and V. R. Icolari, “Extending the usable Ka band spectrum for satellite communications: The CoRaSat project,” in *International Conference on Wireless and Satellite Systems*. Springer, 2015, pp. 119–132.
- [21] N. Chumberre, B. Evans, A. Vanelli-Coralli, J. Krause, J. Grotz, and S. K. Sharma, “FP7 project CoRaSat intermediate results and standardization strategy: Cognitive radio techniques in Ka band SatCom context,” in *Proc. European Conference on Networks and Communications (EuCNC)*, 2014.
- [22] S. K. Sharma, “Interweave underlay cognitive radio techniques and applications in satellite communication systems,” Ph.D. dissertation, University of Luxembourg, Luxembourg, 2014.

- [23] A. Jovicic and P. Viswanath, “Cognitive radio: An information-theoretic perspective,” *IEEE Transactions on Information Theory*, vol. 55, no. 9, pp. 3945–3958, 2009.
- [24] A. J. Goldsmith, S. A. Jafar, I. Maric, and S. Srinivasa, “Breaking spectrum gridlock with cognitive radios: An information theoretic perspective.” *Proceedings of the IEEE*, vol. 97, no. 5, pp. 894–914, 2009.
- [25] M. Costa, “Writing on dirty paper (corresp.),” *IEEE transactions on information theory*, vol. 29, no. 3, pp. 439–441, 1983.
- [26] U. Erez, S. Shamai, and R. Zamir, “Capacity and lattice strategies for canceling known interference,” *IEEE Transactions on Information Theory*, vol. 51, no. 11, pp. 3820–3833, 2005.
- [27] M. V. Eyuboglu and G. D. Forney, “Trellis precoding: Combined coding, precoding and shaping for intersymbol interference channels,” *IEEE Transactions on Information Theory*, vol. 38, no. 2, pp. 301–314, 1992.
- [28] G. Forney, “Trellis shaping,” *IEEE Transactions on Information Theory*, vol. 38, no. 2, pp. 281–300, 1992.
- [29] W. Yu, D. P. Varodayan, and J. M. Cioffi, “Trellis and convolutional precoding for transmitter-based interference presubtraction,” *IEEE Transactions on Communications*, vol. 53, no. 7, pp. 1220–1230.
- [30] Y. Sun, W. Xu, and J. Lin, “Trellis shaping based dirty paper coding scheme for the overlay cognitive radio channel,” in *IEEE 25th Annual International Symposium on Personal, Indoor, and Mobile Radio Communication (PIMRC), 2014*, pp. 1773–1777.
- [31] M. Álvarez-Díaz, M. Neri, C. Mosquera, and G. Corazza, “Trellis shaping techniques for satellite telecommunication systems,” in *IEEE International Workshop on Satellite and Space Communications, 2006*, 2006, pp. 148–152.
- [32] L. B. C. da Silva, T. Benaddi, and L. Franck, “Cognitive radio overlay paradigm towards satellite communications,” in *2018 IEEE International Black Sea Conference on Communications and Networking (BlackSeaCom)*, 2018, pp. 1–5.
- [33] —, “A design method of cognitive overlay links for satellite communications,” in *IEEE 9th Advanced Satellite Multimedia Systems Conference and the 15th Signal Processing for Space Communications Workshop (ASMS/SPSC)*, 2018, pp. 1–6.
- [34] —, “On the feasibility of a secondary service transmission over an existent satellite infrastructure,” in *International Conference on Cognitive Radio Oriented Wireless Networks*. Springer, 2019, pp. 154–167.

- [35] —, “A watermarking like scheme for cubesat communications,” in *10th European CubeSat Symposium*, 2018.
- [36] S. K. Sharma, S. Chatzinotas, and B. Ottersten, “Interference alignment for spectral coexistence of heterogeneous networks,” *EURASIP Journal on Wireless Communications and Networking*, vol. 2013, no. 1, p. 46, 2013.
- [37] —, “Exploiting polarization for spectrum sensing in cognitive satcoms,” in *IEEE 7th International ICST Conference on Cognitive Radio Oriented Wireless Networks and Communications (CROWNCOM)*, 2012, pp. 36–41.
- [38] —, “Transmit beamforming for spectral coexistence of satellite and terrestrial networks,” in *IEEE 8th International Conference on Cognitive Radio Oriented Wireless Networks*, 2013, pp. 275–281.
- [39] A. El Gamal and Y.-H. Kim, *Network information theory*. Cambridge university press, 2011.
- [40] E. Biglieri, A. J. Goldsmith, L. J. Greenstein, N. B. Mandayam, and H. V. Poor, *Principles of cognitive radio*. Cambridge University Press, 2013.
- [41] J. G. Proakis and M. Salehi, *Digital communications*. McGraw-hill New York, 2001, vol. 4.
- [42] A. Abrardo and M. Barni, “Orthogonal dirty paper coding for informed data hiding,” in *Security, Steganography, and Watermarking of Multimedia Contents VI*, vol. 5306. International Society for Optics and Photonics, 2004, pp. 274–285.
- [43] P. Comesana, F. Pérez-González, and F. M. Willems, “Applying erez and tenbrink’s dirty paper codes to data hiding,” in *Security, Steganography, and Watermarking of Multimedia Contents VII*, vol. 5681. International Society for Optics and Photonics, 2005, pp. 298–307.
- [44] Ç. Dikici, K. Idrissi, and A. Baskurt, “Dirty-paper writing based on LDPC codes for data hiding,” in *International Workshop on Multimedia Content Representation, Classification and Security*. Springer, 2006, pp. 114–120.
- [45] P. Singh and R. Chadha, “A survey of digital watermarking techniques, applications and attacks,” *International Journal of Engineering and Innovative Technology (IJEIT)*, vol. 2, no. 9, pp. 165–175, 2013.
- [46] S. Katzenbeisser and F. Petitcolas, “Digital watermarking,” *Artech House, London*, 2000.
- [47] T. Liu and Z.-d. Qiu, “The survey of digital watermarking-based image authentication techniques,” in *IEEE 6th International Conference on Signal Processing, 2002.*, vol. 2, 2002, pp. 1556–1559.

- [48] M. L. Miller, "Watermarking with dirty paper codes," in *IEEE Proceedings International Conference on Image Processing (Cat. No. 01CH37205)*, vol. 2, 2001, pp. 538–541.
- [49] S. Gelfand, "Coding for channel with random parameters," *Probl. Contr. and Inf. Theory*, vol. 9, no. 1, pp. 19–31, 1980.
- [50] T. M. Cover and J. A. Thomas, *Elements of information theory*. John Wiley & Sons, 2012.
- [51] M. Tomlinson, "New automatic equaliser employing modulo arithmetic," *Electronics letters*, vol. 7, no. 5, pp. 138–139, 1971.
- [52] H. Harashima and H. Miyakawa, "Matched-transmission technique for channels with intersymbol interference," *IEEE Transactions on Communications*, vol. 20, no. 4, pp. 774–780, 1972.
- [53] G. D. Forney and M. V. Eyuboglu, "Combined equalization and coding using precoding," *IEEE Communications Magazine*, vol. 29, no. 12, pp. 25–34, 1991.
- [54] U. Erez and R. Zamir, "log (1+ SNR) on the AWGN channel with lattice encoding and decoding," *IEEE Transactions on Information Theory*, vol. 50, no. 10, p. 1, 2004.
- [55] G. D. Forney and L.-F. Wei, "Multidimensional constellations. I. introduction, figures of merit, and generalized cross constellations," *IEEE journal on selected areas in communications*, vol. 7, no. 6, pp. 877–892, 1989.
- [56] G. D. Forney, "Multidimensional constellations. II. voronoi constellations," *IEEE Journal on Selected Areas in Communications*, vol. 7, no. 6, pp. 941–958, 1989.
- [57] R. F. Fischer, *Precoding and signal shaping for digital transmission*. John Wiley & Sons, 2005.
- [58] S. A. Tretter, *Constellation Shaping, Nonlinear Precoding, and Trellis Coding for Voiceband Telephone Channel Modems: With Emphasis on ITU-T Recommendation*. Springer Science & Business Media, 2012, vol. 34.
- [59] M. A. Diaz, C. M. Nartallo, and R. L. Valcarce, "Design of nonlinear precoding and estimation schemes for advanced communication systems," Ph.D. dissertation, Ph. D. dissertation, University Vigo, Spain, 2010.
- [60] G. Ungerboeck, "Channel coding with multilevel/phase signals," *IEEE transactions on Information Theory*, vol. 28, no. 1, pp. 55–67, 1982.
- [61] —, "Trellis-coded modulation with redundant signal sets part i: Introduction," *IEEE Communications magazine*, vol. 25, no. 2, pp. 5–11, 1987.
- [62] —, "Trellis-coded modulation with redundant signal sets part ii: State of the art," *IEEE Communications magazine*, vol. 25, no. 2, pp. 12–21, 1987.

- [63] M. De Sanctis, E. Cianca, G. Araniti, I. Bisio, and R. Prasad, "Satellite communications supporting internet of remote things," *IEEE Internet of Things Journal*, vol. 3, no. 1, pp. 113–123, 2015.
- [64] G. Cocco and C. Ibars, "On the feasibility of satellite M2M systems," in *30th AIAA International Communications Satellite System Conference (ICSSC)*, 2012, p. 15074.
- [65] V. Almonacid Zamora, "Cross-layer design applied to small satellites for data collection," Ph.D. dissertation, 2017, thèse de doctorat dirigée par Despaux, Gilles et Franck, Laurent Électronique Montpellier 2017. [Online]. Available: <http://www.theses.fr/2017MONT079>
- [66] ISIS - Innovative Solutions In Space B.V., "ISIS high data rate S-band transmitter specifications," <https://www.isispace.nl/wp-content/uploads/2016/02/ISIS-Communication-systems-Brochure-v2-compressed.pdf>, (Online); accessed 27 January 2020.
- [67] E.-M. ECSS, "St-10c: Space project management-project planning and implementation," 2009.
- [68] G. Maral and M. Bousquet, *Satellite communications systems: systems, techniques and technology*. John Wiley & Sons, 2011.
- [69] R. Regulations, "Maximum permissible levels of interference in a satellite network (GSO/FSS; non-GSO/FSS; non-GSO/MSS feeder links) for a hypothetical reference digital path in the fixed-satellite service caused by other codirectional FSS networks below 30 ghz," *Recommendation ITU-R S*, vol. 1323, 1997.
- [70] D. Barbarić, J. Vuković, and D. Babic, in *IEEE 41st International Convention on Information and Communication Technology, Electronics and Microelectronics (MIPRO)*.
- [71] W. J. Larson and J. R. Wertz, "Space mission analysis and design," Torrance, CA (United States); Microcosm, Inc., Tech. Rep., 1992.
- [72] M. Arias and F. Aguado, "Small satellite link budget calculation," in *ITU Symposium and Workshop on small satellite regulation and communication systems*, 2016.
- [73] M. Tanahashi and H. Ochiai, "Near constant envelope trellis shaping for psk signaling," *IEEE Transactions on Communications*, vol. 57, no. 2, pp. 450–458, 2009.
- [74] J. J. Spilker Jr, "Digital communications by satellite," *Englewood Cliffs, NJ, Prentice-Hall, Inc., 1977. 685 p.*, 1977.

- [75] M. H. SHARIFI *et al.*, “Effects of transmitter-satellite and receiver timing, frequency, and amplitude instabilities on BPSK and QPSK system performance,” in *1985 IEEE International Conference on Communications (ICC)*, 1985, pp. 499–503.
- [76] Z. Chen and F. F. Dai, “Effects of lo phase and amplitude imbalances and phase noise on M -QAM transceiver performance,” *IEEE Transactions on Industrial electronics*, vol. 57, no. 5, pp. 1505–1517, 2010.
- [77] H. Tsou, “The effect of phase and amplitude imbalance on the performance of BPSK/QPSK communication systems,” *The Telecommunications and Data Acquisition Progress Report 42-130, April–June 1997*, pp. 1–13, 1997.
- [78] A. Georgiadis, “Gain, phase imbalance, and phase noise effects on error vector magnitude,” *IEEE Transactions on Vehicular Technology*, vol. 53, no. 2, pp. 443–449, 2004.
- [79] D. Taggart and R. Kumar, “Impact of phase noise on the performance of the QPSK modulated signal,” in *IEEE Aerospace Conference*, 2011, pp. 1–10.
- [80] R. Krishnan, M. R. Khanzadi, N. Krishnan, Y. Wu, A. G. i Amat, T. Eriksson, and R. Schober, “Linear massive mimo precoders in the presence of phase noise—a large-scale analysis,” *IEEE Transactions on Vehicular Technology*, vol. 65, no. 5, pp. 3057–3071, 2015.
- [81] J. Jones, “Filter distortion and intersymbol interference effects on psk signals,” *IEEE Transactions on Communication Technology*, vol. 19, no. 2, pp. 120–132, 1971.
- [82] A. Azizzadeh and L. Mohammadi, “Degradation of BER by group delay in digital phase modulation,” in *IEEE Fourth Advanced International Conference on Telecommunications*, 2008, pp. 350–354.
- [83] G. D. Forney Jr, “On the role of MMSE estimation in approaching the information-theoretic limits of linear gaussian channels: Shannon meets Wiener,” *arXiv preprint cs/0409053*, 2004.
- [84] —, “Shannon meets Wiener II: On MMSE estimation in successive decoding schemes,” *arXiv preprint cs/0409011*, 2004.
- [85] R. M. Gagliardi, *Satellite communications*. Springer Science & Business Media, 2012.
- [86] EnduroSat, “S-band patch antenna type I user manual,” https://www.endurosat.com/modules-datasheets/S-Band_Patch_User_Manual_Rev1_2.pdf, (Online); accessed 27 January 2020.
- [87] NanoAvionics, “Cubesat S-band patch antenna,” <https://nanoavionics.com/cubesat-components/cubesat-s-band-patch-antenna>, (Online); accessed 27 January 2020.

[88] Anywaves, “Smallsat S-band antenna,” <https://newspace-factory.com/product/cubesat-s-band-antenna>, (Online); accessed 27 January 2020.

Titre : Radio Cognitive Overlay pour communications satellitaires IoT.

Mots clés : Communications par satellites; Radio cognitive; Dirty paper coding; Précodage.

Résumé : La projection favorable vers le segment des satellites pourrait se maintenir, surtout aujourd'hui, puisque la demande de nouveaux services a considérablement augmentée. Cela se justifie par les caractéristiques uniques du satellite, telles que les capacités de multidiffusion et de radiodiffusion, les aspects de mobilité et la couverture mondiale. À titre d'exemple, nous soulignons l'utilisation du satellite pour soutenir les futures communications de machine à machine (M2M). Dans ce contexte, l'un des principaux défis consiste à développer des techniques permettant une meilleure coordination entre les services existants et futurs. C'est dans ce cadre que les techniques de radio cognitive (RC) sont devenues intéressantes pour les applications spatiales. Cette thèse étudie la faisabilité d'une transmission d'un utilisateur cognitif (UC) sur une

infrastructure existante d'utilisateurs primaires en utilisant les techniques de RC de type overlay. Dans cette optique, la première contribution présente une méthodologie de design pour ce paradigme dans le domaine des communications par satellite. Ensuite, nous discutons d'une approche pour contrôler la puissance de sortie de l'UC en abordant la technique de mise en forme du treillis et d'une nouvelle méthode pour récupérer la perte modulo. Ces techniques montrent un compromis entre l'efficacité de puissance, (réduction de la perte modulo), et la complexité, (réduction des opérations de l'encodeur). Enfin, nous examinons les solutions proposées à la lumière d'un scénario satellite réaliste en utilisant des exemples de pièces commerciales (COTS) et en supposant des valeurs pratiques pour le bilan de liaison.

Title : Overlay Cognitive Radio for IoT Satellite Communications

Keywords : Satellite communications; Cognitive radios; Dirty-paper coding; Precoding.

Abstract : The favorable projection towards the satellite segment could be sustained especially today, since the demand for the rising new services has increased considerably. This is justified by the unique satellite characteristics such as multicast and broadcasting capabilities, mobility aspects and global reach, besides the ability to cover and connect remote areas and hostile environments. As a typical example, we point out the use of satellite to support the Machine-to-Machine (M2M) communications. In this context, a main challenge is to develop techniques that enable a better coordination among legacy and future services. It is within this framework that the Cognitive Radio (CR) techniques have also become attractive for space applications. This doctoral thesis studies the feasibility of a Cognitive User (CU) transmission over the primary user infrastructure by using the CR techniques in the overlay paradigm applied to the satellite

context. In this perspective, the first thesis contribution present a framework for overlay paradigms towards satellite communications. In this sense, a low complexity solution is proposed related to the Trellis Shaping based DPC encoder for the CU. Subsequently, we discuss an approach to control the CU output power by addressing the trellis shaping (TS) technique. Moreover, by using auxiliary bits as well as the proper mapping selection, further constellation expansion is performed in order to increase the number of shaping regions. The relation among these implemented techniques provides a trade-off between power efficiency, by the reduction of the modulo loss, and complexity, by the reduction of the encoder operations. Finally, we examine the proposed solutions at the light of a realistic satellite scenario. In this general contribution, by using examples of commercial off-the-shelf (COTS) parts and assuming practical link budget parameters.